DOUBLE-ENDED TRAVELING WAVE-BASED METHOD FOR POLE-TO-GROUND FAULT LOCATION ON HVDC TRANSMISSION LINES

CAIO MULLER SANTOS RIBEIRO

PHD THESIS
ON ELECTRICAL ENGINEERING

DEPARTMENT OF ELECTRICAL ENGINEERING

TECHNOLOGY FACULTY

UNIVERSITY OF BRASÍLIA

University of Brasília
Technology Faculty
Department of Electrical Engineering

Double-Ended Traveling Wave-Based Method for Pole-to-Ground Fault Location on HVDC Transmission Lines

Caio Muller Santos Ribeiro

PHD THESIS SUBMITTED TO THE GRADUATE PROGRAM IN ELECTRICAL ENGINEERING AT THE UNIVERSITY OF BRASÍLIA AS REQUIRED FOR OBTAINING THE PHD DEGREE IN ELECTRICAL ENGINEERING.

APPROVED BY:

Prof. Kleber Melo e Silva, D.Sc. (Advisor)
University of Brasília, Brazil

Prof. Felipe Vigolvino Lopes, D.Sc. (Co-advisor)
Federal University of Paraíba, Brazil

Prof. Flávio Bezerra Costa, D.Sc. (External Examiner)
Michigan Technological University, United States of America

Prof. José Carlos de Melo Vieira Júnior, D.Sc. (External Examiner)
University of São Paulo, Brazil

Prof. Francis Arody Moreno Vásquez, D.Sc. (Internal Examiner)
University of Brasília, Brazil

Publicação: PPGEE.TD 207/24

September 27, 2024
Brasília, Brazil

FICHA CATALOGRÁFICA

RIBEIRO, CAIO MULLER S.
Double-Ended Traveling Wave-Based Method for Pole-to-Ground Fault Location on HVDC Transmission Lines [Distrito Federal] 2024.
ix, 62p., 210 x 297 mm (ENE/FT/UnB, Doutor, Tese de Doutorado – Universidade de Brasília. Faculdade de Tecnologia.
Departamento de Engenharia Elétrica.

1. Eletromagnetic transients 2. Fault location
3. HVDC transmission lines 4. Power systems
5. Traveling waves
I. ENE/FT/UnB II. Título (série)

REFERÊNCIA BIBLIOGRÁFICA

RIBEIRO, CAIO MULLER S. (2024). Double-Ended Traveling Wave-Based Method for Pole-to-Ground Fault Location on HVDC Transmission Lines. Tese de Doutorado em Engenharia Elétrica, Publicação PPGEE.TD 207/24, Departamento de Engenharia Elétrica, Universidade de Brasília, DF, 62p.

CESSÃO DE DIREITOS

Caio Muller Santos Ribeiro
Universidade de Brasília (UnB)
Campus Universitário Darcy Ribeiro
Faculdade de Tecnologia (FT)
Departamento de Engenharia Elétrica (ENE)
Brasília, Distrito Federal, Brasil
CEP 70.919-970

To the Word.

ACKNOWLEDGEMENTS

To ...

... God the Father and the Son and the Holy Spirit.

... Holy Mary, Mother of God.

... my parents Deusira B. S. Ribeiro and José J. Ribeiro.

... my advisors Prof. Kleber M. Silva, D.Sc., and Prof. Felipe V. Lopes., D.Sc.

... my research partners Pedro C. Fernandes, M.Sc., Tiago R. Honorato, M.Sc., Fernando M. Magalhães Jr., M.Sc., and Letícia A. Gama, D.Sc.

... the members of the Power Systems Protection Laboratory (LAPSE).

... the Graduate Program in Electrical Engineering (PPGEE).

... the employees of the Department of Electrical Engineering (ENE).

... the employees of the Technology Faculty (FT).

... the University of Brasília (UnB).

... the Coordenação de Aperfeiçoamento de Pessoal de Nível Superior - Brasil (CAPES) - Finance Code 001.

... the Conselho Nacional de Desenvolvimento Científico e Tecnológico (CNPq).

... the Fundação de Apoio à Pesquisa do Distrito Federal (FAPDF).

... the Ministério da Ciência, Tecnologia e Inovação (MCTI).

RESUMO

Título: Método Baseado na Teoria de Ondas Viajantes Usando Dados de Dois Terminais para Localizar Faltas Polo-Terra em Linhas de Transmissão de Alta Tensão e Corrente Contínua.

Nesta tese, propõe-se um método de localização de faltas polo-terra baseado na teoria das ondas viajantes usando dados de dois terminais para linhas de transmissão de alta tensão em corrente contínua. Faltas polo-terra são mais frequentes e críticas do que faltas polo-polo nessas linhas. Dessa forma, é crucial localizar com precisão as faltas polo-terra para que essas linhas sejam reparadas rapidamente após desligamentos não programados. Ao realizar uma análise da propagação das ondas viajantes lançadas por faltas polo-terra, descobriu-se que as ondas refratadas no ponto de falta podem ser detectadas usando um critério baseado em amplitude e polaridade. Com base nessa descoberta, propõe-se um método de localização de faltas polo-terra, livre da configuração da velocidade de propagação das ondas viajantes e de meios de sincronização de dados. Foram realizadas simulações no sistema do Rio Madeira usando o *Alternative Transients Program*. A linha foi implementada usando o modelo JMarti dependente na frequência e com parâmetros distribuídos. Dos resultados, o método proposto mostrou-se ser preciso, com erros na localização das faltas menores que 0,6 km (0,02% do comprimento da linha) na maioria dos casos. Além disso, o método se revelou imune aos desalinhamentos na sincronização de dados. Ademais, o método se mostrou robusto a diferentes resistências de falta, níveis de ruído, resistividades do solo e frequências de amostragem. Por fim, através de um estudo comparativo, mostrou-se que o método é mais simples, preciso e robusto do que os métodos de localização de faltas baseados em ondas viajantes no estado da arte.

Palavras-chave: Linhas de transmissão de alta tensão em corrente contínua, localização de faltas, ondas viajantes, sistemas de potência, transitórios eletromagnéticos.

ABSTRACT

Title: Double-Ended Traveling Wave-Based Method for Pole-to-Ground Fault Location on HVDC Transmission Lines.

This PhD thesis proposes a double-ended method based on traveling waves (TWs) for locating pole-to-ground (PG) faults on high-voltage direct current (HVDC) transmission lines. PG faults are more likely and critical than pole-to-pole (PP) faults on HVDC lines. Hence, accurate PG fault location is important to quickly restore HVDC systems after unscheduled shutdowns. An analysis of the TWs launched by PG faults reveals that refracted TWs can be easily detected at both line ends using an amplitude- and polarity-based criterion. Based on this finding, a double-ended PG fault location method free of TW propagation velocity settings and data synchronization is proposed. Fault simulations in the Rio Madeira HVDC system using the Alternative Transients Program (ATP) were carried out. The transmission line was implemented using the distributed parameter frequency-dependent JMarti model. Results show that the method is accurate, presenting errors smaller than 0.6 km (0.02% of the line length) in most cases. Also, the method is revealed to be immune to data synchronization misalignments, being robust to different fault resistances, noise levels, soil resistivities, and sampling frequencies. Finally, a comparative study shows that the method is simpler, more accurate, and more robust than the state-of-the-art TW-based fault location (TWFL) methods.

Keywords:

Electromagnetic transients, fault location, HVDC transmission lines, power systems, traveling waves.

TABLE OF CONTENTS

LIST OF FIGURES

LIST OF TABLES

LIST OF SYMBOLS

0	Ground mode
1	Aerial mode
$\alpha_0(\omega)$	Ground mode attenuation
$\alpha_1(\omega)$	Aerial mode attenuation
$\beta_0(\omega)$	Ground mode phase shift
$\beta_1(\omega)$	Aerial mode phase shift
$C_0(\omega)$	Ground line capacitance [F/km]
$C_1(\omega)$	Aerial line capacitance [F/km]
$C_{\mathrm{p}}(\omega)$	Self line capacitance [F/km]
$C_{\mathrm{m}}(\omega)$	Mutual line capacitance [F/km]
d	Fault distance
$\tilde{d}$	Fault distance estimation of method
$d_{\mathrm{ClassicalSETWFL}}$	d estimation by the Classical SETWFL method
$d_{\mathrm{ModalSETWFL}}$	d estimation by the Modal SETWFL method
$d_{\mathrm{SettingsFreeSETWFL}}$	d estimation by the SettingsFree SETWFL method
$d_{\mathrm{EnhancedSETWFL}}$	d estimation by the Enhanced SETWFL method
$d_{\mathrm{ClassicalDETWFL}}$	d estimation by the Classical DETWFL method
$d_{\mathrm{ModalDETWFL}}$	d estimation by the Modal DETWFL method
$d_{\mathrm{SettingsFree1DETWFL}}$	d estimation by the SettingsFree1 DETWFL method
$d_{\mathrm{SettingsFree2DETWFL}}$	d estimation by the SettingsFree2 DETWFL method
$d_{\mathrm{SyncFreeDETWFL}}$	d estimation by the SyncFree DETWFL method
$d_{\mathrm{SyncFreSettingsFreeDETWFL}}$	d estimation by the SyncFreeSettingsFree DETWFL method
$d_{\mathrm{EnhancedDETWFL}}$	d estimation by the Enhanced DETWFL method
ε	Fault location error
$e_0(x,t,\omega)$	Ground mode voltage signal
$e_1(x,t,\omega)$	Aerial mode voltage signal
$e_-(x,t,\omega)$	Voltage signal at negative pole
$e_+(x,t,\omega)$	Voltage signal at positive pole
$E_0(x,\omega)$	Ground mode voltage signal in frequency domain
$E_1(x,\omega)$	Aerial mode voltage signal in frequency domain
$E_{backward}(x,\omega)$	Backward TW voltage in frequency domain
$E_{forward}(x,\omega)$	Forward TW voltage in frequency domain
$E_{backward}(x,\omega)$	Backward TW voltage in frequency domain
$E_{forward}(x,\omega)$	Forward TW voltage in frequency domain
f_{S}	Sampling frequency
$G_0(\omega)$	Ground line conductance [Ω/km]
$G_1(\omega)$	Aerial line conductance [Ω/km]
$G_{\mathrm{p}}(\omega)$	Self line conductance [Ω/km]
$G_{\mathrm{m}}(\omega)$	Mutual line conductance [Ω/km]

$i_0(x,t,\omega)$	Ground mode current signal
$i_1(x,t,\omega)$	Aerial mode current signal
$i_-(x,t,\omega)$	Current signal at negative pole
$i_+(x,t,\omega)$	Current signal at positive pole
$I_0(x,\omega)$	Ground mode voltage signal in frequency domain
$I_1(x,\omega)$	Aerial mode voltage signal in frequency domain
$I_{backward}(x,\omega)$	Backward TW current in frequency domain
$I_{forward}(x,\omega)$	Forward TW current in frequency domain
$I_{backward}(x,\omega)$	Backward TW current in frequency domain
$I_{forward}(x,\omega)$	Forward TW current in frequency domain
$L_0(\omega)$	Ground line inductance [H/km]
$L_1(\omega)$	Aerial line inductance [H/km]
$L_\mathrm{p}(\omega)$	Self line inductance [H/km]
$L_\mathrm{m}(\omega)$	Mutual line inductance [H/km]
$i^{(+)}_\mathrm{Recti}$	Positive pole current signal at rectifier station
$i^{(-)}_\mathrm{Inver}$	Negative pole current signal at inverter station
$i^{(1)}_\mathrm{Recti}$	Aerial mode current signal at rectifier station
$i^{(1)}_\mathrm{Inver}$	Aerial mode current signal at inverter station
$i^{(1,\mathrm{TW})}_\mathrm{Recti}$	Aerial pole TW current signal at rectifier station
$i^{(1,\mathrm{TW})}_\mathrm{Inver}$	Aerial pole TW current signal at inverter station
κ	Data synchronization misalignment
ℓ	Transmission line length
$R_0(\omega)$	Ground line resistance [Ω/km]
$R_1(\omega)$	Aerial line resistance [Ω/km]
$R_\mathrm{p}(\omega)$	Self line resistance [Ω/km]
$R_\mathrm{m}(\omega)$	Mutual line resistance [Ω/km]
R_Fault	Fault resistance [Ω]
$\boldsymbol{T}$	Karrenbauer transformation
$t^{(0)}$	Dependence of ground mode incident TW arrival instant
$k^{(1)}_\mathrm{Incid}$	Aerial mode incident TW arrival sample
$k^{(1)}_\mathrm{Incid}$	Aerial mode refracted TW arrival sample
$k^{(1)}_\mathrm{Recti,Incid}$	Aerial mode incident TW arrival sample at rectifier station
$k^{(1)}_\mathrm{Inver,Incid}$	Aerial mode incident TW arrival sample at inverter station
$k^{(1)}_\mathrm{Recti,Refra}$	Aerial mode refracted TW arrival sample at rectifier station
$k^{(1)}_\mathrm{Inver,Refra}$	Aerial mode refracted TW arrival sample at inverter station
$t^{(0)}_\mathrm{Recti,Incid}$	Ground mode incident TW arrival instant at rectifier station [s]
$t^{(1)}_\mathrm{Recti,Incid}$	Aerial mode incident TW arrival instant at rectifier station [s]
$t^{(0)}_\mathrm{Recti,Refle}$	Ground mode reflected TW arrival instant at rectifier station [s]
$t^{(1)}_\mathrm{Recti,Refle}$	Aerial mode reflected TW arrival instant at rectifier station [s]
$t^{(0)}_\mathrm{Recti,Refra}$	Ground mode refracted TW arrival instant at rectifier station [s]
$t^{(1)}_\mathrm{Recti,Refra}$	Aerial mode refracted TW arrival instant at rectifier station [s]
$t^{(0)}_\mathrm{Inver,Incid}$	Ground mode incident TW arrival instant at inverter station [s]
$t^{(1)}_\mathrm{Inver,Incid}$	Aerial mode incident TW arrival instant at inverter station [s]
$t^{(0)}_\mathrm{Inver,Refle}$	Ground mode reflected TW arrival instant at inverter station [s]
$t^{(1)}_\mathrm{Inver,Refle}$	Aerial mode reflected TW arrival instant at inverter station [s]

$t^{(0)}_{\text{Inver,Refra}}$	Ground mode refracted TW arrival instant at inverter station [s]
$t^{(1)}_{\text{Inver,Refra}}$	Aerial mode refracted TW arrival instant at inverter station [s]
$t^{(0*)}_{\text{Inver,Incid}}$	$t^{(0)}_{\text{Inver,Incid}} + \kappa$ misaligment [s]
$t^{(1*)}_{\text{Inver,Incid}}$	$t^{(1)}_{\text{Inver,Incid}} + \kappa$ misaligment [s]
$t^{(0*)}_{\text{Inver,Refle}}$	$t^{(0)}_{\text{Inver,Refle}} + \kappa$ misaligment [s]
$t^{(1*)}_{\text{Inver,Refle}}$	$t^{(1)}_{\text{Inver,Refra}} + \kappa$ misaligment [s]
$t^{(0*)}_{\text{Inver,Refra}}$	$t^{(0)}_{\text{Inver,Refra}} + \kappa$ misaligment [s]
$t^{(1*)}_{\text{Inver,Refra}}$	$t^{(1)}_{\text{Inver,Refra}} + \kappa$ misaligment [s]
t_{Refle}	Dependence of reflected TW arrival instant
v_{p}	TW propagation velocity [km/s]
$v^{(0)}_{\text{p}}$	Ground mode TW propagation velocity [km/s]
$v^{(1)}_{\text{p}}$	Aerial mode TW propagation velocity [km/s]
$v^{(0')}_{\text{p}}$	Ground mode lossless TW propagation velocity [km/s]
$v^{(1')}_{\text{p}}$	Aerial mode lossless TW propagation velocity [km/s]
$\gamma_0(\omega)$	Ground mode propagation coefficient
$\gamma_1(\omega)$	Aerial mode propagation coefficient
$Z^{(0)}_{\text{C}}$	Ground mode characteristic impedance [Ω]
$Z^{(1)}_{\text{C}}$	Aerial mode characteristic impedance [Ω]
$Z^{(0)}_{\text{Surge}}$	Ground mode surge impedance [Ω]
$Z^{(1)}_{\text{Surge}}$	Aerial mode surge impedance [Ω]
$\Upsilon_{\text{Fault,Refle}}$	Reflection coefficient at fault point
$\Upsilon_{\text{Fault,Refra}}$	Refraction coefficient at fault point
ρ	Soil resistivity

GLOSSARY

AC	Alternating Current
ATP	Alternative Transients Program
DC	Direct Current
DETWFL	Double-Ended TWFL
HVAC	High-Voltage Alternating Current
HVDC	High-Voltage Direct Current
LCC	Line Commutated Converter
MMC	Modular Multi-Level Converter
PhD	Doctor of Philosophy
PG	Pole-to-Ground
PP	Pole-to-Pole
SETWFL	Single-Ended TWFL
SNR	Signal-to-Noise Ratio
TW	Traveling Wave
TWFL	Traveling Wave-Based Fault Location
VSC	Voltage Source Converter

CHAPTER 1

INTRODUCTION

1.1 BACKGROUND

Electricity plays a crucial role in today's world. A wide variety of devices and instruments, including industrial motors, street lights, household appliances, medical equipment, and computers, depend on electrical energy. A reliable and uninterrupted power supply is a fundamental requirement for maintaining social stability and well-being. Consequently, the development of robust and dependable power systems has become vital for modern societies.

Essentially, a power system is divided into three basic parts: generation, transmission, and distribution. Among them, transmission is of particular interest due to its role in facilitating the flow of electricity from main generation plants to distribution and consumption. Therefore, reliable transmission lines are of utmost importance to robust and reliable power systems.

A transmission line may operate in either alternating current (AC) or direct current (DC). When operating at high voltage levels, these lines are designated as high-voltage AC (HVAC) or high-voltage DC (HVDC) lines, respectively. Today, HVDC lines are key to modern power systems initiatives (Hitachi Energy, 2023). These lines are highly efficient for bulk power transmission over very long distances (ALASSI *et al.*, 2019), renewable energy sources interconnection (Hitachi Energy, 2023) etc. Table 1.1 illustrates some examples of HVDC lines. As can be seen, growing economies and large land masses like Brazil, China and India have long-length bulk-power HVDC systems in place. However, due to their long lengths, these lines are subject to hard-geographical and environmental conditions. Consequently, HVDC lines are highly susceptible to faults (WU *et al.*, 2021), which can result in power supply interruptions.

In order to overcome these challenges, solutions to locate faults in HVDC lines are of great interest. Also, in several countries, among them Brazil, the revenue of transmission grid companies are based on the amount of time the assets availability, rather than the amount of energy are transmitted by them (HOFF *et al.*, 2021). Financial penalties are applied when the

transmission line is unexpectedly taken out of service, such as due to a permanent fault (HOFF *et al.*, 2021). Therefore, fault locating schemes are an important tool to provide a starting point for maintenance crews during the inspection of faulted lines. As a consequence, the repairing times can be reduced, and the transmission lines are returned to electrical power system as quickly as possible, avoiding financial penalties and power supply interruptions.

Faults on HVDC lines can be classified into pole-to-pole (PP) and pole-to-ground (PG). In general, PG faults are more likely and critical than PP faults (WU *et al.*, 2021; TüNNERHOFF *et al.*, 2018; HALEEM; RAJAPAKSE, 2019). Indeed, whenever small current PG faults take place, the HVDC converter station is not isolated, and the line can continue on service, damaging the system (WU *et al.*, 2021). Therefore, among two types of faults on HVDC systems, accurate PG fault location is of greater importance to provide fast line repair (WU *et al.*, 2021).

Table 1.1: Examples of HVDC transmission lines.

Project Name	**Country**	**Comissioning Year**	**Voltage [kV]**	**Power [MW]**	**Length [km]**
Xiangjiaba – Shanghai	China	2010	±800	7200	1980
Nuozhadu – Guangdong	China	2013	±800	5000	1451
Jinping – Sunan	China	2013	±800	7200	2090
Rio Madeira*	Brazil	2014	±600	6300	2450
Xiluodu – Guangdong*	China	2014	±500	6400	1286
Xiluodu – Zhejiang	China	2014	±1100	8000	1680
Zhundong – Sichuan	China	2016	±1100	10000	2600
Champa – Kurukshetra	India	2016	±800	3000	1365
Belo Monte*	Brazil	2017/2019	±800	8000	2076/2543
Raigarh – Pugalur	India	2019	±800	6000	1830
Changji – Guquan	China	2019	±1100	12000	3324

* Two bipoles.

Source: Own Authorship.

1.2 PROBLEM STATEMENT

Nowadays, TW-based fault location methods (TWFL) represent the most accurate solution for HVDC lines (LAN *et al.*, 2019). These methods provide a fault location accuracy in the order of hundreds of meters (SCHWEITZER *et al.*, 2013), with few or even no user-defined settings (SEL INC., 2022). Basically, a TWFL method is a formulation for estimating the real fault distance using TW arrival instants at the line ends. Nevertheless, despite the advantages of TWFL principles, the existing TWFL methods have drawbacks that may result in erroneous fault location when applied in HVDC systems.

The initial limitation of TWFL methods when applied to HVDC systems is the dependence of ground mode quantities (FERNANDES *et al.*, 2020). Typically, the TW phenomenon in multi-pole systems is analyzed in the modal domain, resulting in the calculation of aerial-mode and ground-mode quantities. Some TWFL methods are based on ground mode TWs, as exemplified by the approaches proposed by Liu *et al.* (2012) and Lopes (2016). Nevertheless, ground-mode TWs are significantly attenuated in HVDC lines due to their long lengths (WEI *et al.*, 2023; LIU *et al.*, 2023), which can result in the inability to detect TW arrival instants, and, consequently, the unfeasibility of TWFL methods. Accordingly, aerial-mode TWFL methods are preferred to applications on HVDC systems (FERNANDES *et al.*, 2020).

Among the TWFL methods that uses only aerial-mode TWs, two drawbacks are commonly reported: TW propagation velocity setting dependence (FAYAZI *et al.*, 2023; ZHANG *et al.*, 2019; HUAI *et al.*, 2020; DARDENGO *et al.*, 2021; HUAI *et al.*, 2021) and data synchronization requirement (CHEN *et al.*, 2022; WANG *et al.*, 2021; FERNANDES *et al.*, 2020). TW propagation velocity is affected by the frequency-dependence of line electrical parameters, making it difficult to calculate a certain TW propagation velocity value to set the TWFL method. On the other hand, data synchronization are supported by several solutions, such as global positioning system (LOPES *et al.*, 2015; MONTEIRO *et al.*, 2022). However, these solutions can fail (LOPES *et al.*, 2015; MONTEIRO *et al.*, 2022). Thus, efforts have been made to develop TWFL methods free of TW propagation velocity setting and data synchronization.

Recently, TW propagation velocity setting- and data synchronization-free methods have been proposed (SCHWEITZER *et al.*, 2016; LOPES *et al.*, 2018; HUAI *et al.*, 2020; ZHU *et al.*, 2022). These methods seem promising for fault location on HVDC lines (ZHU *et al.*, 2022). The drawback of these existing TW propagation velocity setting- and data synchronization-

free methods is the need to detect the TWs reflected from the fault point (HUAI *et al.*, 2020; ZHU *et al.*, 2022). False detections of these reflections result in significant fault location errors (FERNANDES *et al.*, 2020; ZHANG *et al.*, 2019; VIEIRA *et al.*, 2023). The challenge of detecting reflected TWs in HVDC lines is more prominent in PG faults (FERNANDES *et al.*, 2020), due to confusion with refracted TWs and aerial-mode TWs generated by the mixing mode phenomenon (LIN *et al.*, 2021; DE MAGALHÃES JR.; LOPES, 2021b). Therefore, power utilities have demonstrated great interest in the development of reliable and accurate TWFL methods capable of overcoming practical issues on detecting reflected TWs that usually arise in this critical and likely type of fault.

1.3 OBJECTIVE

To propose a TW propagation velocity setting- and data synchronization-free TWFL method using only aerial mode quantities to deal with PG faults on HVDC lines without the use of reflected TWs. To achieve this objective, sub-goals are pursued as follows.

- To identify drawbacks of the state-of-the-art TWFL methods;
- To investigate the TW phenomenon on HVDC lines;
- To compare the proposed method to the state-of-the-art methods.

1.4 CONTRIBUTION

This PhD thesis introduces a TWFL method for HVDC lines that addresses drawbacks of existing TWFL methods. Specifically, proposed method eliminates the dependence on ground mode quantities, TW propagation velocity settings, data synchronization, and reflected TWs, which have been identified as significant challenges in the state-of-the-art TWFL methods.

1.5 SCOPE AND LIMITATIONS

The proposed method is developed to deal with PG faults on HVDC lines. Therefore, PP faults are outside the scope of this thesis. Existing solutions, such as the one presented in Zhu *et al.* (2022), can be used for this type of fault, since reflected TWs are easy to detect in PP

faults (FERNANDES *et al.*, 2020). Furthermore, the proposed method has not been tested on non-homogeneous systems, which are lines composed of overhead, underground and submarine cables. Finally, the proposed method was conceived for point-to-point HVDC systems. Therefore, multi-terminal HVDC systems are outside the scope of this thesis.

1.6 OUTLINE

The rest of this thesis is organized as follows.

- Chapter 2 elucidates the fundamental concepts and mathematical principles that form the basis of TWs;
- Chapter 3 presents a historical overview of TWFL methods, emphasizing the limitations of these techniques;
- Chapter 4 proposes an innovative TW propagation velocity setting- and data synchronization-free TWFL method to deal with PG faults on HVDC lines;
- Chapter 5 evaluates the proposed method's performance and compares the proposed method to the state-of-the-art TWFL methods;
- Chapter 6 exposes the conclusions and future directions;
- Appendix A presents a list of scientific publications.

CHAPTER 2

FUNDAMENTALS

First studies on TWs date back to the early 20th century (STEINMETZ, 1908; STEINMETZ, 1909; CARSON, 1919; CARSON, 1925; CARSON, 1928). Today, there are several books about this content (GREENWOOD, 1991; IZYKOWSKI, 2008; PHADKE; THORP, 2009; SAHA *et al.*, 2010; FERRER; SCHWEITZER, 2010; GLOVER *et al.*, 2015; DONG, 2022). Therefore, this field is already extensively supported from literature. In this way, this chapter restricts to perform a brief overview of these fundamentals.

2.1 BASIC CONCEPTS

Figure 2.1 shows a fault on a monopolar HVDC line. After the fault takes place, electromagnetic transients are launched towards the rectifier and inverter stations. These transients are known as traveling waves (TWs). The velocity of a TW, depicted here as v_{p} [km/s], depends on the line electrical parameters: resistance, inductance, conductance, and capacitance, which are a function of frequency, tower geometry, and soil resistivity (SAHA *et al.*, 2010). The amplitude and polarity of a TW depend on the fault conditions: fault resistance R_{Fault} [Ω] and pre-fault voltage at fault point (DE MAGALHÃES JR.; LOPES, 2021a). Moreover, the TWs are reflected and refracted at line discontinuities, which are points where the electrical parameters abruptly change, such as at the line terminations and the fault point. Finally, the TWs attenuate as they propagate throughout the line, and reflect and refract at the line discontinuities until they are completely attenuated (AURANGZEB *et al.*, 2000).

Figure 2.1: Fault on a monopolar HVDC line.

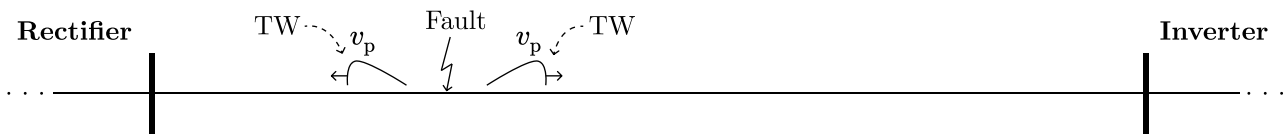

Source: Own Authorship.

In monopolar HVDC systems, TWs propagate at a single v_p. However, in multi-pole systems, for example, bipolar HVDC lines, the conductors are generally mutually coupled, thus, different v_p exist (MAGNAGO; ABUR, 1998). Therefore, to analyze TWs in multi-pole lines, pole domain signals are decoupled into modal components (MAGNAGO; ABUR, 1998). For this purpose, modal transformations are used, among which the most popular are Clarke and Karrenbauer transforms (FARIA; BRICENO, 1997). Figure 2.2 shows TWs in the modal domain soon after a fault takes place on a bipolar HVDC line. Two modal TWs are obtained, namely, ground '0' and aerial '1' modes. In general, ground-mode TWs are less advantageous than aerial-mode TWs. Ground-mode TWs attenuate more than aerial-mode ones during the propagation throughout the line (WEI *et al.*, 2023; LIU *et al.*, 2023). Another challenge of analyzing ground-mode TWs is dispersion. Due to line electrical parameters being frequency-dependent (MARTI *et al.*, 1993), different frequency components have different attenuation values, which distorts the wavefronts and lengthens the fall or rise time of TWs. Therefore, it is difficult to accurately determine the arrival instants of ground-mode TWs (LIU *et al.*, 2023). Moreover, ground-mode TW propagation velocity $v_p^{(0)}$ is more affected by uncertainties in line electrical parameters and frequency dependence than aerial-mode TW propagation velocity $v_p^{(1)}$ (RIBEIRO *et al.*, 2022). In short, the attenuation and dispersion effect of ground-mode TWs, and high uncertainty in $v_p^{(0)}$ decrease the accuracy and reliability of TWFL methods that use these mode quantities (FERNANDES *et al.*, 2020). As a consequence, most TWFL methods use aerial-mode TWs instead of ground mode ones (FERNANDES *et al.*, 2020).

Although TWs offer advantages in aerial mode, they also present certain challenges. The aerial-mode TW propagation velocity $v_p^{(1)}$ also changes with the frequency-dependent characteristics of line electrical parameters, which makes it difficult to accurately calculate $v_p^{(1)}$ (RIBEIRO *et al.*, 2022; ZHU *et al.*, 2022). Experts have discussed and tried to solve the problem of determining $v_p^{(1)}$ accurately, but there is still no solution (RIBEIRO *et al.*, 2022). In AC sys-

Figure 2.2: Fault on a bipolar HVDC line.

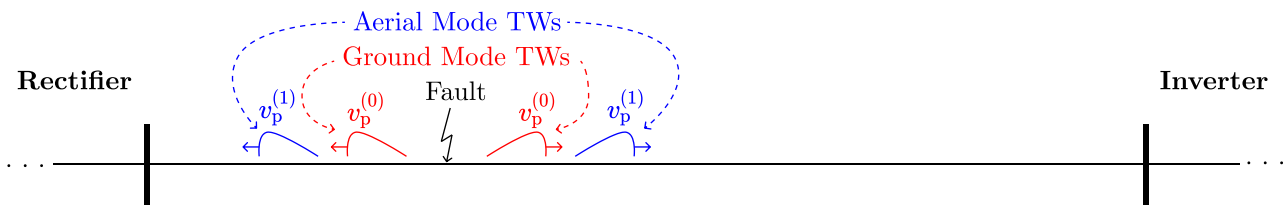

Source: Own Authorship.

tems, an energization test is recommended (KASZTENNY *et al.*, 2016). However, no analogous considerations are available for DC systems. In TWFL methods, $v_{\mathrm{p}}^{(1)}$ is often an user-predefined setting. In consequence of the aforementioned uncertainties in $v_{\mathrm{p}}^{(1)}$, this can lead to fault location errors (KASZTENNY *et al.*, 2016). Consequently, v_{p} setting-free methods have been considered promising TWFL solutions (LOPES *et al.*, 2021; ZHU *et al.*, 2022).

Regarding the line discontinuity points, two are more important: the line terminations and the fault point. The first TWs that arrive at the line terminations are known as incident TWs. In general, after an incident TW reaches a line termination, a TW travels back to the fault point and travels back to line discontinuity. This TW that travels back to the same line discontinuity is typically called reflected TW. Whereas, an incident TW that reaches a line termination travels back to the fault point, and passes through the opposite line termination is commonly called refracted TW. Incident, reflected, and refracted TWs are the most important TWs used in TWFL methods (LOPES *et al.*, 2021).

After arriving at a discontinuity, a TW can change in amplitude and polarity. The relationship of amplitude and polarity between a reflected or refracted TW before and after a discontinuity is given by the difference between the line electrical parameters upstream and downstream of this discontinuity point (SAHA *et al.*, 2010). This relationship is accounted by the reflection and refraction coefficients. Due to these variations in amplitude and polarity, the detection of each TW has particular challenges.

Incident TWs are the first and the highest energy electromagnetic transients in the signals (DONG, 2022). Of all the TWs that arrive at a line terminal, incident TWs are the easiest to detect (DONG, 2022). On the other hand, detecting reflected and refracted TWs is not always an easy task (ZHU *et al.*, 2022). Especially in PG faults on HVDC systems, the detection of reflected TWs has been shown to be a difficult task (FERNANDES *et al.*, 2020; VIEIRA *et al.*, 2023). In PG faults, a phenomenon called as mixing mode generates aerial-mode TWs from ground-mode TWs, and vice-versa (LIN *et al.*, 2021; DE MAGALHÃES JR.; LOPES, 2021b). Thus, TWs from the mixing mode phenomenon can appear around reflected and refracted TWs. As a result, false detections of reflected or refracted TWs can occur, leading to fault location errors (FERNANDES *et al.*, 2020; VIEIRA *et al.*, 2023). Therefore, procedures to correctly detect reflected and refracted TWs have been considered as a trend (LOPES *et al.*, 2021), especially for PG faults on HVDC systems (FERNANDES *et al.*, 2020).

Another challenge of TWFL methods is data synchronization (LOPES *et al.*, 2015; MONTEIRO *et al.*, 2022). Double-ended TWFL (DETWFL) solutions have been considered more reliable than single-ended TWFL (SETWFL) techniques (MONTEIRO *et al.*, 2022). However, two-terminal measurements are taken from distant stations, therefore, data must be aligned (LOPES *et al.*, 2015; MONTEIRO *et al.*, 2022). In several DETWFL solutions, the rectifier and inverter data synchronization is mandatory, otherwise can lead to fault location errors (SAHA *et al.*, 2010; MONTEIRO *et al.*, 2022). Various data synchronization solutions are available in real-world applications, such as real-time clocks, precise time protocol, network time protocol, inter-range instrumentation group time codes, and global positioning systems (MONTEIRO *et al.*, 2022). Although data synchronization solutions are available in the market, these solutions can maloperate. Therefore, data synchronization-free methods have been considered as promising TWFL solutions (HUAI *et al.*, 2020; ZHU *et al.*, 2022).

Aiming to facilitate the comprehension and visualization of TWs, Bewley (1931) propose a time-space graphical representation of the TW propagation paths throughout a transmission line. Figure 2.3 presents an example of this chart for a fault on a bipolar HVDC line. The diagram is formed by orthogonal axes, being the horizontal and vertical axes related to the space and time representations, respectively. Also, in this example, the red dashed and blue continuous lines represent the ground '0' and aerial '1' mode TWs, respectively. The slopes

Figure 2.3: Lattice diagram for a fault on a bipolar HVDC line.

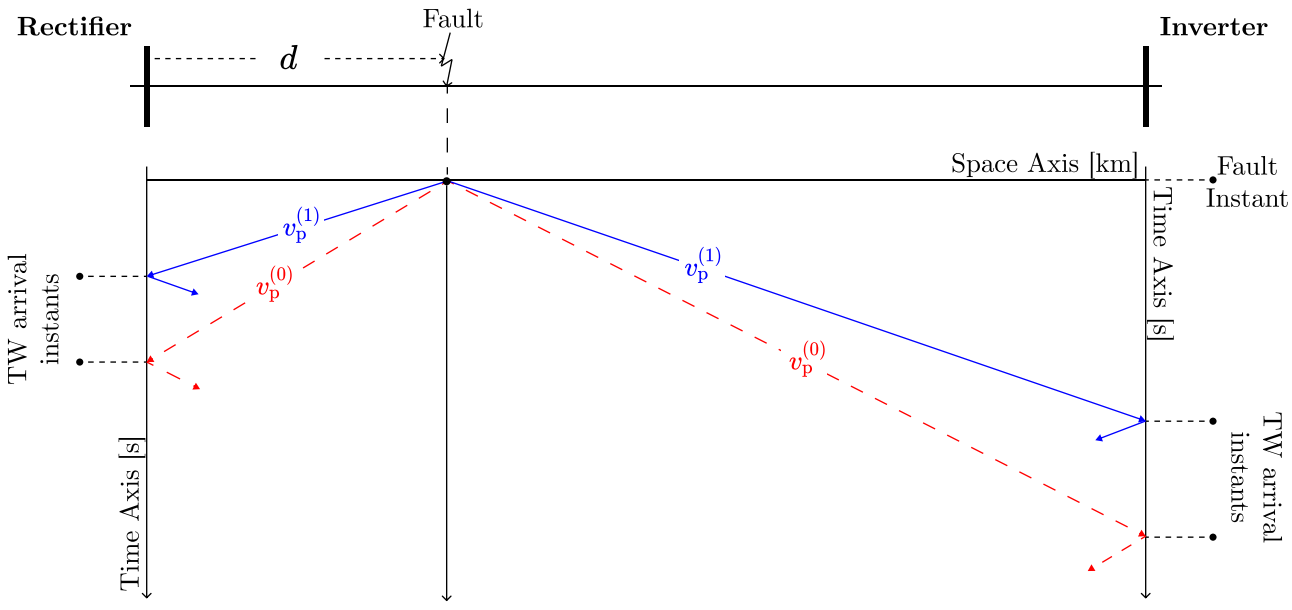

Source: Own Authorship.

of each lattice are proportional to each modal v_{p}. Based on the patterns created by TWs in the Bewley diagrams, and considering trigonometric identities, TWFL methods are created to estimate the fault distance d. Since this graphic looks like a lattice, it is also known as Bewley's lattice diagram or lattice diagram (DATTA; CHATTERJEE, 2012).

Figure 2.4 shows a lattice diagram for a fault on a bipolar HVDC line highlighting these eight main TW arrival instants. Subscripts 'Recti' and 'Inver' stand for the rectifier and inverter stations, 'Incid', 'Refle' and 'Refra' stand for the incident, reflected and refracted TWs, and superscripts '0' and '1' represent ground and aerial modes. Also, $v_{\mathrm{p}}^{(0)}$ and $v_{\mathrm{p}}^{(1)}$ represent ground and aerial mode v_{p}, respectively. Finally, '*' denotes $t_{\mathrm{Inver}}^{(*)} = t_{\mathrm{Inver}} + \kappa$, being κ the data synchronization misalignment at the inverter station ($\kappa = 0$ if synchronized data are considered). Therefore, considering a fault distance d and a transmission line length ℓ, each arrival instant at both line ends can be derived as:

Figure 2.4: Main TW arrival instants used in TWFL methods.

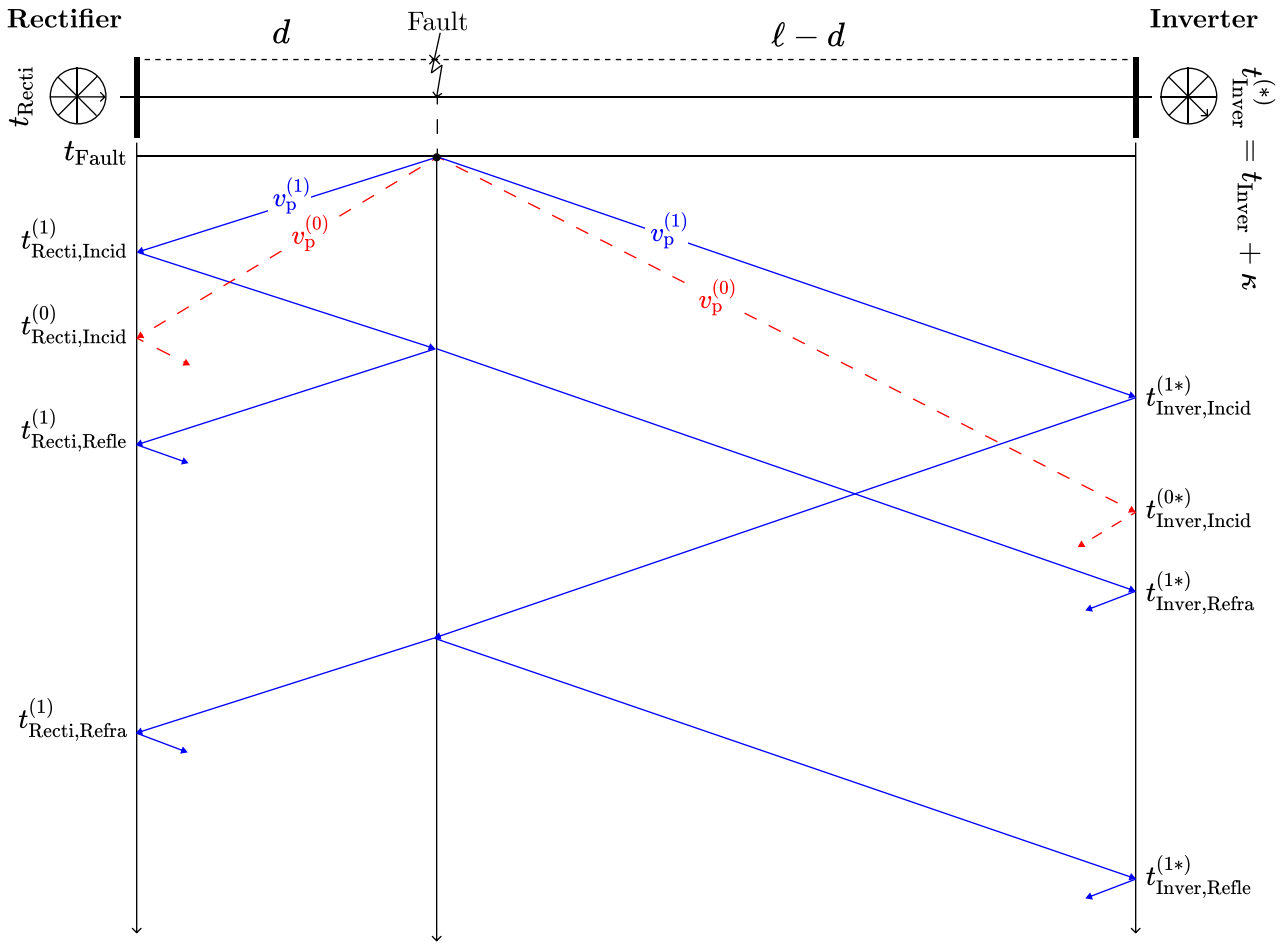

Source: Own Authorship.

$$t^{(1)}_{\text{Recti,Incid}} = t_{\text{Fault}} + \frac{d}{v^{(1)}_{\text{p}}} \ , \tag{2.1}$$

$$t^{(0)}_{\text{Recti,Incid}} = t_{\text{Fault}} + \frac{d}{v^{(0)}_{\text{p}}} \ , \tag{2.2}$$

$$t^{(1)}_{\text{Recti,Refle}} = t_{\text{Fault}} + \frac{3 \cdot d}{v^{(1)}_{\text{p}}} \ , \tag{2.3}$$

$$t^{(1)}_{\text{Recti,Refra}} = t_{\text{Fault}} + \frac{\ell - d}{v^{(1)}_{\text{p}}} + \frac{\ell}{v^{(1)}_{\text{p}}} \ , \tag{2.4}$$

$$t^{(1*)}_{\text{Inver,Incid}} = t_{\text{Fault}} + \frac{\ell - d}{v^{(1)}_{\text{p}}} \ , \tag{2.5}$$

$$t^{(0*)}_{\text{Inver,Incid}} = t_{\text{Fault}} + \frac{\ell - d}{v^{(0)}_{\text{p}}} \ , \tag{2.6}$$

$$t^{(1*)}_{\text{Inver,Refra}} = t_{\text{Fault}} + \frac{d}{v^{(1)}_{\text{p}}} + \frac{\ell}{v^{(1)}_{\text{p}}} \ , \tag{2.7}$$

$$t^{(1*)}_{\text{Inver,Refle}} = t_{\text{Fault}} + \frac{3 \cdot (\ell - d)}{v^{(1)}_{\text{p}}} \ . \tag{2.8}$$

Based on these TW arrival instants, TWFL methods are developed. In the Chapter 3, a literature review of TWFL methods is presented using these eight TW arrival instants. In the next Section, a review of mathematical principles of TWs is presented. The goal is highlight these TW arrival instants are affected by the line electrical parameters.

2.2 MATHEMATICAL PRINCIPLES

Fig. 2.5 shows an incremental section of a line model Δx long of a bipolar HVDC system. By applying Kirchhoff's voltage and current laws (KVL and KCL, respectively), when $\Delta x \to 0$, it is obtained that:

$$-\frac{\partial}{\partial x}\begin{bmatrix} e_+(x,t,\omega) \\ e_-(x,t,\omega) \end{bmatrix} = \begin{bmatrix} R_{\text{p}}(\omega) & R_{\text{m}}(\omega) \\ R_{\text{m}}(\omega) & R_{\text{p}}(\omega) \end{bmatrix} \cdot \begin{bmatrix} i_+(x,t,\omega) \\ i_-(x,t,\omega) \end{bmatrix} + \begin{bmatrix} L_{\text{p}}(\omega) & L_{\text{m}}(\omega) \\ L_{\text{m}}(\omega) & L_{\text{p}}(\omega) \end{bmatrix} \cdot \frac{\partial}{\partial t}\begin{bmatrix} i_+(x,t,\omega) \\ i_-(x,t,\omega) \end{bmatrix}, \tag{2.9}$$

$$-\frac{\partial}{\partial x}\begin{bmatrix} i_+(x,t,\omega) \\ i_-(x,t,\omega) \end{bmatrix} = \begin{bmatrix} G_{\text{p}}(\omega) & G_{\text{m}}(\omega) \\ G_{\text{m}}(\omega) & G_{\text{p}}(\omega) \end{bmatrix} \cdot \begin{bmatrix} e_+(x,t,\omega) \\ e_-(x,t,\omega) \end{bmatrix} + \begin{bmatrix} C'_{\text{p}}(\omega) & C_{\text{m}}(\omega) \\ C_{\text{m}}(\omega) & C'_{\text{p}}(\omega) \end{bmatrix} \cdot \frac{\partial}{\partial t}\begin{bmatrix} e_+(x,t,\omega) \\ e_-(x,t,\omega) \end{bmatrix}, \tag{2.10}$$

where e_+, e_-, i_+ and i_- are the voltages and current at positive and negative poles, respectively; $R_{\text{p}}(\omega)$ and $R_{\text{m}}(\omega)$ are the self and mutual line resistance, respectively; $L_{\text{p}}(\omega)$ and $L_m(\omega)$ are the self and mutual line inductances, respectively; $G_{\text{p}}(\omega)$ and $G_{\text{m}}(\omega)$ are the self and mutual line conductance, respectively; and $C'_{\text{p}}(\omega)$ and $C_{\text{m}}(\omega)$ are the self and mutual line capacitances,

respectively, being $C'_{\mathrm{p}}(\omega) = -C_{\mathrm{p}}(\omega) - C_{\mathrm{m}}(\omega)$. Furthermore, x, t and ω are the space, time and angular frequency representation, respectively, being $\omega = 2\pi f$ where f is frequency.

The Karrenbauer transformation $\boldsymbol{T}$ (DOMMEL, 1969; DOMMEL; MEYER, 1974) is used here to decouple the voltage and current pole signals expressed in (2.9) and (2.10) into their respective ground '0' and aerial '1' mode quantities using:

$$\begin{bmatrix} e_+(x,t,\omega) \\ e_-(x,t,\omega) \end{bmatrix} = \boldsymbol{T} \cdot \begin{bmatrix} e_0(x,t,\omega) \\ e_1(x,t,\omega) \end{bmatrix}, \tag{2.11}$$

$$\begin{bmatrix} i_+(x,t,\omega) \\ i_-(x,t,\omega) \end{bmatrix} = \boldsymbol{T} \cdot \begin{bmatrix} i_0(x,t,\omega) \\ i_1(x,t,\omega) \end{bmatrix}, \tag{2.12}$$

being:

$$\boldsymbol{T} = \frac{1}{\sqrt{2}} \begin{bmatrix} 1 & 1 \\ 1 & -1 \end{bmatrix}. \tag{2.13}$$

Thereby, applying (2.11), (2.12) and (2.13) in (2.9) and (2.10) yields:

$$-\frac{\partial}{\partial x} \begin{bmatrix} e_0(x,t,\omega) \\ e_1(x,t,\omega) \end{bmatrix} = \begin{bmatrix} R_0(\omega) & 0 \\ 0 & R_1(\omega) \end{bmatrix} \cdot \begin{bmatrix} i_0(x,t,\omega) \\ i_1(x,t,\omega) \end{bmatrix} + \begin{bmatrix} L_0(\omega) & 0 \\ 0 & L_1(\omega) \end{bmatrix} \cdot \frac{\partial}{\partial t} \begin{bmatrix} i_0(x,t,\omega) \\ i_1(x,t,\omega) \end{bmatrix}, \tag{2.14}$$

$$-\frac{\partial}{\partial x} \begin{bmatrix} i_0(x,t,\omega) \\ i_1(x,t,\omega) \end{bmatrix} = \begin{bmatrix} G_0(\omega) & 0 \\ 0 & G_1(\omega) \end{bmatrix} \cdot \begin{bmatrix} e_0(x,t,\omega) \\ e_1(x,t,\omega) \end{bmatrix} + \begin{bmatrix} C_0(\omega) & 0 \\ 0 & C_1(\omega) \end{bmatrix} \cdot \frac{\partial}{\partial t} \begin{bmatrix} e_0(x,t,\omega) \\ e_1(x,t,\omega) \end{bmatrix}, \tag{2.15}$$

Figure 2.5: Incremental section of a bipolar HVDC lossy line.

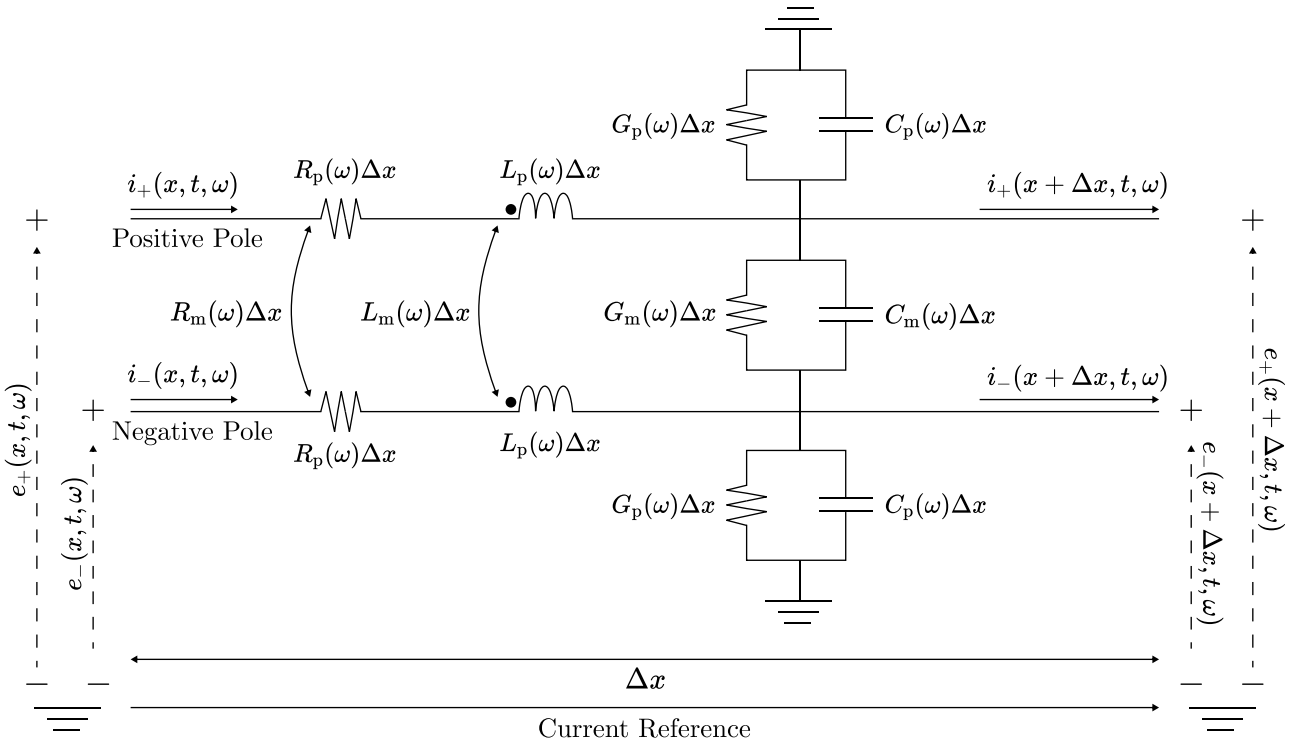

Source: Own Authorship.

being $R_0(\omega) = R_\mathrm{p}(\omega) + R_\mathrm{m}(\omega)$, $R_1(\omega) = R_\mathrm{p}(\omega) - R_\mathrm{m}(\omega)$, $L_0(\omega) = L_\mathrm{p}(\omega) + L_\mathrm{m}(\omega)$, $L_1(\omega) = L_\mathrm{p}(\omega) - L_\mathrm{m}(\omega)$, $G_0(\omega) = G_\mathrm{p}(\omega) + G_\mathrm{m}(\omega)$, $G_1(\omega) = G_\mathrm{p}(\omega) - G_\mathrm{m}(\omega)$, $C_0(\omega) = -C_\mathrm{p}(\omega)$ and $C_1(\omega) = -C_\mathrm{p}(\omega) - 2C_\mathrm{m}(\omega)$, where $R_0(\omega)$ and $R_1(\omega)$ are the ground and aerial mode line resistances, respectively. $L_0(\omega)$ and $L_1(\omega)$ are the ground and aerial mode line inductances, respectively. $G_0(\omega)$ and $G_1(\omega)$ are the ground and aerial mode line conductances, respectively. Finally, $C_0(\omega)$ and $C_1(\omega)$ are the ground and aerial mode line capacitances, respectively.

By applying the Fourier transform (FOURIER, 1822) to (2.14) and (2.15) yields:

$$-\frac{\partial}{\partial x}\begin{bmatrix}E_0(x,\omega)\\E_1(x,\omega)\end{bmatrix} = \begin{bmatrix}R_0(\omega)+j\omega L_0(\omega) & 0\\0 & R_1(\omega)+j\omega L_1(\omega)\end{bmatrix}\cdot\begin{bmatrix}I_0(x,\omega)\\I_1(x,\omega)\end{bmatrix}, \tag{2.16}$$

$$-\frac{\partial}{\partial x}\begin{bmatrix}I_0(x,\omega)\\I_1(x,\omega)\end{bmatrix} = \begin{bmatrix}G_0(\omega)+j\omega C_0(\omega) & 0\\0 & G_1(\omega)+j\omega C_1(\omega)\end{bmatrix}\cdot\begin{bmatrix}E_0(x,\omega)\\E_1(x,\omega)\end{bmatrix}. \tag{2.17}$$

By differentiating (2.16) and (2.17) with respect to x and appropriately substituting (2.16) and (2.17) in the obtained derivatives, one can find that (GLOVER *et al.*, 2015):

$$-\frac{\partial^2}{\partial x^2}\begin{bmatrix}E_0(x,\omega)\\E_1(x,\omega)\end{bmatrix} = \begin{bmatrix}\gamma_0(\omega) & 0\\0 & \gamma_1(\omega)\end{bmatrix}^2\cdot\begin{bmatrix}E_0(x,\omega)\\E_1(x,\omega)\end{bmatrix}, \tag{2.18}$$

$$-\frac{\partial^2}{\partial x^2}\begin{bmatrix}I_0(x,\omega)\\I_1(x,\omega)\end{bmatrix} = \begin{bmatrix}\gamma_0(\omega) & 0\\0 & \gamma_1(\omega)\end{bmatrix}^2\cdot\begin{bmatrix}I_0(x,\omega)\\I_1(x,\omega)\end{bmatrix}, \tag{2.19}$$

where $\gamma_0(\omega)$ and $\gamma_1(\omega)$ are the ground and aerial mode propagation coefficients, which are defined as functions of the line electrical parameters as:

$$\gamma_0(\omega) = \sqrt{[R_0(\omega)+j\omega L_0(\omega)]\cdot[G_0(\omega)+j\omega C_0(\omega)]}, \tag{2.20}$$

$$\gamma_1(\omega) = \sqrt{[R_1(\omega)+j\omega L_1(\omega)]\cdot[G_1(\omega)+j\omega C_1(\omega)]}. \tag{2.21}$$

The propagation coefficients are often formulated as follows:

$$\gamma_0(\omega) = \alpha_0(\omega) + j\beta_0(\omega), \tag{2.22}$$

$$\gamma_1(\omega) = \alpha_1(\omega) + j\beta_1(\omega), \tag{2.23}$$

being $\alpha_0(\omega)$ and $\alpha_1(\omega)$ the attenuation constants, and $\beta_0(\omega)$ and $\beta_1(\omega)$ the phase shift.

Still considering such characteristic parameters, ground and aerial mode TW propagation velocities $v_{\mathrm{p},0}$ and $v_{\mathrm{p},1}$ can be calculated as:

$$v_\mathrm{p}^{(0)}(\omega) = \frac{\omega}{\beta_0(\omega)}, \tag{2.24}$$

$$v_{\mathrm{p}}^{(1)}(\omega) = \frac{\omega}{\beta_1(\omega)}. \tag{2.25}$$

The solutions of (2.18) and (2.19) are reported in (GLOVER *et al.*, 2015) as:

$$E_0(x,\omega) = E_0^{forward}(\omega) \cdot \exp\left[-\gamma_0(\omega) \cdot x\right] + E_0^{backward}(\omega) \cdot \exp\left[\gamma_0(\omega) \cdot x\right], \tag{2.26}$$

$$E_1(x,\omega) = E_1^{forward}(\omega) \cdot \exp\left[-\gamma_1(\omega) \cdot x\right] + E_1^{backward}(\omega) \cdot \exp\left[\gamma_1(\omega) \cdot x\right], \tag{2.27}$$

$$I_0(x,\omega) = I_0^{forward}(\omega) \cdot \exp\left[-\gamma_0(\omega) \cdot x\right] + I_0^{backward}(\omega) \cdot \exp\left[\gamma_0(\omega) \cdot x\right], \tag{2.28}$$

$$I_1(x,\omega) = I_1^{forward}(\omega) \cdot \exp\left[-\gamma_1(\omega) \cdot x\right] + I_1^{backward}(\omega) \cdot \exp\left[\gamma_1(\omega) \cdot x\right], \tag{2.29}$$

where $E_0^{forward}$, $E_1^{forward}$, $E_0^{backward}$, $E_1^{backward}$, $I_0^{forward}$, $I_1^{forward}$, $I_0^{backward}$, $I_1^{backward}$ are the voltage and current forward and backward TW equations in ground and aerial mode domains, respectively.

Ground and aerial mode voltage and current signals are related between themselves by the ground and aerial line characteristic impedances $Z_{\mathrm{C}}^{(0)}(\omega)$ and $Z_{\mathrm{C}}^{(1)}(\omega)$. Thus, considering the Ohm's law, one can obtain:

$$Z_{\mathrm{C}}^{(0)}(\omega) = \frac{E_0^{forward}(\omega)}{I_0^{forward}(\omega)} = -\frac{E_0^{backward}(\omega)}{I_0^{backward}(\omega)} = \sqrt{\frac{R_0(\omega) + j\omega L_0(\omega)}{G_0(\omega) + j\omega C_0(\omega)}}, \tag{2.30}$$

$$Z_{\mathrm{C}}^{(1)}(\omega) = \frac{E_1^{forward}(\omega)}{I_1^{forward}(\omega)} = -\frac{E_1^{backward}(\omega)}{I_1^{backward}(\omega)} = \sqrt{\frac{R_1(\omega) + j\omega L_1(\omega)}{G_1(\omega) + j\omega C_1(\omega)}}. \tag{2.31}$$

When performing high-frequency ($\omega \to \infty$) studies, such as on fault-induced electromagnetic transients, $R_0 \ll L_0$, $G_0 \ll C_0$, $R_1 \ll L_1$, and $G_1 \ll C_1$. Therefore, ground and aerial characteristic impedances $Z_{\mathrm{C}}^{(0)}(\omega)$ and $Z_{\mathrm{C}}^{(1)}(\omega)$ can be approximated respectively by the ground and aerial surge impedances $Z_{\mathrm{Surge}}^{(0)}(\omega)$ and $Z_{\mathrm{Surge}}^{(1)}(\omega)$:

$$Z_{\mathrm{Surge}}^{(0)}(\omega) = \lim_{R_0 \to 0 \text{ and } G_0 \to 0} Z_{\mathrm{C}}^{(0)}(\omega) = \sqrt{\frac{L_0(\omega)}{C_0(\omega)}}, \tag{2.32}$$

$$Z_{\mathrm{Surge}}^{(1)}(\omega) = \lim_{R_1 \to 0 \text{ and } G_1 \to 0} Z_{\mathrm{C}}^{(1)}(\omega) = \sqrt{\frac{L_1(\omega)}{C_1(\omega)}}. \tag{2.33}$$

Analogously, the ground and aerial TW propagation velocities $v_{\mathrm{p}}^{(0)}(\omega)$ and $v_{\mathrm{p}}^{(1)}(\omega)$ can be approximated by the lossless ground and aerial $v_{\mathrm{p}}^{(1')}(\omega)$ and $v_{\mathrm{p}}^{(0')}(\omega)$ TW propagation velocities, which are calculated as:

$$v_{\mathrm{p}}^{(0')}(\omega) = \lim_{R_0 \to 0 \text{ and } G_0 \to 0} v_{\mathrm{p},0}(\omega) = \frac{1}{\sqrt{L_0(\omega) \cdot C_0(\omega)}}, \tag{2.34}$$

$$v_{\mathrm{p}}^{(1')}(\omega) = \lim_{R_1 \to 0 \text{ and } G_1 \to 0} v_{\mathrm{p},1}(\omega) = \frac{1}{\sqrt{L_1(\omega) \cdot C_1(\omega)}}. \tag{2.35}$$

To exemplify the behavior of the aforementioned variables, Figure 2.6 shows the ground and aerial mode line electrical parameters of the Rio Madeira HVDC system, (see Chapter 5) obtained by means the .lis file of JMarti model using the ATP software. Figure 2.6(a) shows that resistance increases with frequency, being the ground-mode resistance R_0 greater than the aerial-mode resistance R_1. This difference is due to the soil resistivity effect. As a consequence, the attenuation effect is more prominent in high frequencies than low frequencies (see Figure 2.6(e)). Also, ground-mode TWs attenuate more than aerial-mode TWs. By this reason, the majority of TWFL methods use aerial-mode TWs instead of ground-mode ones. From Figs. 2.6(c)and 2.6(d), the conductances and capacitances are practically constant in frequency. Moreover, Figure 2.6(b) shows that the aerial-mode inductance L_1 is also basically invariant in frequency. Nevertheless, the ground-mode inductance L_0 decreases as the frequency increases. This feature affects the characteristic and surge line impedances and TW propagation velocity. In this way, from Figure 2.6(i), the ground-mode surge impedance is greater than the aerial-mode one, reflecting the inductance curve. Finally, comparing Figs. 2.6(i) and 2.6(g), as observed that the surge impedance is almost the same the absolute value of characteristic impedance in high frequencies. Then, the approximation of these variables is acceptable for TW analysis, which is a high-frequency analysis. By comparing Figs. 2.6(f) and 2.6(j), the approximation of a lossless line is also acceptable for high frequencies. Moreover, the TW propagation velocity of ground-mode component change greatly with frequency. In contrast, the TW propagation velocity of aerial-mode component tends to be stable in the high frequency band. By this reason, aerial-mode TWs are preferred for TWFL methods.

Figure 2.6: Ground and aerial mode line electrical parameters of the Rio Madeira HVDC system obtained by means the .lis file of JMarti model using the ATP software.

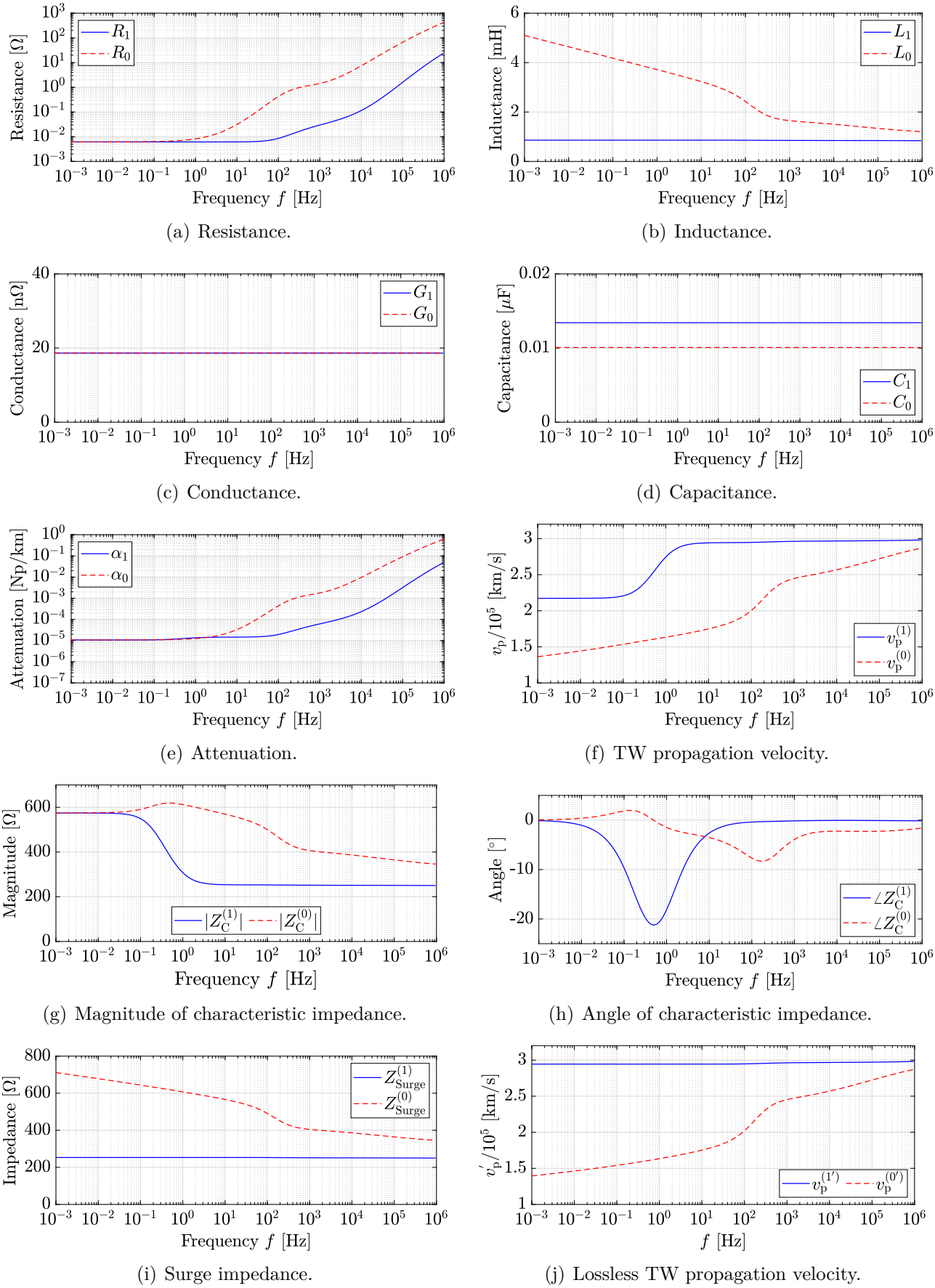

(a) Resistance.

(b) Inductance.

(c) Conductance.

(d) Capacitance.

(e) Attenuation.

(f) TW propagation velocity.

(g) Magnitude of characteristic impedance.

(h) Angle of characteristic impedance.

(i) Surge impedance.

(j) Lossless TW propagation velocity.

Source: Own Authorship.

CHAPTER 3

STATE OF THE ART

Earliest TWFL methods were reported between the 1920s and 1930s (CARSON, 1926; BEWLEY, 1929; KARAPETOFF, 1929; MCEACHRON *et al.*, 1930a; MCEACHRON *et al.*, 1930b; BEWLEY, 1931; ROHRIG, 1931; DOWELL, 1931; RORDEN, 1932; ALLEN; GROSS, 1935). Throughout these almost 100 years, several TWFL methods have been proposed. Next, a brief review of this history is presented.

During the 1940s, TWFL methods were widely adopted for use on de-energized underground cables (GALE *et al.*, 1993). In the late 1940s engineers who had worked on radar during World War II began to investigate whether pulse echo techniques could be used for fault location on overhead lines (CROSSLEY *et al.*, 1993). For many years, the inaccuracies of impedance and reactance-based approaches have been acknowledged, and the hunt for TWFL methods was widely reported during the 1950s (STEVENS; STRINGFIELD, 1948; HUGHES; WEINTRAUB, 1950; LEWIS, 1951; STRINGFIELD *et al.*, 1957). However, the costs associated with the installation, operation, and maintenance of the equipment used in TWFL methods were unbearable, thereby, limiting the applications of TWFL methods (GALE *et al.*, 1993).

In 1955, several studies on fault location for overhead lines and underground cables had already been published, among which TWFL solutions. Aiming to summarize these techniques, AIEE Committee Report (1955) published a review paper of the methods available to date. According to the authors, a total of 30 studies on TWFL methods, eight solutions based on fault-generated surges, and 22 approaches using pulse radar, had already been reported. The authors highlighted that the maximum fault location error of TWFL methods is equal to 1% of line length, whereas other solutions presented errors of up to 20% of line. Therefore, TWFL solutions already showed to be promising at that time (SNEDDOM; GALE, 1997).

Still in that decade, TWFL methods were classified according to operation mode (fault-generated TWs or pulse injection signals) and the number of monitored ends (single-ended SETWFL or double-ended DETWFL) (GALE *et al.*, 1993; CROSSLEY *et al.*, 1993). Initially,

the methods were divided in seven types using the letters of the alphabet, being: Types A and D those which do not include any pulse generating circuitry but rely on the fault-induced TWs (GALE *et al.*, 1993); Types B, C, F, and K are those which use a pulse, or a signal, injected onto the line or communication system (GALE *et al.*, 1993; CROSSLEY *et al.*, 1993; STRINGFIELD *et al.*, 1957); and Type E, which consists of methods that use transients produced by circuit breaker operations. Each type is defined next:

- Type A are SETWFL methods, which measure the time required for the fault-generated TW to travel from the end to the fault and back, i.e. reflected TWs (CROSSLEY *et al.*, 1993).
- Types B are DETWFL methods and have three subdivisions known as Types B1, B2, and B3. Type B1 used a radio timing pulse sent over a microwave channel, Type B2 used a power line carrier, and Type B3 used the injection of a DC pulse onto the line (GALE *et al.*, 1993; CROSSLEY *et al.*, 1993).
- Type C are SETWFL methods that operate using the radar principle. A pulse is applied to the line and the round tip back time for travel to the fault and back is measured (CROSSLEY *et al.*, 1993). The reflection of the injected pulse into the line by the unit itself is used to locate the fault (GALE *et al.*, 1993).
- Type D are DETWFL methods which detect the time arrival at each end of the line of the initial fault generated TW, i.e. the first incident TW at both line ends (CROSSLEY *et al.*, 1993).
- Type F is similar to Type C, except it uses repetitive pulse injections (STRINGFIELD *et al.*, 1957).
- Type K is a variation of Type F. The essential characteristic of Type K is the use of a beam switching tube, which is the use of a series of lamps to indicate distance, instead of a trace on a cathode-ray tube screen (STRINGFIELD *et al.*, 1957).
- Type E are SETWFL methods which use the transients created when a line is re-energized by closing a circuit breaker (SNEDDOM; GALE, 1997).

Solutions based on pulse injection, especially the Type B TWFL method, predominated until the 1980s (STRINGFIELD *et al.*, 1957; MARIHART; HAAGENSON, 1972). After that,

TWFL methods that do not use any pulse injection, i.e. Types A and D, predominated over the others (LOPES *et al.*, 2021). The predominance of Types A and D types is due to several factors, with the simplicity of the solutions that do not use pulse injection being a notable distinguishing feature (LOPES *et al.*, 2021).

Although all types of TWFL methods provided better accuracy than previously reported in the 1950s, their usefulness from the practical point of view were limited due to reliability and maintenance problems (SNEDDOM; GALE, 1997). Forty years later, in the 1990s, the TWFL methods are once more being applied to overhead lines (SNEDDOM; GALE, 1997). Two main factors explain the re-birth of the TWFL methods: the market demanded fast and accurate fault location on strategically important very long high voltage lines; and the re-examination of the behavior of TWs on power systems and, in particular, how TWs might be detected and used for fault location purposes led these methods to become more reliable (SNEDDOM; GALE, 1997). Finally, other important motivating factors to the reported spread of TWFL methods resulted from the new technical advances in high-speed data acquisition, data synchronization, and improvements in remote control and communication systems (SNEDDOM; GALE, 1997).

Few studies on TWFL methods have been published during the 1950-1990 historical gap. In the 1970s, Marihart & Haagenson (1972) presented an automatic electronic fault locator and its application to a large high-voltage power line grid power. This device has been equipped with a Type B method, which was applied to a 500 kV AC power line and an 800 kV DC system. The authors highlighted many operational difficulties, such as not recording information because of the line attenuation and low sensitivity of the coupling equipment. Despite these application challenges, the speed and accuracy of the TWFL method were pointed out, awakening the potential of using TWFL methods.

As mentioned earlier, Type B was the most used TWFL method for HVDC lines until the 1980s (STRINGFIELD *et al.*, 1957; MARIHART; HAAGENSON, 1972). This type is simple and accurate but requires a wide-band microwave channel, which was expensive (ANDO *et al.*, 1985b). Hence, in the next decade, some studies for new Type A methods began to be proposed. Among them, Ando *et al.* (1985a), Ando *et al.* (1985b) introduce a Type A TWFL method using three consecutive TW arrival instants (incident, reflected, and refracted TWs). The authors proposes to estimate the fault distance as follows. If $d \leq \ell/2$:

$$\tilde{d}_{\text{ClassicalSETWFL}}\ [\text{km}] = \frac{\left[t^{(1)}_{\text{Recti,Refle}} - t^{(1)}_{\text{Recti,Incid}}\right] \cdot v^{(1)}_{\text{p}}}{2}\ , \tag{3.1}$$

otherwise $d > \ell/2$:

$$\tilde{d}_{\text{ClassicalSETWFL}}\ [\text{km}] = \ell - \frac{\left[t^{(1)}_{\text{Recti,Refra}} - t^{(1)}_{\text{Recti,Incid}}\right] \cdot v^{(1)}_{\text{p}}}{2}\ , \tag{3.2}$$

where $t^{(1)}_{\text{Recti,Incid}}$ [s], $t^{(1)}_{\text{Recti,Refle}}$ [s], and $t^{(1)}_{\text{Recti,Refra}}$ [s] are the aerial mode incident, reflected, and refracted TWs arrival instants at the rectifier station. Also, $v^{(1)}_{\text{p}}$ [km/s] is the aerial mode TW propagation velocity. Among the required TW arrival instants, $t^{(1)}_{\text{Recti,Incid}}$ is the easiest TW arrival instant to detect (DONG, 2022). However, the detection of $t^{(1)}_{\text{Recti,Refle}}$ and $t^{(1)}_{\text{Recti,Refra}}$ is a challenge (SCHWEITZER *et al.*, 2016; HUAI *et al.*, 2020; ZHU *et al.*, 2022). Ando *et al.* (1985b) suggest using polarity for identifying reflected and refracted TWs and, consequently, the faulty half line. However, detection and identification of these TWs is the drawback of this method. Finally, this method requires $v^{(1)}_{\text{p}}$ as a user predefined setting, which can lead to fault location errors due to frequency-dependence and uncertainties in line electrical parameters (LOPES *et al.*, 2021). Due to be the first SETWFL solution, this method is named here as Classical SETWFL.

In the mid-1990s, Gale *et al.* (1993) presented again the definition of Types A, B, C, and D. As mentioned earlier, Types A and D solutions have been preferred after the 1980s due to simplicity reasons (LOPES *et al.*, 2021). Type A is the SETWFL method presented by Ando *et al.* (1985b), and Type D solution is a DETWFL method. The Type D method presented by Gale *et al.* (1993) calculates the fault distance on an HVDC system as:

$$\tilde{d}_{\text{ClassicalDETWFL}}\ [\text{km}] = \frac{\ell}{2} + \frac{\left[t^{(1*)}_{\text{Inver,Incid}} - t^{(1)}_{\text{Recti,Incid}}\right] \cdot v^{(1)}_{\text{p}}}{2}\ , \tag{3.3}$$

where $t^{(1)}_{\text{RetInc}}$ [s] and $t^{(1*)}_{\text{Inver,Incid}}$ [s] are the aerial mode incident TWs that arrives at rectifier and inverter stations, being $t^{(1*)}_{\text{Inver,Incid}} = t^{(1)}_{\text{Inver,Incid}} + \kappa$, where κ is the data synchronization misalignment. Both $t^{(1)}_{\text{RetInc}}$ [s] and $t^{(1*)}_{\text{Inver,Incid}}$ [s] instants are relatively easy to detect. However, κ is required due to the subtraction of data from different ends. This requirement is a drawback that can jeopardize this DETWFL method (GALE *et al.*, 1993; FERNANDES *et al.*, 2020). Moreover, this method requires v_{p} as a user predefined setting. As aforementioned, v_{p} is affected by the frequency-dependent and uncertainties in line electrical parameters, leading in fault location errors. Due to be the first DETWFL solution, this method is named here as Classical DETWFL.

In the late 1990s, Magnago & Abur (1998) suggests an application of Classical SETWFL and Classical DETWFL using Wavelet Transform. Almost ten years later, Chen *et al.* (2006)

reviewed the basic principles of Classical SETWFL and Classical DETWFL and suggest the application of these approaches in HVDC transmission lines. However, both papers do not present a solution to overcome the drawbacks to detect reflected and refracted TWs, κ misalignments, and v_{p} settings dependence.

After the beginning of the 21st century, TWFL methods aiming to overcome drawbacks observed in Classical SETWFL and Classical DETWFL formulas have been proposed. The first one is presented by Gilany *et al.* (2007). This method was originally proposed for underground cable AC lines and is adapted here for DC systems. The authors propose a DETWFL formula using the arrival instants of first incident TWs at both line ends and the arrival instant of reflected TW at the local end. The fault distance is estimated as:

$$\tilde{d}_{\mathrm{SettingsFree1DETWFL}}\ [\mathrm{km}] = \left\{ \frac{\left[t^{(1)}_{\mathrm{Recti,Refle}} - t^{(1)}_{\mathrm{Recti,Incid}}\right]}{\left[t^{(1)}_{\mathrm{Recti,Refle}} - t^{(1)}_{\mathrm{Recti,Incid}}\right] + \left[t^{(1*)}_{\mathrm{Inver,Incid}} - t^{(1)}_{\mathrm{Recti,Incid}}\right]} \right\} \cdot \frac{\ell}{2}\ , \qquad (3.4)$$

where $t^{(1)}_{\mathrm{Recti,Incid}}$ [s], $t^{(1*)}_{\mathrm{Inver,Incid}}$ [s], and $t^{(1)}_{\mathrm{Recti,Refle}}$ [s] are instants that the first incident and reflected TWs arrives at rectifier and inverter stations, respectively. The goal of Gilany *et al.* (2007) is to eliminate the v_{p} dependence. As a consequence, the advantage of this method is not be affected by uncertainties in v_{p} setting. Nevertheless, this solution depends on reflected TW at one terminal, which is a well-known challenging task (ZHU *et al.*, 2022). Moreover, this approach still requires data synchronization, which can be an issue when there are data misalignments in the signals (GALE *et al.*, 1993; MONTEIRO *et al.*, 2022). Due to be the first DETWFL solution that is free of v_{p} settings, this method is named here as SettingsFree1 DETWFL.

In 2011, Nanayakkara *et al.* (2011) present a performance evaluation of Classical SETWFL and Classical DETWFL applied to HVDC lines using different procedures. The authors present a comparison of Discrete Wavelet Transform and Continuous Wavelet Transform to identify the TW arrival instants. The use of Continuous Wavelet Transform coefficients yields more robust and accurate wavefront detection compared to the scheme that uses Discrete Wavelet Transform coefficients. In conclusion, the authors suggest using the Continuous Wavelet Transform. However, no solution to overcome the drawbacks (dependence of reflected TWs and v_{p} settings of Classical SETWFL and data synchronization and v_{p} settings of Classical DETWFL) was not proposed.

To overcome the dependence of the reflected TW in the Classical SETWFL, Liu *et al.* (2012) proposed a TWFL method using ground mode TWs. This method was originally proposed for AC lines but was adapted for DC systems by Fernandes *et al.* (2020). The formula is presented

as follows.

$$\tilde{d}_{\text{ModalSETWFL}}\ [\text{km}] = \frac{\left[t^{(0)}_{\text{Recti,Incid}} - t^{(1)}_{\text{Recti,Incid}}\right] \cdot v_{\text{p}}^{(1)} \cdot v_{\text{p}}^{(0)}}{v_{\text{p}}^{(1)} - v_{\text{p}}^{(0)}}\ , \tag{3.5}$$

where $t^{(0)}_{\text{Recti,Incid}}$ [s] and $t^{(1)}_{\text{Recti,Incid}}$ [s] are the arrival instants that ground and aerial mode incident TWs arrives at the rectifier station, respectively. Also, $v_{\text{p}}^{(0)}$ [km/s] and $v_{\text{p}}^{(1)}$ [km/s] are the ground and aerial TW propagation velocities, respectively. The main advantage of this method is not depend on reflected TWs. However, ground mode typically presents a considerable attenuation (WEI *et al.*, 2023; LIU *et al.*, 2023), which leads to becomes difficult to detect the arrival instant of these TWs. Moreover, (3.5) depends on ground $v_{\text{p}}^{(0)}$ [km/s] and aerial $v_{\text{p}}^{(1)}$ [km/s], which are both affected by uncertainties due to line electrical parameters and frequency dependence, mainly $v_{\text{p}}^{(0)}$ [km/s] (RIBEIRO *et al.*, 2022). This dependence might affect the method's performance. Due to be a solution that use ground mode quantities, this method is named here as Modal SETWFL.

Inspired by this last paper, Lopes (2016) propose a DETWFL method using ground mode TWs. This method was originally proposed for AC lines and is adapted here for DC systems. This solution is presented next.

$$\tilde{d}_{\text{ModalDETWFL}}\ [\text{km}] = \left\{ \frac{\left[t^{(0)}_{\text{Recti,Incid}} - t^{(1)}_{\text{Recti,Incid}}\right]}{\left[t^{(0)}_{\text{Recti,Incid}} - t^{(1)}_{\text{Recti,Incid}}\right] + \left[t^{(0*)}_{\text{Inver,Incid}} - t^{(1*)}_{\text{Inver,Incid}}\right]} \right\} \cdot \ell\ , \tag{3.6}$$

where $t^{(0)}_{\text{Recti,Incid}}$ [s], $t^{(1)}_{\text{Recti,Incid}}$ [s], $t^{(0*)}_{\text{Inver,Incid}}$ [s] and $t^{(1*)}_{\text{Inver,Incid}}$ [s] are the time instants that zero and aerial mode TWs arrives at rectifier and inverter stations, respectively. This formula does not depend on any v_{p} [km/s] (neither zero $v_{\text{p}}^{(0)}$ [km/s] nor aerial $v_{\text{p}}^{(1)}$ [km/s]). Therefore, this is a v_{p} setting-free TWFL solution. Furthermore, (3.6) does not require data synchronization κ, being immune to κ misalignments. However, the dependence on ground mode quantities is the main drawback of this formula. Ground mode TWs are highly affected by attenuation and dispersion (FERNANDES *et al.*, 2020). As a consequence, $t^{(0)}_{\text{Recti,Incid}}$ and $t^{(0)}_{\text{Inver,Incid}}$ might not be detected (FERNANDES *et al.*, 2020). This dependence on ground mode TWs can lead to fault location errors or even make the method impractical to be used. Due to be a solution that use ground mode TWs, this method is named here as Modal DETWFL.

In the same year, Schweitzer *et al.* (2016) proposed a SETWFL method using incident, reflected and refracted TWs at the local end. This method was originally proposed for AC lines and was adapted for DC systems by Zhu *et al.* (2022). This formula is presented next.

$$\tilde{d}_{\text{SettingsFreeSETWFL}}\ [\text{km}] = \left[\frac{t^{(1)}_{\text{Recti,Refle}} - t^{(1)}_{\text{Recti,Incid}}}{t^{(1)}_{\text{Recti,Refle}} - t^{(1)}_{\text{Recti,Incid}} + t^{(1)}_{\text{Recti,Refra}} - t^{(1)}_{\text{Recti,Incid}}} \right] \cdot \ell\ , \tag{3.7}$$

where $t^{(1)}_{\text{Recti,Incid}}$ [s], $t^{(1)}_{\text{Recti,Refle}}$ [s] and $t^{(1)}_{\text{Recti,Refra}}$ [s] are the aerial mode incident, reflected and refracted TWs arrival instants at the rectifier station, respectively. This formula does not depend on v_{p} settings. Then, this solution is not affected by the frequency-dependence and uncertainties in line electrical parameters. The main drawback of this method is correctly detecting the reflected and refracted TWs (FERNANDES *et al.*, 2020; ZHU *et al.*, 2022). False detections of these TWs can lead to fault location errors (FERNANDES *et al.*, 2020; ZHANG *et al.*, 2019; ZHU *et al.*, 2022; VIEIRA *et al.*, 2023). Due to be a solution free of v_{p} settings, this method is named here as SettingsFree SETWFL.

In the next year, Dardengo *et al.* (2018) proposes a DETWFL using incident and refracted TWs. This method estimates the fault distance as:

$$\tilde{d}_{\text{SettingsFree2DETWFL}}\ [\text{km}] = \frac{\left[t^{(1)}_{\text{Recti,Refra}} - t^{(1)}_{\text{Recti,Incid}}\right] + \left[t^{(1*)}_{\text{Inver,Incid}} - t^{(1)}_{\text{Recti,Incid}}\right]}{2 \cdot \left[t^{(1)}_{\text{Recti,Refra}} - t^{(1*)}_{\text{Inver,Incid}}\right]} \cdot \ell \ , \tag{3.8}$$

where $t^{(1)}_{\text{Recti,Incid}}$ [s], $t^{(1*)}_{\text{Inver,Incid}}$ [s], and $t^{(1*)}_{\text{Inver,Refra}}$ [s] are the instants that incident and reflected arrive at rectifier and inverter stations, respectively. The main advantage of this method is not require v_{p} settings. However, this solution is affected by κ misalignments. Due to be the second DETWFL method free of v_{p} settings, this method is named here as SettingsFree2 DETWFL.

In the same year, Lopes *et al.* (2018) proposed a DETWFL method free of both κ misalignments and v_{p} settings. This method was originally proposed for AC lines and was adapted for DC systems by Zhu *et al.* (2022). This method estimates the fault location as:

$$\tilde{d}_{\text{SyncFreeSettingsFreeDETWFL}}\ [\text{km}] = \left(\frac{t^{(1)}_{\text{Recti,Refle}} - t^{(1)}_{\text{Recti,Incid}}}{t^{(1)}_{\text{Recti,Refle}} - t^{(1)}_{\text{Recti,Incid}} + t^{(1*)}_{\text{Inver,Refle}} - t^{(1*)}_{\text{Inver,Incid}}} \right) \cdot \ell \ , \tag{3.9}$$

where $t^{(1)}_{\text{Recti,Incid}}$ [s], $t^{(1)}_{\text{Recti,Refle}}$ [s], $t^{(1*)}_{\text{Inver,Incid}}$ [s], and $t^{(1*)}_{\text{Inver,Refle}}$ [s] are the instants that incident and reflected arrive at rectifier and inverter stations, respectively. Although this method does not depend on $v^{(1)}_{\text{p}}$ settings nor data synchronization means, the dependence of detecting reflected TWs at both stations is an important drawback. As aforementioned, false detections of these TWs can lead to fault location errors (FERNANDES *et al.*, 2020; ZHANG *et al.*, 2019; ZHU *et al.*, 2022; VIEIRA *et al.*, 2023). Due to be a method free of both κ misalignments and v_{p} settings, this method named here as SyncFreeSettingsFree DETWFL.

In 2019, Naidu & Pradhan (2019) propose a DETWFL method using reflected TWs. This method was originally proposed for AC lines and is adapted here for DC systems. This method estimates the fault distance as:

If $d \leq \ell/2$:

$$\tilde{d}_{\text{SyncFreeDETWFL1}}\ [\text{km}] = \frac{\left[t^{(1)}_{\text{Recti,Refle}} - t^{(1)}_{\text{Recti,Incid}} + t^{(1*)}_{\text{Inver,Refra}} - t^{(1*)}_{\text{Inver,Incid}}\right] \cdot v^{(1)}_{\text{p}}}{4}\ , \tag{3.10}$$

otherwise $d > \ell/2$:

$$\tilde{d}_{\text{SyncFreeDETWFL2}}\ [\text{km}] = \frac{\left[t^{(1)}_{\text{Recti,Refra}} - t^{(1)}_{\text{Recti,Incid}} + t^{(1*)}_{\text{Inver,Refle}} - t^{(1*)}_{\text{Inver,Incid}}\right] \cdot v^{(1)}_{\text{p}}}{4}\ , \tag{3.11}$$

where $t^{(1)}_{\text{Recti,Incid}}$ [s], $t^{(1)}_{\text{Recti,Refle}}$ [s], $t^{(1)}_{\text{Recti,Refra}}$ [s], $t^{(1*)}_{\text{Inver,Incid}}$ [s], $t^{(1*)}_{\text{Inver,Refle}}$ [s], and $t^{(1*)}_{\text{Inver,Refra}}$ [s] are incident, reflected and refracted TW arrival times at rectifier and inverter stations, respectively. The main advantage of this method is that it is free of κ misalignments. However, reflected and refracted TW arrival instants are used to overcome the κ requirement, but detecting these TWs is a challenge in real-world applications. Furthermore, this method is still affected by uncertainties in $v^{(1)}_{\text{p}}$ [km/s], which can be a source of fault location errors when there are uncertainties in the line electrical parameters. Due to be a method free of κ misalignments, this method is named here as SyncFree DETWFL.

In 2019, Silva *et al.* (2019) evaluated Classical SETWFL and Classical DETWFL using Real-Time Stationary Wavelet Transform and Real-Time Boundary Stationary Wavelet Transform applied to bipolar HVDC systems. The challenge of detecting reflected TWs was highlighted. In the same direction as Ando *et al.* (1985b), Silva *et al.* (2019) suggests considering the polarity of reflected TWs to identify reflected TWs. A relationship between the HVDC converter characteristic and reflected TWs was developed. This relationship is an important finding for applying and developing TWFL methods for HVDC systems.

At the beginning of the third decade of the 21st century, Fernandes *et al.* (2020) present a performance evaluation of the four methods: Classical SETWFL, Modal SETWFL, Classical DETWFL, and Modal DETWFL applied to HVDC systems. The challenge of detecting ground mode quantities in HVDC systems due to attenuation is highlighted. Moreover, the impact of κ misalignments in Classical DETWFL is shown. In addition, the authors show that reflected TWs are specially difficult to detect in PG faults on HVDC systems. Therefore, solutions to overcome the challenge of detecting reflected TWs in PG fault on HVDC lines seems as a contribution to the state of the art.

In the same year, Huai *et al.* (2020) presents a SETWFL using incident and refracted TWs.

This method estimated the fault distance as:

$$\tilde{d}_{\text{EnhancedSETWFL}} = \frac{\left\{2 \cdot \ell + \left[t^{(1)}_{\text{Recti,Incid}} - t^{(1)}_{\text{Recti,Refra}}\right] \cdot v^{(1)}_{\text{p,Recti,Refra}}\right\} \cdot v^{(1)}_{\text{p,Recti,Incid}}}{v^{(1)}_{\text{p,Recti,Incid}} + v^{(1)}_{\text{p,Recti,Refra}}} \,, \tag{3.12}$$

where $v^{(1)}_{\text{p,Recti,Incid}}$ and $v^{(1)}_{\text{p,Recti,Refra}}$ are the $v^{(1)}_{\text{p}}$ at the rectifier station at incident and refracted TW arrival instants, respectively. This formula takes into account different $v^{(1)}_{\text{p}}$ values at each terminal. A TWFL procedure is used to estimate $v^{(1)}_{\text{p,Recti,Incid}}$ and $v^{(1)}_{\text{p,Recti,Refra}}$, such as Hilbert-Huang Transform (HUAI *et al.*, 2020). However, TWFL methods that use this formula still depend on line electrical parameters (HUAI *et al.*, 2020; WANG *et al.*, 2021; CHEN *et al.*, 2022). Due to be a method that is an enhancement of Classical SETWFL, this method is named here as Enhanced SETWFL.

As aforementioned, several TWFL methods have been proposed so far. In 2021, Lopes *et al.* (2021) published a review paper about the past, present, and future trends of TWFL methods. According to the authors, TWFL methods are evolving towards overcoming drawbacks that might arise due to uncertainties in v_{p} settings and κ misalignments. Hence, v_{p} settings-free methods without κ requirement are classified as future trends (LOPES *et al.*, 2021). Based on that, TWFL solutions using reflected or refracted TWs are a tendency. In this sense, advances in TWFL procedures to correctly detect TWs are also future trends. In this opportunity, (LOPES *et al.*, 2021) propose three more types of TWFL methods. Each type is described in detail as follows:

- Type T are DETWFL methods independent of data synchronization, but requiring settings, such as v_{p};

- Type S are TWFL methods that do not depend on settings, i.e. settings-free solutions. This type is divided into two sub-types. Type S1 are settings-free SETWFL methods, and Type S2 are settings-free DETWFL approaches but require data synchronization.

- Type V are DETWFL methods that do not depend on either v_{p}, i.e. it is a settings-free solution, or data synchronization κ means.

In the same year, by knowing that uncertainties in v_{p} settings lead to fault location errors, Wang *et al.* (2021) propose adaptations in the Classical DETWFL, resulting in the following

method.

$$\tilde{d}_{\text{EnhancedDETWFL}}\ [\text{km}] = \frac{\left\{\left[t^{(1*)}_{\text{Inver,Incid}} - t^{(1)}_{\text{Recti,Incid}}\right] \cdot v^{(1)}_{\text{p,Recti,Incid}} \cdot v^{(1)}_{\text{p,Inver,Incid}}\right\} + v^{(1)}_{\text{p,Recti,Incid}} \cdot \ell}{v^{(1)}_{\text{p,Recti,Incid}} + v^{(1)}_{\text{p,Inver,Incid}}}\ , \tag{3.13}$$

where $v^{(1)}_{\text{p,Recti,Incid}}$ and $v^{(1)}_{\text{p,Inver,Incid}}$ are $v^{(1)}_{\text{p}}$ at incident TW arrival instant at the rectifier and inverter stations, respectively. This formula takes into account different $v^{(1)}_{\text{p}}$ values at each terminal. A TWFL procedure is used to estimate $v^{(1)}_{\text{p,Recti,Incid}}$ and $v^{(1)}_{\text{p,Inver,Recti}}$, such as Stockwell transform (WANG *et al.*, 2021). However, TWFL methods that use this formula still depend on a curve of $v^{(1)}_{\text{p}}$ and frequency, consequently, this method still depends on line electrical parameters (WANG *et al.*, 2021). Due to be a method that is an enhancement of Classical DETWFL, this method is named here as Enhanced DETWFL. In the same direction of Wang *et al.* (2021), Chen *et al.* (2022) propose the Enhanced DETWFL formula using Empirical Mode Decomposition and Hilbert-Huang Transform. However, both solutions proposed by Wang *et al.* (2021) or Chen *et al.* (2022) are still affected by uncertainties in line electrical parameters. Moreover, formula (3.13) requires data synchronization.

In recent years, several TWFL procedures based on mathematical tools have been proposed. Oliveira *et al.* (2022) present applications of Hilbert-Huang Transform and Stockwell Transfom in the Classical DETWFL method. In the same direction, Vieira *et al.* (2022) present a study of application challenges of the Classical SETWFL and Classical DETWFL applied to HVDC systems. In the same year, Zeng *et al.* (2022) propose the Enhanced DETWFL method based on Successive Variational Mode Decomposition, which takes into account variations in v_{p}. Even so, since settings are required, inaccuracies in v_{p} treatment can compromise the fault location accuracy. Fayazi *et al.* (2023) propose the Classical SETWFL method based on Discrete Wavelet Transform. Zhang *et al.* (2019) propose the Classical SETWFL method based on Wavelet Transform Modulus Maxima. Huai *et al.* (2021) propose the Classical SETWFL method based on Variational Mode Decomposition and Teager Energy Operator. Huai *et al.* (2020) propose a single-ended method based on Stationary Wavelet Transform and Singular Value Decomposition. Zhu *et al.* (2022) propose the SettingsFree SETWFL and SyncFreeSettingsFree DETWFL methods based on the Hilbert-Huang Transform. The goal of most of these methods is using mathematical tools to correctly detect reflected TWs (HUAI *et al.*, 2020; ZHU *et al.*, 2022). Therefore, a solution that overcome the requirement of detecting reflected TWs seems as a contribution to the state of the art.

Figure 3.1 shows a timeline of TWFL methods. As can be seen, first studies on TWs date back to the 1920s. In 1950, solutions that later became known as Classical TWFL methods were proposed. Between the 1950s and 1990s, only a few papers were published. This period is a historical gap in TWFL solutions due to the technological barriers. After the 1990s, the quest to avoid the drawbacks of Classical TWFL methods has gained interest. In the 21st century, TWFL methods free of drawbacks have been proposed. However, each solution has at least one drawback. Therefore, in order to consolidate this review, two Tables are presented next. Table 3.1 summarizes the types of TWFL methods and Table 3.2 shows the drawbacks of TWFL methods. From Table 3.1, Type V TWFL solutions show to be a potential trend. Type V methods do not use pulse injection, and do not require v_{p} settings nor data synchronization κ means. Based on the aforementioned considerations, TWFL methods that use fault-induced TWs predominated over those based on pulse injection. Moreover, methods free of v_{p} settings and κ means are of great interest. Therefore, new Type V methods are indeed a great contribution to the literature. However, Type V methods commonly require reflected TWs, which are a challenge to detect them. In this sense, advances in TW procedures are also reported as a trend, since good procedures are essential to make these Type V approaches feasible in the field. However, state-of-the-art TWFL procedures are based on complex mathematical tools, such as Hilbert-Huang Transform, Empirical Mode Decomposition, Teager Energy Operator etc. In conclusion, a Type V method based on a relatively simple procedure is a potential contribution to the current technological context. According to Table 3.2, the TWFL methods available on literature face a trade-off between four drawbacks, namely: ground mode TW arrival instants $t^{(0)}_{\mathrm{Recti,Incid}}$ or $t^{(0)}_{\mathrm{Inver,Incid}}$, data synchronization κ, v_{p} settings, and reflected TW arrival instants $t^{(1)}_{\mathrm{Recti,Refle}}$ or $t^{(1*)}_{\mathrm{Inver,Refle}}$ dependence. Modal SETWFL and Modal DETWFL methods require $t^{(0)}_{\mathrm{Recti,Incid}}$ or $t^{(0)}_{\mathrm{Inver,Incid}}$. Classical SETWFL, Modal SETWFL, Classical DETWFL, and Sync-Free DETWFL methods are susceptible to uncertainties in v_{p} settings. Classical DETWFL, SettingsFree1 DETWFL, SettingsFree2 DETWFL, and Enhanced DETWFL methods are susceptible to κ misalignments. Finally, Classical SETWFL, SettingsFree SETWFL, SettingsFree1 DETWFL, SettingsFree2 DETWFL, SyncFree DETWFL, SyncFreeSettingsFree DETWFL depend on reflected TWs. As a conclusion, a TWFL method free of these four drawbacks is an interesting contribution. In the next Chapter, a Type V method free of $t^{(0)}_{\mathrm{Recti,Incid}}$ or $t^{(0)}_{\mathrm{Inver,Incid}}$, data synchronization κ, v_{p} settings, and reflected TWs is proposed. As it will be shown, the proposed formula (4.9) overcomes these four drawbacks.

Figure 3.1: Timeline of TWFL Methods.

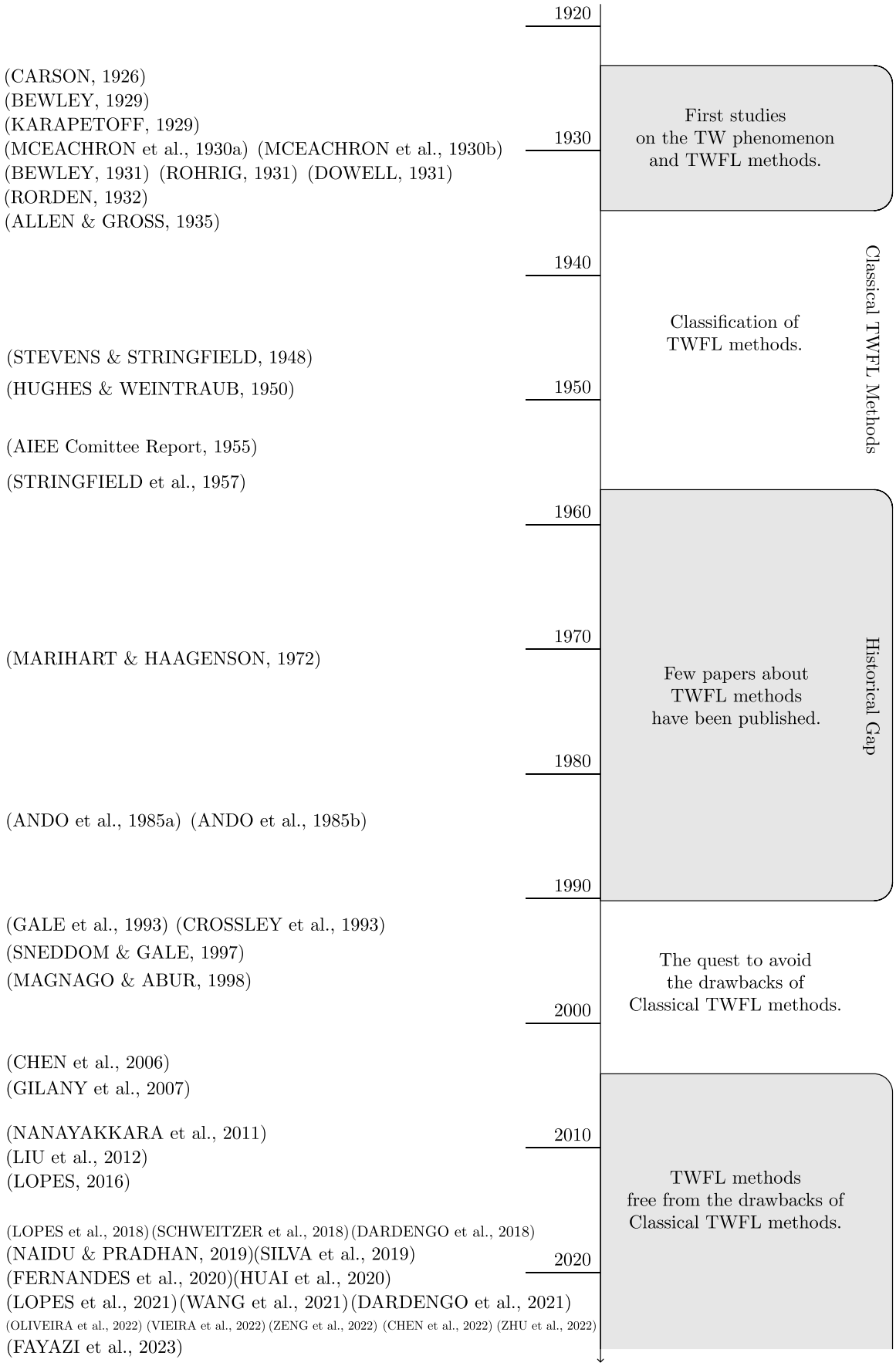

Source: Own Authorship.

Table 3.1: Types of TWFL methods.

Type	-Ended	Pulse injection not used	Essential characteristic
A	Single	✓	Reflected TW t_{Refle} or refracted TW t_{Refra} required
B1	Double		Radio timing pulse
B2	Double		Power lines carrier
B3	Double		Direct current pulse
C	Single		Radar principle
D	Double	✓	Data synchronization κ required
E	Single	✓	Transients induced by circuit breakers
F	Single		Repetitive pulses
K	Single		Beam switching tube
T	Double	✓	Free of data synchronization κ means but v_{p} setting required
S1	Single	✓	Free of v_{p} settings
S2	Double	✓	Data synchronization κ required
V	Double	✓	Free of v_{p} settings and data synchronization κ means

Source: Own Authorship.

Table 3.2: Drawbacks of TWFL methods.

					Free of			
	Nickname	Type	Reference	Formula	$t^{(0)}$	v_{p}	κ	t_{Refle}
SETWFL	Classical	A	Ando *et al.* (1985b)	(3.1)(3.2)	✓		✓	
	Modal		Liu *et al.* (2012)	(3.5)			✓	✓
	SettingsFree	S1	Schweitzer *et al.* (2016)	(3.7)	✓	✓	✓	
	Enhanced	A	Huai *et al.* (2020)	(3.12)	✓	*	✓	✓
DETWFL	Classical	D	Gale *et al.* (1993)	(3.3)	✓			✓
	Modal	V	Lopes (2016)	(3.6)		✓	✓	✓
	SettingsFree1	S2	Gilany *et al.* (2007)	(3.4)	✓	✓		
	SettingsFree2	S2	Dardengo *et al.* (2018)	(3.8)	✓	✓		
	SyncFree	T	Naidu & Pradhan (2019)	(3.10)(3.11)	✓		✓	
	SyncFreeSettingsFree	V	Lopes *et al.* (2018)	(3.9)	✓	✓	✓	
	Enhanced	D	Wang *et al.* (2021)	(3.13)	✓	*		✓
	Proposed	V	This thesis	(4.9)	✓	✓	✓	✓

* Free of v_{p} settings but require a v_{p} versus frequency graph like Figure 2.6(f).

Source: Own Authorship.

CHAPTER 4

PROPOSED METHOD

This chapter introduces a Type V TWFL method to deal with PG faults on HVDC lines.

4.1 FOUNDATION

First, an analysis of the TW phenomenon in HVDC lines is conducted. The goal is to identify TWs that can be used in the method by employing a straightforward procedure. Ground-mode TWs are not considered in this analysis. In the previous Chapters, the disadvantages of using these TWs were highlighted. Thus, only aerial-mode TWs are considered to be used in the method. Figure 4.1 shows a lattice diagram for a fault d far from the rectifier station, which starts at t_{Fault} instant on an HVDC line ℓ long. The arrival instants of the aerial-mode incident, reflected, and refracted TWs at rectifier and inverter stations are given by $t^{(1)}_{\text{Recti,Incid}}$ and $t^{(1)}_{\text{Inver,Incid}}$, $t^{(1)}_{\text{Recti,Refle}}$ and $t^{(1)}_{\text{Inver,Refle}}$, and $t^{(1)}_{\text{Recti,Refra}}$ and $t^{(1)}_{\text{Inver,Refra}}$, respectively. The superscript (1) stands for the aerial-mode, so that $v^{(1)}_{\text{p}}$ is the aerial-mode TW propagation velocity.

Compared to reflected or refracted TWs, incident TWs are easy to detect (DONG, 2022). Incident TWs are the first and the highest energy TWs in the fault signals. Therefore, $t^{(1)}_{\text{Recti,Incid}}$ and $t^{(1)}_{\text{Inver,Incid}}$ are considered to be used in the method. Nevertheless, methods that depend

Figure 4.1: Lattice diagram for a fault on an HVDC line.

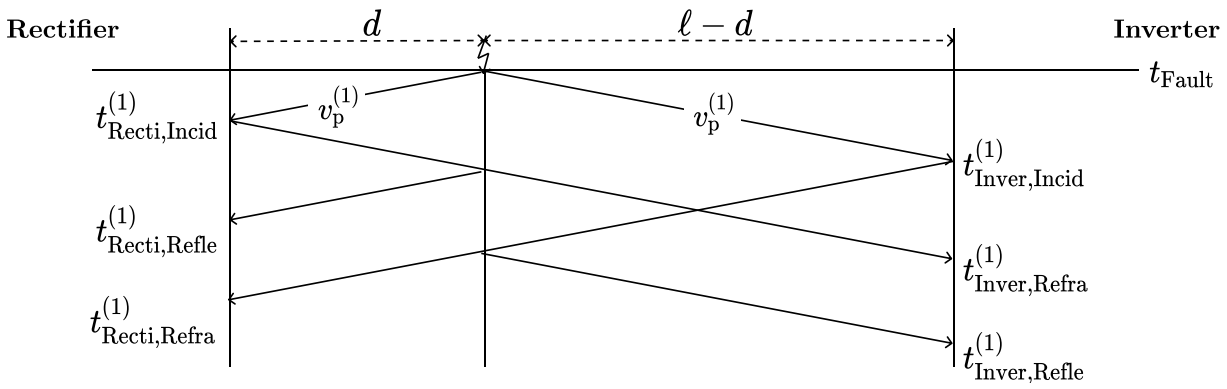

Source: Own Authorship.

only on incident TWs are affected by inaccuracies in $v_{\mathrm{p}}^{(1)}$ settings and data synchronization misalignments (GALE *et al.*, 1993; FERNANDES *et al.*, 2020). Therefore, this thesis also investigates the behavior of reflected and refracted TWs. The goal is to identify which of these TWs are easier to detect and can be used in the method.

The amplitude of reflected and refracted TWs depends mainly on the reflection $\Upsilon_{\mathrm{Fault,Refle}}$ and refraction $\Upsilon_{\mathrm{Fault,Refra}}$ coefficients at the fault point, respectively (LIN *et al.*, 2021; LAN *et al.*, 2021; YU *et al.*, 2023). For PG faults, these coefficients for current TWs are expressed as presented in (LIN *et al.*, 2021; LAN *et al.*, 2021; YU *et al.*, 2023):

$$\Upsilon_{\mathrm{Fault,Refle}} = \frac{Z_{\mathrm{Surge}}^{(1)}}{Z_{\mathrm{Surge}}^{(1)} + Z_{\mathrm{Surge}}^{(0)} + 4R_{\mathrm{Fault}}} \,, \tag{4.1}$$

$$\Upsilon_{\mathrm{Fault,Refra}} = \frac{Z_{\mathrm{Surge}}^{(0)} + R_{\mathrm{Fault}}}{Z_{\mathrm{Surge}}^{(1)} + Z_{\mathrm{Surge}}^{(0)} + 4R_{\mathrm{Fault}}} \,, \tag{4.2}$$

where $Z_{\mathrm{Surge}}^{(0)}$, $Z_{\mathrm{Surge}}^{(1)}$, and R_{Fault} are the ground- and aerial-mode line surge impedance, and fault resistance, respectively. The superscript (0) stands for the ground mode.

From (4.2), $|\Upsilon_{\mathrm{Fault,Refra}}| \neq 0$ regardless of R_{Fault}. Moreover, from (4.1) and (4.2), $|\Upsilon_{\mathrm{Fault,Refra}}| > |\Upsilon_{\mathrm{Fault,Refle}}|$ because $Z_{\mathrm{Surge}}^{(0)} > Z_{\mathrm{Surge}}^{(1)}$ in overhead multi-pole transmission lines (KIMBARK, 1970; ZHANG *et al.*, 2012; ZHANG *et al.*, 2021). Thereby, refracted TWs have larger amplitudes than reflected ones in PG faults. Thus, this is the first finding of this analysis. In other words, refracted TWs seem to be easier to detect than reflected TWs in PG faults.

Aiming to increase the reliability of detection procedures applied to identify the refracted TWs, the polarity of these TWs is investigated. The polarity of refracted TWs depends on the HVDC converter characteristic (ANDO *et al.*, 1985b; WANG *et al.*, 2019; WANG; ZHANG, 2022a). This characteristic can be inductive or capacitive. For instance, the characteristic of modular multi-level converter (MMC) is inductive (WANG; ZHANG, 2022a). Line commutated converter (LCC) Type-A is inductive (WANG; ZHANG, 2022a), but the LCC Type-B is capacitive (WANG; ZHANG, 2022a). Also, voltage source converter (VSC) is capacitive (WANG *et al.*, 2019). Figure 4.2 shows lattice diagrams with the four inductive and capacitive HVDC converter characteristic combinations. If the characteristic of one end is inductive, the polarities of the incident and refracted TWs in the opposite end are the same. Conversely, if the characteristic of one end is capacitive, the polarities of the incident and refracted TWs in the opposite end are different. Such a well-established polarity pattern is the second finding of this analysis.

Figure 4.2: Polarity of current TWs for different HVDC converter characteristics.

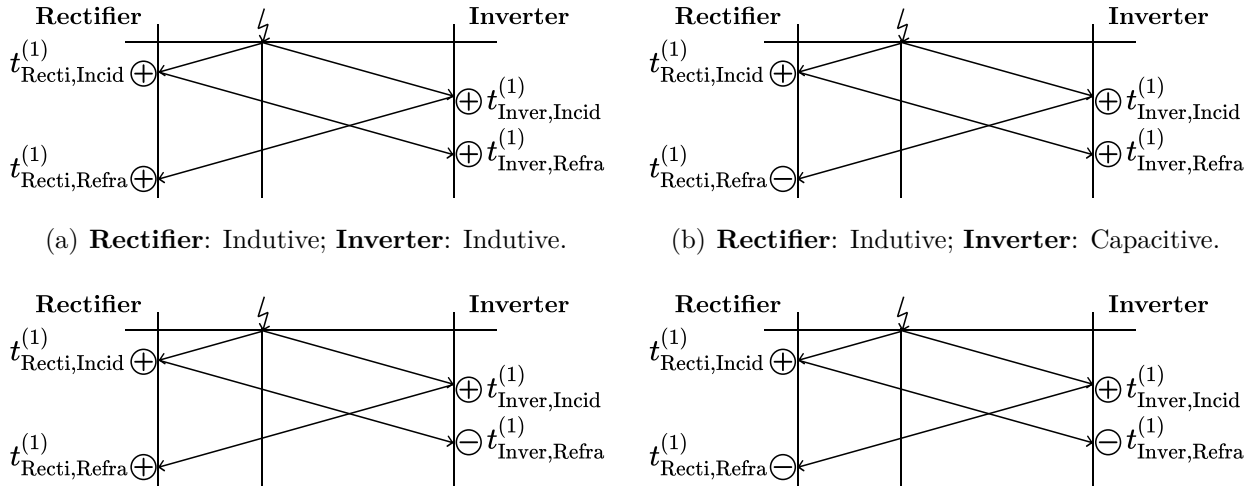

(a) **Rectifier**: Indutive; **Inverter**: Indutive.

(b) **Rectifier**: Indutive; **Inverter**: Capacitive.

(c) **Rectifier**: Capacitive; **Inverter**: Indutive.

(d) **Rectifier**: Capacitive; **Inverter**: Capacitive.

Source: Own Authorship.

Up to this point, two findings were identified. Firstly, refracted TWs have high amplitudes in PG faults. Secondly, a well-established polarity pattern of refracted TWs in HVDC systems. Therefore, refracted TWs can be easily detected using a amplitude- and polarity-based criterion for PG faults. These two findings and the proposed criterion are a major contribution of this PhD thesis. Then, since incident TWs are easy to detect, a PG fault location method is designed using only incident and refracted TWs at both stations. In other words, a method is developed considering only the TW arrival instants $t^{(1)}_{\text{Recti,Incid}}$, $t^{(1)}_{\text{Inver,Incid}}$, $t^{(1)}_{\text{Recti,Refra}}$, and $t^{(1)}_{\text{Inver,Refra}}$ (see Fig. 4.1). As these four TW arrival instants are easy to detect, the method aims to be simple and reliable. Further details on the formulation used in the solution are presented next.

4.2 FORMULA

From Figure 4.1, incident and refracted TW arrival instants at both ends are derived as:

$$\left[t^{(1)}_{\text{Recti,Incid}} - t_{\text{Fault}}\right] \cdot v^{(1)}_{\text{p}} = d \ , \tag{4.3}$$

$$\left[t^{(1*)}_{\text{Inver,Incid}} - t_{\text{Fault}}\right] \cdot v^{(1)}_{\text{p}} = \ell - d \ , \tag{4.4}$$

$$\left[t^{(1)}_{\text{Recti,Refra}} - t_{\text{Fault}}\right] \cdot v^{(1)}_{\text{p}} = \ell + \ell - d \ , \tag{4.5}$$

$$\left[t^{(1*)}_{\text{Inver,Refra}} - t_{\text{Fault}}\right] \cdot v^{(1)}_{\text{p}} = \ell + d \ , \tag{4.6}$$

Subtracting (4.5) from (4.3) and (4.6) from (4.4) yields:

$$\left[t^{(1)}_{\text{Recti,Refra}} - t^{(1)}_{\text{Recti,Incid}}\right] \cdot v^{(1)}_{\text{p}} = 2 \cdot \ell - 2 \cdot d \ , \tag{4.7}$$

$$\left[t^{(1*)}_{\text{Inver,Refra}} - t^{(1*)}_{\text{Inver,Incid}}\right] \cdot v^{(1)}_{\text{p}} = 2 \cdot d \ . \tag{4.8}$$

From (4.7) and (4.8), the following fault location formula is proposed:

$$\tilde{d} = \left\{ \frac{\left[t^{(1*)}_{\text{Inver,Refra}} - t^{(1*)}_{\text{Inver,Incid}}\right]}{\left[t^{(1*)}_{\text{Inver,Refra}} - t^{(1*)}_{\text{Inver,Incid}}\right] + \left[t^{(1)}_{\text{Recti,Refra}} - t^{(1)}_{\text{Recti,Incid}}\right]} \right\} \cdot \ell \ . \tag{4.9}$$

being $t^{(1*)}_{\text{Inver,Incid}} = t^{(1)}_{\text{Inver,Incid}} + \kappa$ and $t^{(1*)}_{\text{Inver,Refra}} = t^{(1)}_{\text{Inver,Refra}} + \kappa$, by substituting in (4.9):

$$\tilde{d} = \left\{ \frac{\left\{\left[t^{(1)}_{\text{Inver,Refra}} + \kappa\right] - \left[t^{(1)}_{\text{Inver,Incid}} + \kappa\right]\right\}}{\left\{\left[t^{(1)}_{\text{Inver,Refra}} + \kappa\right] - \left[t^{(1)}_{\text{Inver,Incid}} + \kappa\right]\right\} + \left[t^{(1)}_{\text{Recti,Refra}} - t^{(1)}_{\text{Recti,Incid}}\right]} \right\} \cdot \ell \ , \tag{4.10}$$

by re-arranging the equation:

$$\tilde{d} = \left\{ \frac{\left\{\left[t^{(1)}_{\text{Inver,Refra}} - t^{(1)}_{\text{Inver,Incid}}\right] + [\kappa - \kappa]\right\}}{\left\{\left[t^{(1)}_{\text{Inver,Refra}} - t^{(1)}_{\text{Inver,Incid}}\right] + [\kappa - \kappa]\right\} + \left[t^{(1)}_{\text{Recti,Refra}} - t^{(1)}_{\text{Recti,Incid}}\right]} \right\} \cdot \ell \ . \tag{4.11}$$

by eliminating κ in the equation:

$$\tilde{d} = \left\{ \frac{\left\{\left[t^{(1)}_{\text{Inver,Refra}} - t^{(1)}_{\text{Inver,Incid}}\right] + 0\right\}}{\left\{\left[t^{(1)}_{\text{Inver,Refra}} - t^{(1)}_{\text{Inver,Incid}}\right] + 0\right\} + \left[t^{(1)}_{\text{Recti,Refra}} - t^{(1)}_{\text{Recti,Incid}}\right]} \right\} \cdot \ell \ . \tag{4.12}$$

Therefore, κ is eliminated, resulting in:

$$\tilde{d} = \left\{ \frac{\left[t^{(1)}_{\text{Inver,Refra}} - t^{(1)}_{\text{Inver,Incid}}\right]}{\left[t^{(1)}_{\text{Inver,Refra}} - t^{(1)}_{\text{Inver,Incid}}\right] + \left[t^{(1)}_{\text{Recti,Refra}} - t^{(1)}_{\text{Recti,Incid}}\right]} \right\} \cdot \ell \ . \tag{4.13}$$

Formula (4.9) does not require $v^{(1)}_{\text{p}}$ setting. Thus, the method is free of the effects of uncertainties in $v^{(1)}_{\text{p}}$ settings. As result, the method is not affected by uncertainties in line electrical parameters and frequency dependence on $v^{(1)}_{\text{p}}$. Also, formula (4.9) does not perform double-ended data crossing. In other words, the TW arrival instants are subtracted individually at each station, as shown in each square bracket in (4.9). Hence, data synchronization is not required. As proven, κ misalignment is mathematically eliminated. Furthermore, the method uses only aerial-mode TW arrival instants, overcoming drawbacks due to attenuation and dispersion, as typically verified in ground-mode TWs (WEI *et al.*, 2023; LIU *et al.*, 2023). Moreover, since only easy-to-detect TWs are taken into account, the method has a simple and reliable procedure as described next.

4.3 PROCEDURE

Figure 4.3 shows the method flowchart, which is explained next.

#1 The positive and negative pole current signals are sampled at rectifier station [$i^{(+)}_{\text{Recti}}$ and $i^{(-)}_{\text{Recti}}$], and at inverter station [$i^{(+)}_{\text{Inver}}$ and $i^{(-)}_{\text{Inver}}$].

#2 Using the Karrenbauer modal transformation (DOMMEL; MEYER, 1974), the aerial-mode current signal at rectifier $i^{(1)}_{\text{Recti}}$ station, and at $i^{(1)}_{\text{Inver}}$ inverter station are calculated. This calculation is performed as: $i^{(1)}[k] = \{i^{(+)}[k] - i^{(-)}[k]\}/\sqrt{2}$. This modal transformation is often used to analyze signals on HVDC systems (FERNANDES *et al.*, 2020; DONG, 2022; WANG *et al.*, 2020).

#3 By using a high pass filter, the aerial mode TW current signals at $i^{(1,\text{TW})}_{\text{Recti}}$ rectifier station and at inverter $i^{(1,\text{TW})}_{\text{Inver}}$ station are obtained. The filtering process is performed as proposed in Wang *et al.* (2020). This filter is often used to analyze signals on HVDC systems (WANG *et al.*, 2021; WANG *et al.*, 2022; CHEN *et al.*, 2022; WANG *et al.*, 2023).

$$i^{(1,\text{TW})}[k] = -0.9048 \cdot i^{(1,\text{TW})}[k-1] + 0.9524 \cdot i^{(1)}[k] - 0.9524 \cdot i^{(1)}[k-1] \tag{4.14}$$

Figure 4.3: Proposed method's flowchart.

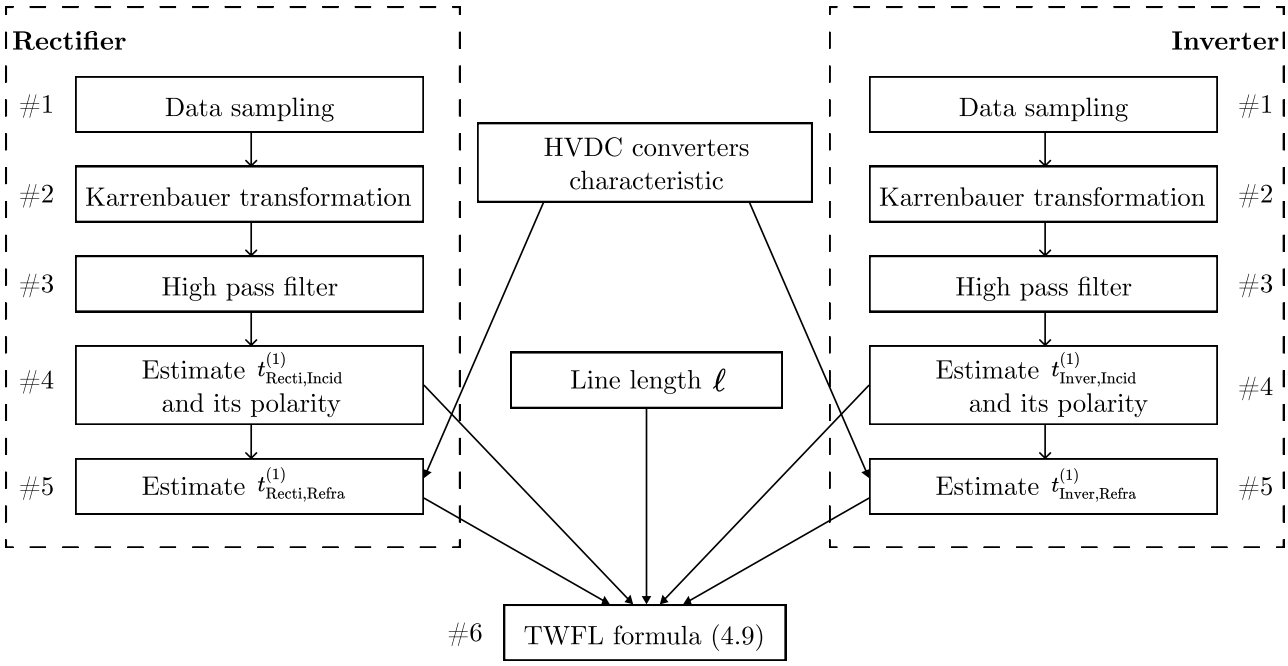

Source: Own Authorship.

#4 By using $i^{(1,\mathrm{TW})}_{\mathrm{Recti}}$ and $i^{(1,\mathrm{TW})}_{\mathrm{Inver}}$ signals, the aerial-mode incident TW arrival samples at rectifier $k^{(1)}_{\mathrm{Recti,Incid}}$ and inverter $k^{(1)}_{\mathrm{Inver,Incid}}$ stations are estimated. This estimation for rectifier station is performed as follows:

$$k^{(1)}_{\mathrm{Recti,Incid}} = \max\left\{\mathrm{abs}\left\{i^{(1,\mathrm{TW})}_{\mathrm{Recti}}[1:\mathrm{end}]\right\}\right\} \ , \tag{4.15}$$

where max and abs are the maximum and absolute functions, respectively. After that, the polarity of the incident TW is estimated as follows.

$$\mathrm{sign}\left\{i^{(1,\mathrm{TW})}_{\mathrm{Recti}}[k^{(1)}_{\mathrm{Recti,Incid}}]\right\} \ , \tag{4.16}$$

where sign returns $+1$ and -1 for a positive and negative polarity, respectively. The estimation for inverter station is similar. Finally, $k^{(1)}_{\mathrm{Recti,Incid}}$ and $k^{(1)}_{\mathrm{Inver,Incid}}$ are converted to TW arrival instants $t^{(1)}_{\mathrm{Recti,Incid}}$ and $t^{(1)}_{\mathrm{Inver,Incid}}$, which are used in the method.

#5 The refracted TW arrival instants are obtained using an amplitude- and polarity-based criterion. From Section 4.1, these TWs can be detected by searching the max or min value after the incident TW. For instance, if the opposite end is inductive and if the polarity of the incident TW at the monitored end is positive (sign = 1), the refracted TW arrival sample $k^{(1)}_{\mathrm{Refra}}$ in such a monitored end is estimated as:

$$k^{(1)}_{\mathrm{Refra}} = \max\left\{\mathrm{peakvalley}\left[i^{(1,\mathrm{TW})}\left[k^{(1)}_{\mathrm{Incid}}:\mathrm{end}\right]\right]\right\} \ , \tag{4.17}$$

where peakvalley returns an array with peaks and valleys. Otherwise, if the polarity of the incident TW at the monitored end is negative (sign = -1), the refracted $k^{(1)}_{\mathrm{Refra}}$ TW arrival sample at the monitored end is estimated by changing max to min in (4.17). On the other hand, if the characteristic of the opposite end is capacitive, $k^{(1)}_{\mathrm{Refra}}$ of the monitored end is estimated by changing the order of max and min in the previous explanation. Finally, $k^{(1)}_{\mathrm{Recti,Refra}}$ and $k^{(1)}_{\mathrm{Inver,Refra}}$ are converted to TW arrival times $t^{(1)}_{\mathrm{Recti,Refra}}$ and $t^{(1)}_{\mathrm{Inver,Refra}}$, which are used in the method. As shown in Section 4.1, the HVDC converter characteristic (inductive or capacitive) is determined from the converter type (MMC, LCC Type-A, LCC Type-B, or VSC). Since for a particular system, the converter type is known beforehand, therefore, the HVDC converter characteristic is consistent and invariant. During commissioning procedures, a test can be done to confirm the HVDC converter characteristic.

#6 From the TW arrival instants $t^{(1)}_{\mathrm{Recti,Incid}}$, $t^{(1)}_{\mathrm{Inver,Incid}}$, $t^{(1)}_{\mathrm{Recti,Refra}}$ and $t^{(1)}_{\mathrm{Inver,Refra}}$, and the line length ℓ, the fault location $\tilde{d}$ is estimated using (4.9).

CHAPTER 5

RESULTS

Fault simulations were carried out in the Bipole 1 of Rio Madeira HVDC system. Figure 5.1 presents this bipole, which consists of a ±600 kV transmission line $\ell = 2450$ km long. Both HVDC converter stations are based on the LCC Type-B technology (WANG; ZHANG, 2022b). This system was modeled using the Alternative Transients Program (ATP). The line was implemented using the distributed parameter frequency-dependent JMarti model (MARTI, 1982; MEYER; LIU, 1992). The tower geometry data are available in (LUZ *et al.*, 2014). An ATP time step equal to 0.5 μs was set (DOMMEL, 1996; MEYER; LIU, 1992).

Results are presented taking into account fault location errors ε (km). The ε index is defined as $\varepsilon = \text{abs}(\tilde{d} - d)$, where $\tilde{d}$ is the fault distance estimated by a TWFL method, d is the real fault distance, and abs is the absolute value function.

Figure 5.1: Bipole 1 of the Rio Madeira HVDC System

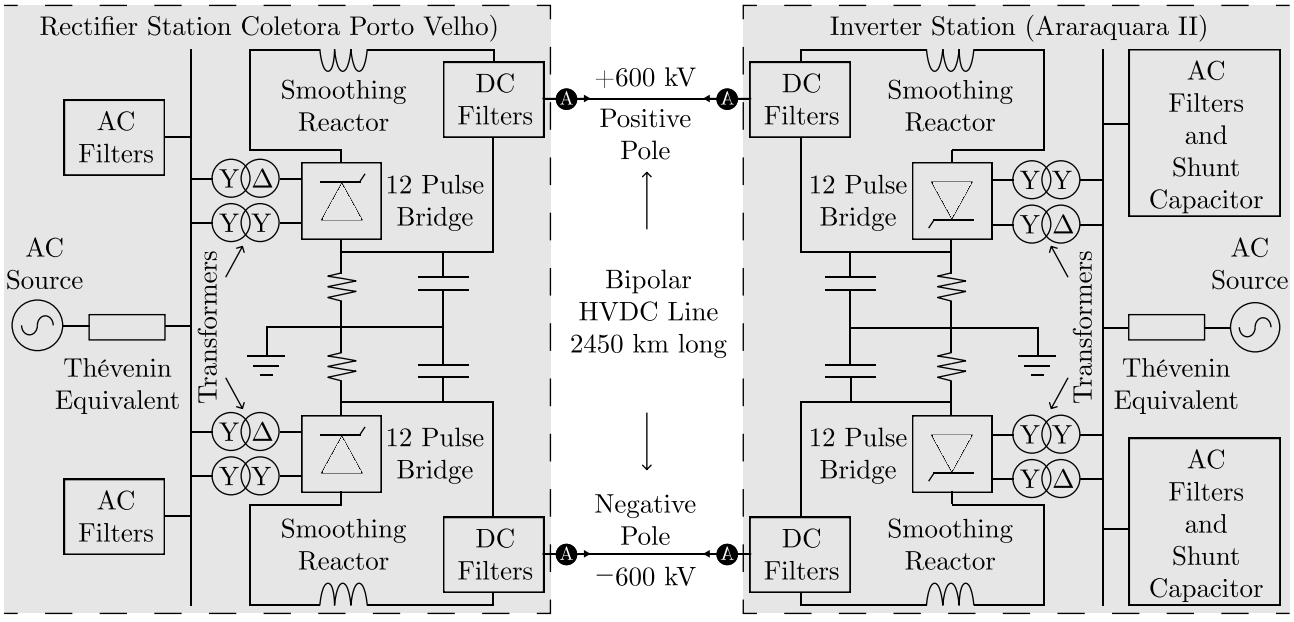

Source: Own Authorship.

5.1 CASE STUDY

To exemplify the proposed method's procedure, two case studies are presented. First, a fault at 30% of the line from the Rectifier Station. Second, a fault at the middle of the line, which is critical due to the overlapping of refracted and reflected TWs.

5.1.1 Fault at 30% of the Line from the Rectifier Station

This case consists in a PG fault at $d = 735$ km (30% of the transmission line length ℓ from rectifier station). Figure 5.2 shows the positive and negative pole current signals at the rectifier $i^{(+)}_{\text{Recti}}$ and $i^{(-)}_{\text{Recti}}$, and at the inverter $i^{(+)}_{\text{Inver}}$ and $i^{(-)}_{\text{Inver}}$ stations, being $t_{\text{Fault}} = 0$ s. Based on these pole signals and using Karrenbauer modal transformation, the aerial mode current signals at rectifier $i^{(1)}_{\text{Recti}}$ and inverter $i^{(1)}_{\text{Inver}}$ stations are obtained as shown in Figure 5.3(a). Based on these aerial-mode current signals and using the high pass filter, the aerial-mode TW current

Figure 5.2: Positive and negative pole currents at rectifier and inverter stations.

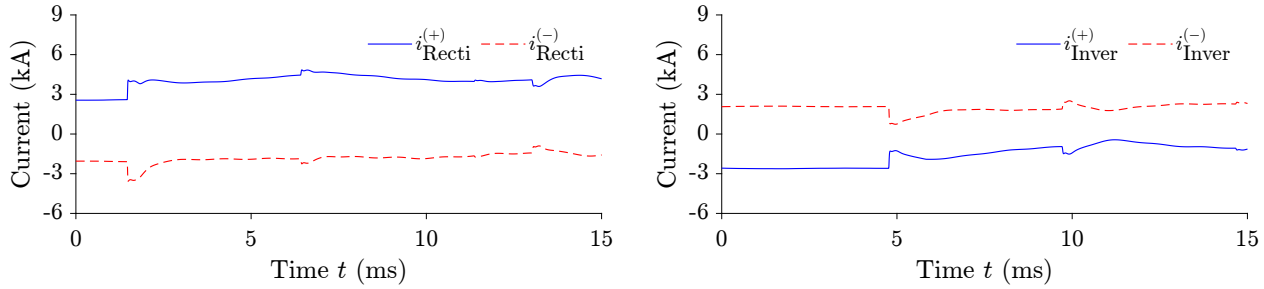

(a) Rectifier station. (b) Inverter station.

Source: Own Authorship.

Figure 5.3: Aerial mode current and TW current at rectifier and inverter stations.

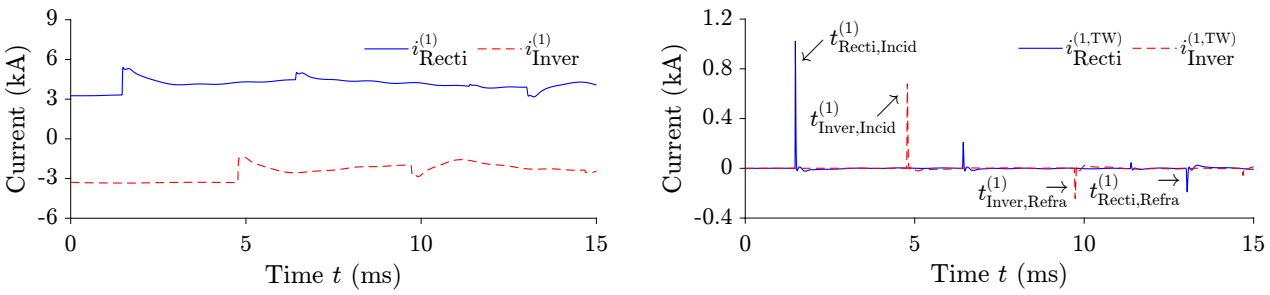

(a) Aerial mode currents. (b) Aerial mode TW currents.

Source: Own Authorship.

signals at rectifier $i^{(1,\mathrm{TW})}_{\mathrm{Recti}}$ and inverter $i^{(1,\mathrm{TW})}_{\mathrm{Inver}}$ stations are obtained as depicted in Figure 5.3(b). From these filtered signals, the TW arrival times are estimated as $t^{(1)}_{\mathrm{Recti,Incid}} = 1.4790$ ms, $t^{(1)}_{\mathrm{Inver,Incid}} = 4.7820$ ms, $t^{(1)}_{\mathrm{Recti,Refra}} = 13.0380$ ms, and $t^{(1)}_{\mathrm{Inver,Refra}} = 9.7350$ ms. By knowing that $\ell = 2450$ km and then applying (4.9), $\tilde{d} = 734.9110$ km is estimated. Thus, a fault location error $\varepsilon = 0.0890$ km is calculated. As can be seen, the method has quite simple procedures and provides a high accurate fault location estimation.

5.1.2 Fault at the Middle of the Line

This case consists in a PG fault at $d = 1225$ km (50% of the transmission line length ℓ). Figure 5.4 shows the positive and negative pole current signals at the rectifier $i^{(+)}_{\mathrm{Recti}}$ and $i^{(-)}_{\mathrm{Recti}}$, and at the inverter $i^{(+)}_{\mathrm{Inver}}$ and $i^{(-)}_{\mathrm{Inver}}$ stations, being $t_{\mathrm{Fault}} = 0$ s. Based on these pole signals and using Karrenbauer modal transformation, the aerial mode current signals at rectifier $i^{(1)}_{\mathrm{Recti}}$ and inverter $i^{(1)}_{\mathrm{Inver}}$ stations are obtained as shown in Figure 5.5(a). Based on these aerial-mode

Figure 5.4: Positive and negative pole currents at rectifier and inverter stations.

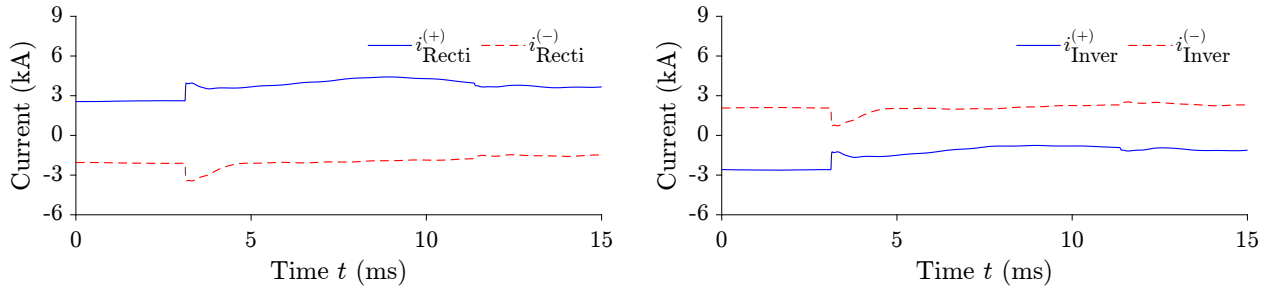

(a) Rectifier station. (b) Inverter station.

Source: Own Authorship.

Figure 5.5: Aerial mode current and TW current at rectifier and inverter stations.

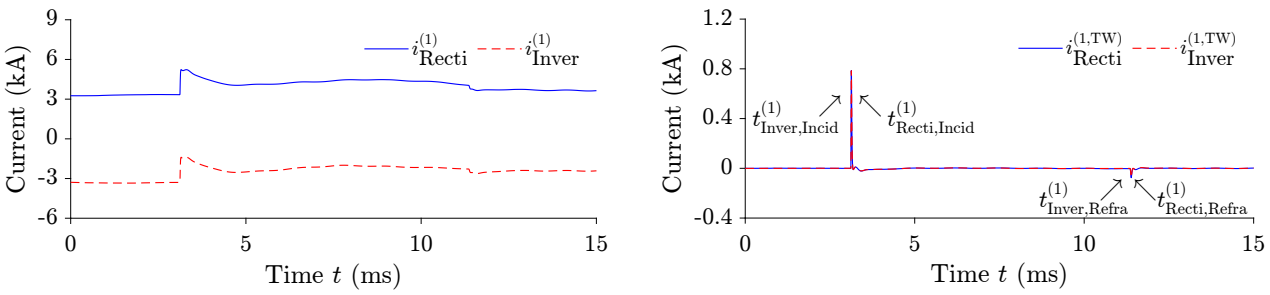

(a) Aerial mode currents. (b) Aerial mode TW currents.

Source: Own Authorship.

current signals and using the high pass filter, the aerial-mode TW current signals at rectifier $i^{(1,\mathrm{TW})}_{\mathrm{Recti}}$ and inverter $i^{(1,\mathrm{TW})}_{\mathrm{Inver}}$ stations are obtained as shown in Figure 5.5(b). From these filtered signals, the TW arrival times are estimated as $t^{(1)}_{\mathrm{Recti,Incid}} = 4.1300$ ms, $t^{(1)}_{\mathrm{Inver,Incid}} = 4.1300$ ms, $t^{(1)}_{\mathrm{Recti,Refra}} = 12.3870$ ms, and $t^{(1)}_{\mathrm{Inver,Refra}} = 12.3870$ ms. By knowing that $\ell = 2450$ km and then applying (4.9), $\tilde{d} = 1224.9998$ km is estimated. Thus, a fault location error $\varepsilon = 0.0002$ km is calculated. As can be seen, even in a critical case in which reflected and refracted TWs overlap, the method provides a highly accurate fault location estimate, demonstrating its robustness.

5.2 MASSIVE STUDY

To validate the proposed method's performance under different scenarios, a massive study was conducted. Fault location errors ε are presented using box plots as shown in Figure 5.6. Each box plot summarizes the ε values for 99 different fault distances (from 1% to 99% of ℓ regarding the Rectifier Station). The borders of the blue box represent the upper (75% of cases) and lower (25% of cases) quartiles. The whiskers represent the minimum and maximum ε values. The red line represents the median (50% of cases), and the red markers represent the outliers. As shown in (4.9), the proposed method is free of v_{p} settings. Hence, tests with different values of the v_{p} setting are not necessary. Therefore, five scenarios were created and taken into account different data synchronization κ misalignments, fault resistances R_{Fault}, signal-to-noise ratio (SNR) levels, soil resistivities ρ, and sampling frequencies f_{S}. When one of these variable is shifted, the other variables were considered as: synchronized signals ($\kappa = 0$ s), solid fault $R_{\mathrm{Fault}} = 0\ \Omega$, noiseless signals, $\rho = 1000\ \Omega$·m, and $f_{\mathrm{S}} = 1$ MHz.

Figure 5.6: Example of a box plot.

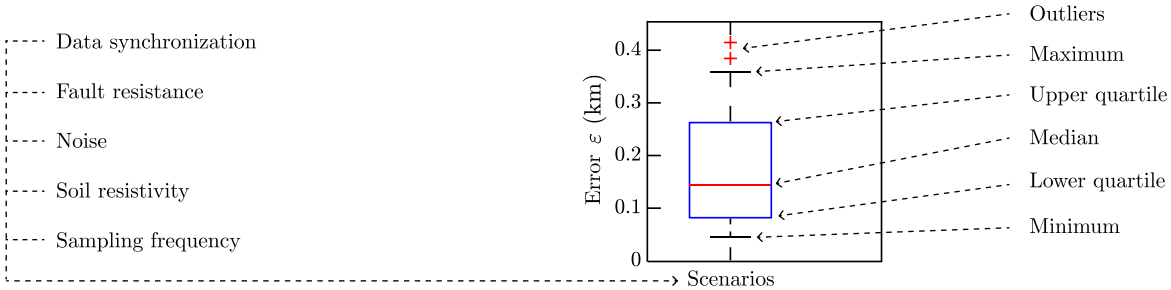

Source: Own Authorship.

5.2.1 Data Synchronization

Aiming to prove the method's independence of data synchronization κ, six situations were carried out as shown in Figure 5.7. Misalignments are applied to the data at the inverter station regarding the rectifier station. Synchronized signals ($\kappa = 0$ s), and unsynchronized signals with $\kappa = 10$ μs, 50 μs, 100 μs, 500 μs, and 1 ms are considered. Results show that the method is not affected by κ. In all scenarios, the fault location errors ε are smaller than 0.6 km.

5.2.2 Fault Resistance

To validate the accuracy of the method under different fault resistances, seven situations were carried out as shown in Figure 5.8. The fault resistance R_{Fault} was set to 0 Ω, 50 Ω, 100 Ω, 200 Ω, 400 Ω, 600 Ω, and 800 Ω. The method is robust to high R_{Fault} values. The fault location errors ε including outliers did not exceed 0.6 km. The medians are ≈ 0.1 km, showing the high accuracy of the method.

Figure 5.7: Fault location error ε with different data synchronization κ misalignments.

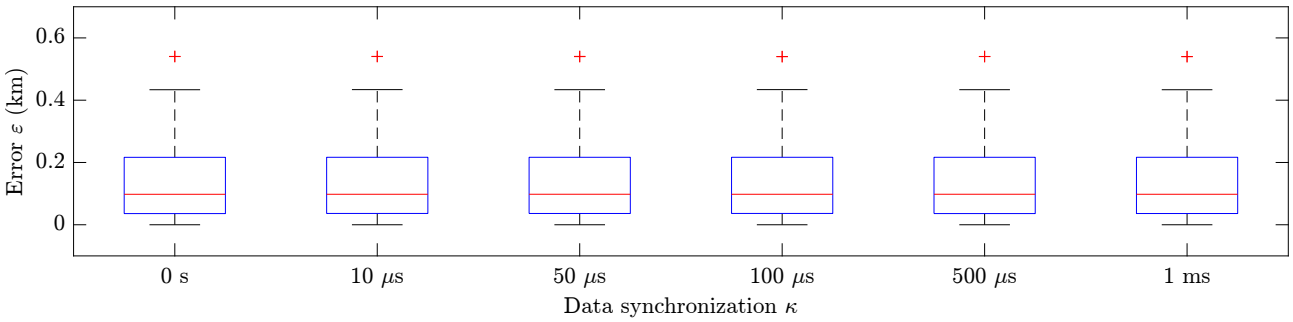

Source: Own Authorship.

Figure 5.8: Fault location error ε with different fault resistance R_{Fault} values.

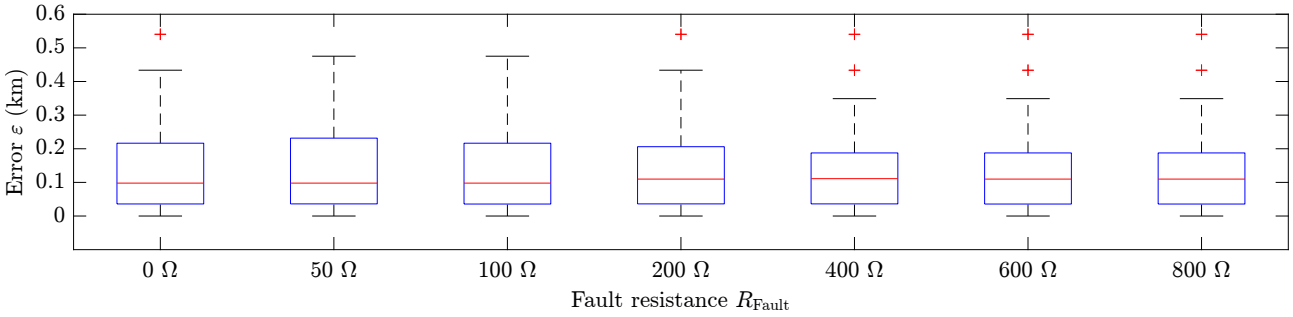

Source: Own Authorship.

5.2.3 Noise

To test the impact of noise, six situations were carried out as shown in Figure 5.9. The SNR is set to noiseless, 60 dB, 55 dB, 50 dB, 45 dB, and 40 dB. As expected for TWFL solutions, the method is affected by noise level. The SNR decreases, the ε increases. However, the median and upper quartile of ε are smaller than 0.5 km and 1 km, respectively, under SNR = 40 dB noisy signals. Therefore, the proposed method proves to be robust against noise.

5.2.4 Soil Resistivity

To study the influence of soil resistivity ρ on the method, six situations were carried out as shown in Figure 5.10. The ρ value is set 0 Ω·m, 1 Ω·m, 10 Ω·m, 100 Ω·m, 1000 Ω·m, 10000 Ω·m. The method's performance is affected by the ρ value. Indeed, soil resistivity impacts the propagation of TWs (DARDENGO *et al.*, 2021). However, the upper quartile (75% of cases) of $\varepsilon < 0.6$ km in all scenarios, showing the high accuracy of the method.

Figure 5.9: Fault location error ε with different noise SNR levels.

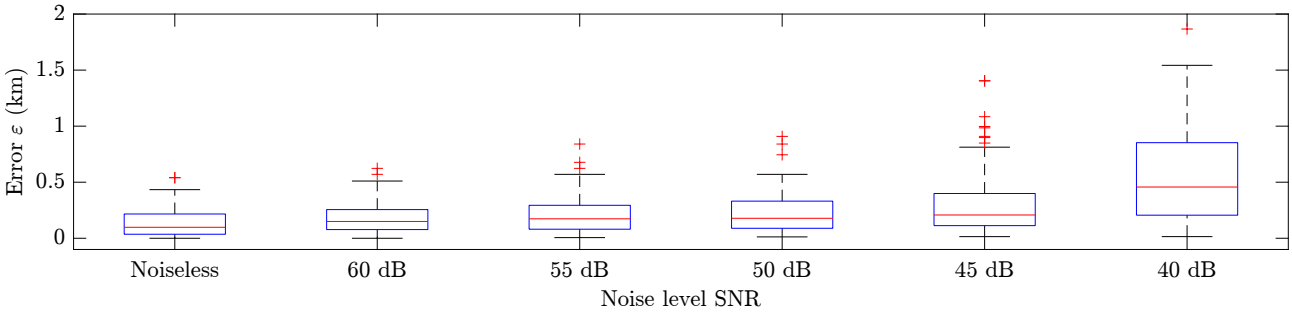

Source: Own Authorship.

Figure 5.10: Fault location error ε with different soil resistivity ρ values.

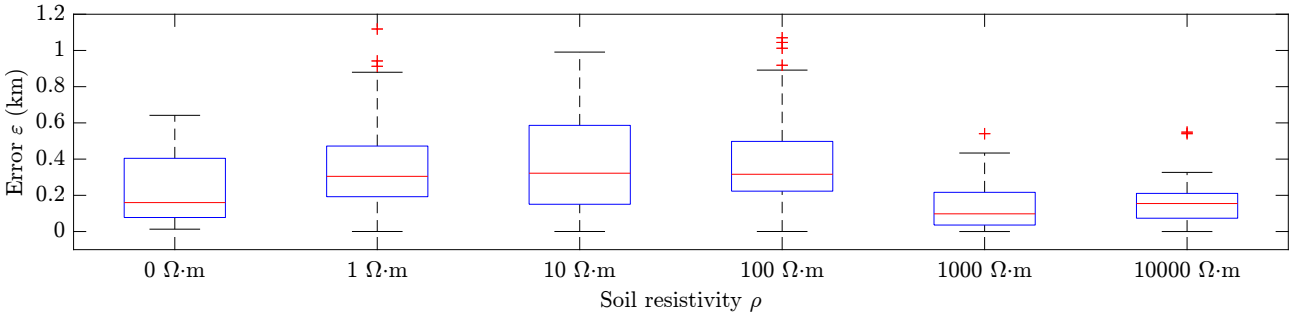

Source: Own Authorship.

5.2.5 Sampling Frequency

To analyze the impact of f_S, six situations were carried out as shown in Figure 5.11. The f_S is set to 10 kHz, 20 kHz, 50 kHz, 100 kHz, 500 kHz, and 1 MHz. The method's accuracy is affected by the f_S value. The higher the f_S, the smaller the ε errors. Using $f_S = 10$ kHz, the maximum error ε is greater than 15 km, so, this f_S is not recommended. For maximum errors, $\varepsilon = 6$ km, 3 km, and 2 km, $f_S = 20$ kHz, 50 kHz, and 100 kHz, respectively, can be used. Nevertheless, to obtain a high accuracy ($\varepsilon < 0.6$ km), as expected for TWFL methods, $f_S > 500$ kHz is recommended. Devices using $f_S = 1$ MHz or greater are readily available on the market and have been widely used in real-world applications, therefore, high f_S values are no longer a technological barrier (DONG, 2022; SEL INC., 2022; GE, 2022; SIEMENS, 2023).

5.3 COMPARATIVE STUDY

To compare the proposed method's performance to the state-of-the-art TWFL solutions, the eleven methods listed in Table 3.2 were implemented. The signal processing performed for the proposed method was used (see Steps #1 to #3 in Section 4.3). Further details of additional implementations are presented next.

- All methods require at least one aerial mode incident TW arrival instant. These instants are estimated as described in Step #4 in Section 4.3;
- In the methods that required ground mode TW arrival instants (Modal SETWFL and Modal DETWFL), these instants are estimated in a similar way as described in Step #4 in Section 4.3 for aerial mode incident TW instants but using ground mode TW signals;

Figure 5.11: Fault location error ε with different sampling frequency f_S values.

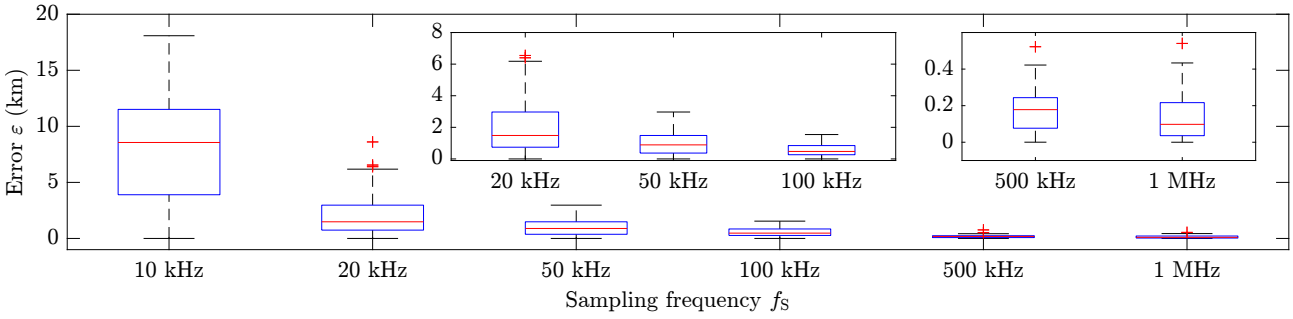

Source: Own Authorship.

- In the methods that require refracted TW arrival instants (Classical SETWFL, Settings-Free SETWFL, Enhanced SETWFL, SettingsFree2 DETWFL, and SyncFree DETWFL), these instants were estimated as described in Step #5 in Section 4.3.

- In the methods that require reflected TWs (Classical SETWFL, SettingsFree SETWFL, SettingsFree1 DETWFL, SettingsFree2 DETWFL, SyncFree DETWFL, and SyncFree-SettingsFree DETWFL), these instants were estimated in a similar way described in Step #5 in Section 4.3 for refracted TW instants but changing max to min and vice versa.

- In the methods that require v_{p} settings (Classical SETWFL, Modal SETWFL, Classical DETWFL, SyncFree DETWFL), three values were considered: $v_{\mathrm{p,20\ kHz}}$, $v_{\mathrm{p,100\ kHz}}$, and $v_{\mathrm{p,Light}}$. First, $v_{\mathrm{p,20\ kHz}}$ and $v_{\mathrm{p,100\ kHz}}$ are computed considering the line electrical parameters obtained by means the .lis file of JMarti model using the ATP software for the HVDC system analyzed in this thesis (see Figure 2.6(f)) at 20 kHz and 100 kHz. Finally, $v_{\mathrm{p,Light}}$ is defined as a percentage (85% for ground mode and 95% for aerial mode) of the speed of light in free space (National Institute of Standards and Technology (NIST), 2023). Thereby, three pairs of $v_{\mathrm{p}}^{(0)}$ and $v_{\mathrm{p}}^{(1)}$ could be obtained, being made available to the setting-dependent TWFL algorithms. The following values were obtained : $v_{\mathrm{p,20\ kHz}}^{(0)} = 261.0308$ km/s, $v_{\mathrm{p,20\ kHz}}^{(1)} = 296.8636$ km/s, $v_{\mathrm{p,100\ kHz}}^{(0)} = 272.1607$ km/s, $v_{\mathrm{p,100\ kHz}}^{(1)} = 297.1816$ km/s. Finally, $v_{\mathrm{p,Light}}^{(0)} = 254.8236$ km/s, and $v_{\mathrm{p,Light}}^{(1)} = 284.8028$ km/s.

- In the methods that require faulted half line identification (Classical SETWFL and Sinc-Free DETWFL), this information was obtained using the real fault distance d.

- In the methods that use instantaneous frequency to set v_{p} (Enhanced SETWFL and DETWFL), the Stockwell transform was used as proposed by Wang *et al.* (2021).

Now, errors ε are presented using line plots in a logarithmic scale. Each line plot presents the ε values for 99 different fault distances. Similar to previous Section, five scenarios were created and taken into account different κ misalignments, R_{Fault}, SNR levels, ρ, and f_{S}. In this Section, besides the ε variable, another index is considered, namely: convergence percentage Ψ [%]. This Ψ index is defined as the percentage of cases that TWFL methods return feasible fault location estimations. In other words, if $0 < \tilde{d} < \ell$. Finally, an information of 2 tower spans (1 tower span $\approx$ 500 m) is shown in each plot. This value is not a maximum acceptable ε but only a reference adopted in this thesis to help in the graphical interpretation.

5.3.1 TW Propagation Velocity

From Table 3.2, Classical SETWFL, Modal SETWFL, Classical DETWFL, and SyncFree DETWFL depend on v_p settings. Figure 5.12 shows Ψ and ε results for solid ($R_{Fault} = 0\ \Omega$) PG faults using synchronized data, noiseless signals, $f_S = 1$ MHz, and $\rho = 1000\ \Omega$·m. Three pairs of v_p values previously described are taken into account. From the results, Modal SETWFL presents the greatest errors ε and the smallest Ψ values. Such a performance results from the dependence of $t^{(0)}_{RecInc}$, which are difficult to detect due to their high attenuation (FERNANDES *et al.*, 2020). Moreover, $v_p^{(0)}$ presents an uncertainty level higher than $v_p^{(1)}$ (WEI *et al.*, 2023; LIU *et al.*, 2023) (see Figure 2.6(f)). Hence, since an unique $v_p^{(0)}$ setting is considered, higher ε values are verified if compared to approaches that depend only on aerial-mode TWs. For the other methods, ε is reduced when these techniques are set using $v_{p,20\ kHz}$, but these v_p information is not always available. On the other hand, proposed method resulted in $\Psi = 100\%$, regardless of v_p setting, presenting $\varepsilon < 540$ m, the best performance among the TWFL methods.

Figure 5.12: Convergence percentage Ψ and fault location error ε with different v_p settings.

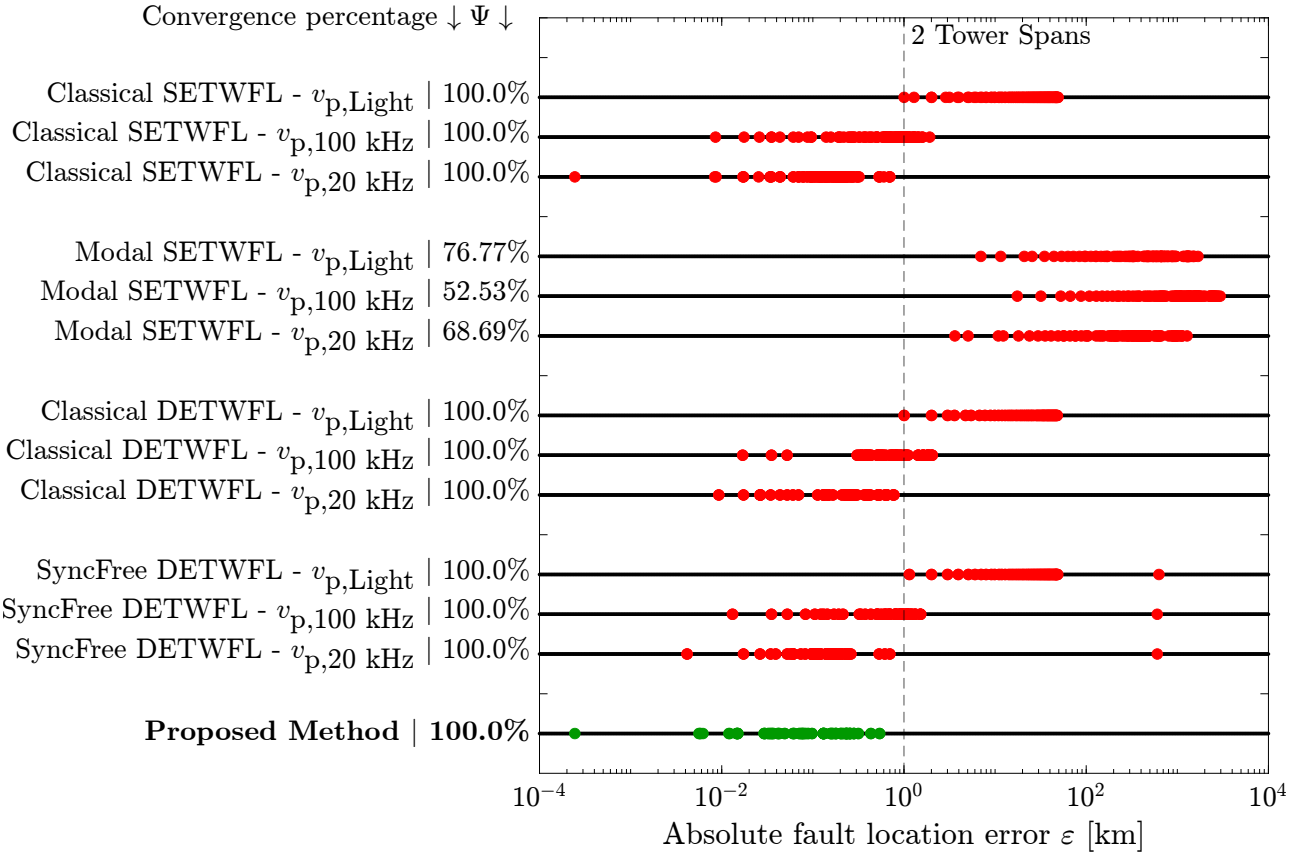

Source: Own Authorship.

5.3.2 Data Synchronization

According to Table 3.2, four approaches are affected by κ misalignments, namely, Classical DETWFL, SettingsFree1 DETWFL, SettingsFree2 DETWFL, and Enhanced DETWFL. Figure 5.13 shows Ψ and ε values for solid ($R_{\text{Fault}} = 0\ \Omega$) PG faults, $f_{\text{S}} = 1$ MHz, $\rho = 1000\ \Omega\cdot$m using noiseless signals under three scenarios: synchronized ($\kappa = 0$ s) and unsynchonized data with $\kappa = 100\ \mu$s and $\kappa = 1$ ms. Also, Classical DETWFL method was set with $v_{\text{p}}^{(1)} = v_{\text{p,20 kHz}}^{(1)}$, since this velocity resulted in the best performance of such technique (see Subsection 5.3.1). From the results, Ψ is almost 100% for synchronized and unsynchronized data but ε presented greater values when unsynchronized measurements were considered. The greater the κ the greater ε for the TWFL methods. Thus, Classical DETWFL, SettingsFree1 DETWFL, SettingsFree2 DETWFL, and Enhanced DETWFL are affected by unsynchronized data. On the other hand, the proposed method resulted in $\Psi = 100\%$ and $\varepsilon < 540$ m for synchronized and unsynchonized data, showing the immunity of κ misalignments of the proposed solution.

Figure 5.13: Convergence percentage Ψ and fault location error ε with different data synchronization κ misalignments.

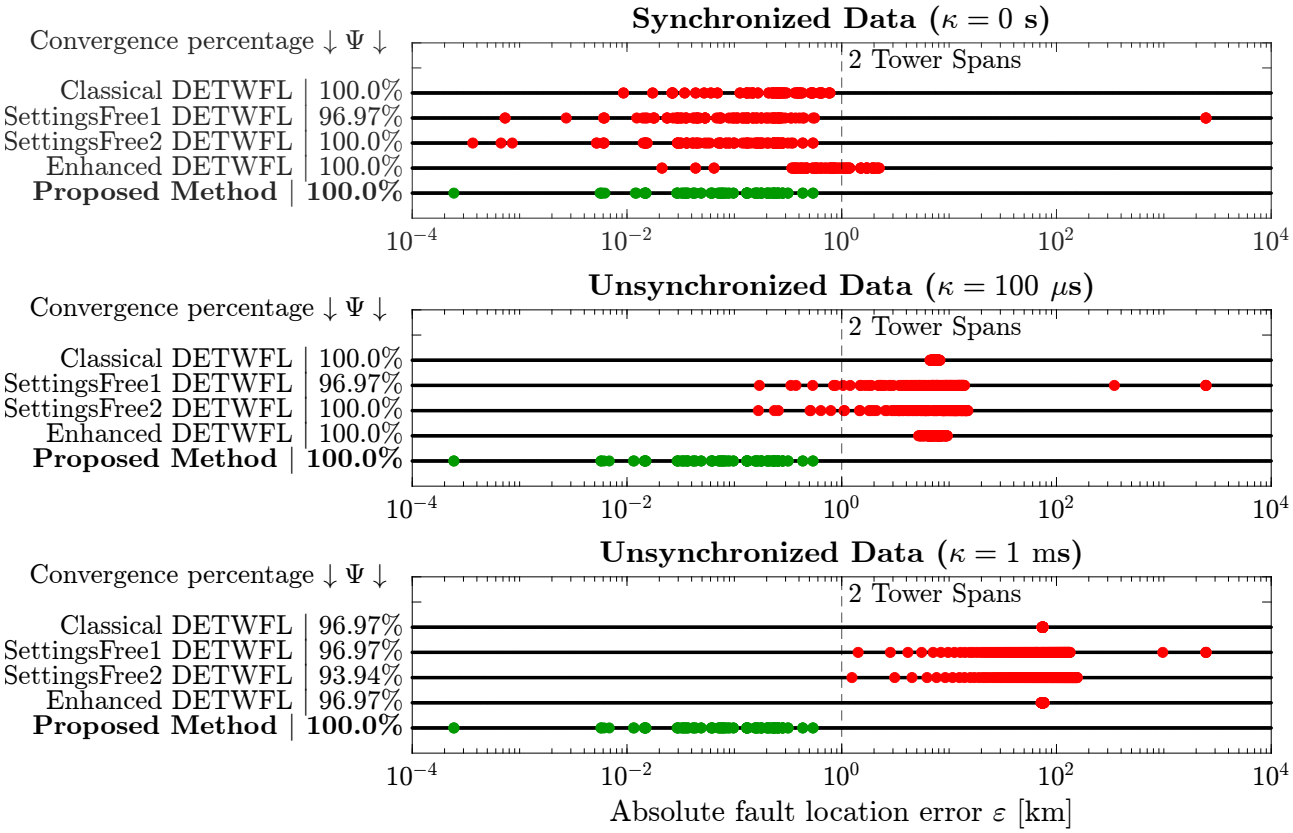

Source: Own Authorship.

5.3.3 Fault Resistance

All methods listed in Table 3.2 are affected by the R_{Fault} value. Figure 5.14 shows the Ψ and ε values for PG faults, when $\kappa = 0$ s, $f_{\text{S}} = 1$ MHz, $\rho = 1000$ Ω·m, noiseless signals, R_{Fault} equal to 0 Ω (solid fault), 100 Ω, 400 Ω and 800 Ω. In solid fault cases, Ψ values were equal to 100% for all TWFL methods, except Modal SETWFL and SettingsFree1 DETWFL. The errors ε did not exceed 2 tower spans in all methods, except Modal SETWFL, Modal DETWFL, Enhanced SETWFL and Enhanced DETWFL. As expected, methods that depend on ground-mode TWs (Modal SETWFL and Modal DETWFL) presented the worst performances. Enhanced SETWFL and Enhanced DETWFL are directly dependent on the instantaneous frequency estimation. The other methods present $\varepsilon < 2$ tower spans. For $R_{\text{Fault}} = 100$ Ω, SettingsFree SETWFL and SettingsFree1 DETWFL, and SyncFreeSettingsFree DETWFL result in errors ε of hundred kilometers. These methods depends on reflected TWs. For $R_{\text{Fault}} = 400$ Ω and $R_{\text{Fault}} = 800$ Ω, all methods, except Classical DETWFL and SettingsFree2 DETWFL presented reduced ε values. Classical DETWFL does not depend on reflected TWs, and SettingsFree2 DETWFL depends on refracted TWs instead of reflected TWs. However, these both methods are affected by data synchronization, as shown in the previous Subsection. On the other hand, proposed method yielded $\Psi = 100\%$ and $\varepsilon < 900$ m for all R_{Fault} values, revealing itself to be quite robust for real applications. These results prove that the use of refracted TWs instead of reflected ones reduces the impacts of R_{Fault} on TWFL procedures.

5.3.4 Noise

All methods listed in Table 3.2 might be affected by the presence of noise in the signals. Figure 5.15 shows the Ψ and ε results for solid ($R_{\text{Fault}} = 0$ Ω) PG faults using synchronized data, $f_{\text{S}} = 1$ MHz, $\rho = 1000$ Ω·m for four situations: noiseless signals and noisy signals with a SNR = 60 dB, 50 dB, and 40 dB. Methods that depends on v_{p} settings, $v_{\text{p}}^{(1)} = v_{\text{p,20 kHz}}^{(1)}$ was set, which resulted in the smallest ε values in the previous cases. From the results, all methods are affected by noise signals. All methods presents $\varepsilon >$ of hundred kilometers when noisy signals with SNR = 40 dB is considered. On the other hand, proposed method resulted in $\Psi = 100\%$ and $\varepsilon < 1.87$ km even under noisy signals with a SNR = 40 dB, showing the its robustness.

Figure 5.14: Convergence percentage Ψ and fault location error ε with different fault resistance R_{Fault} values.

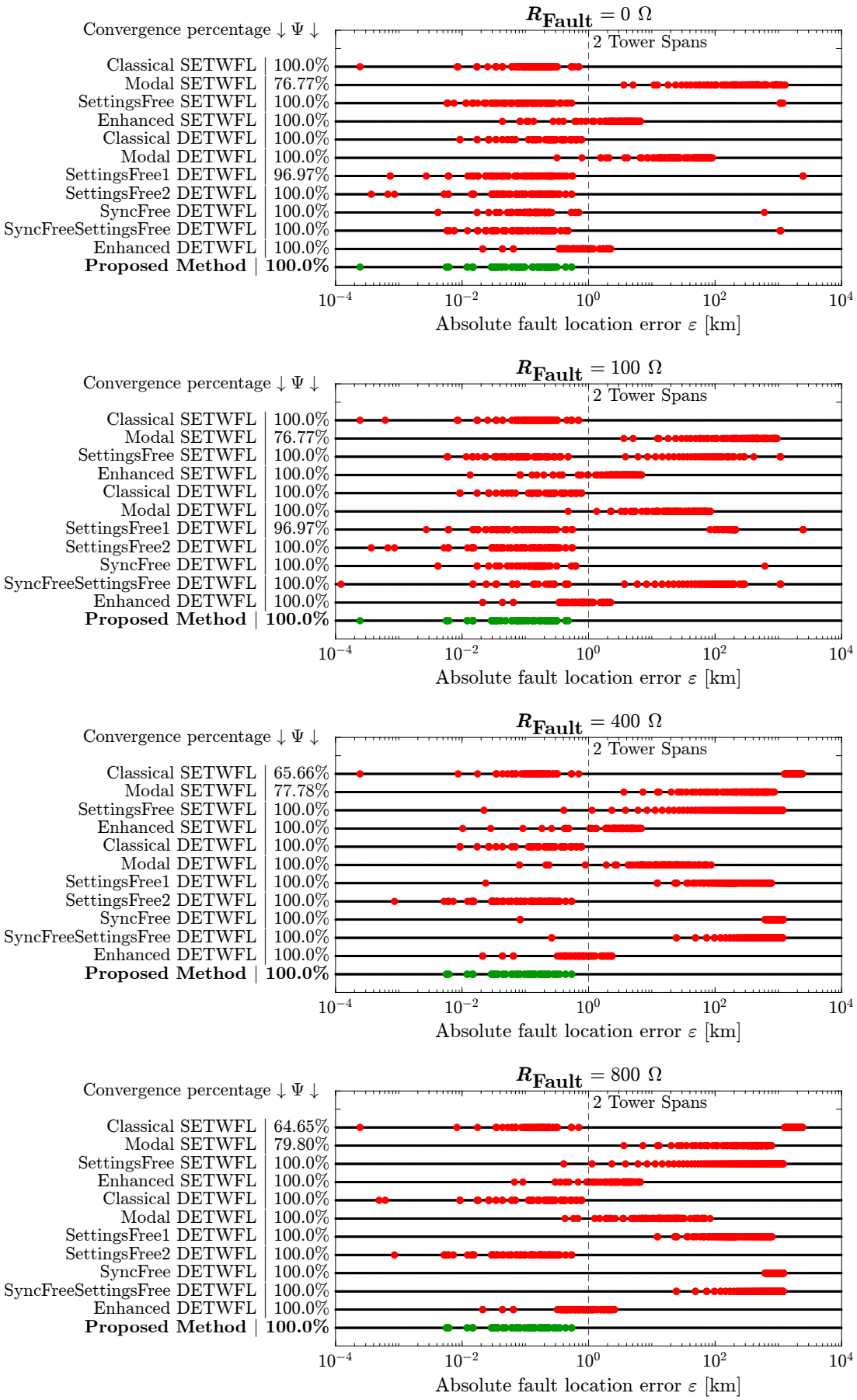

Source: Own Authorship.

Figure 5.15: Convergence percentage Ψ and fault location error ε with different noise SNR levels.

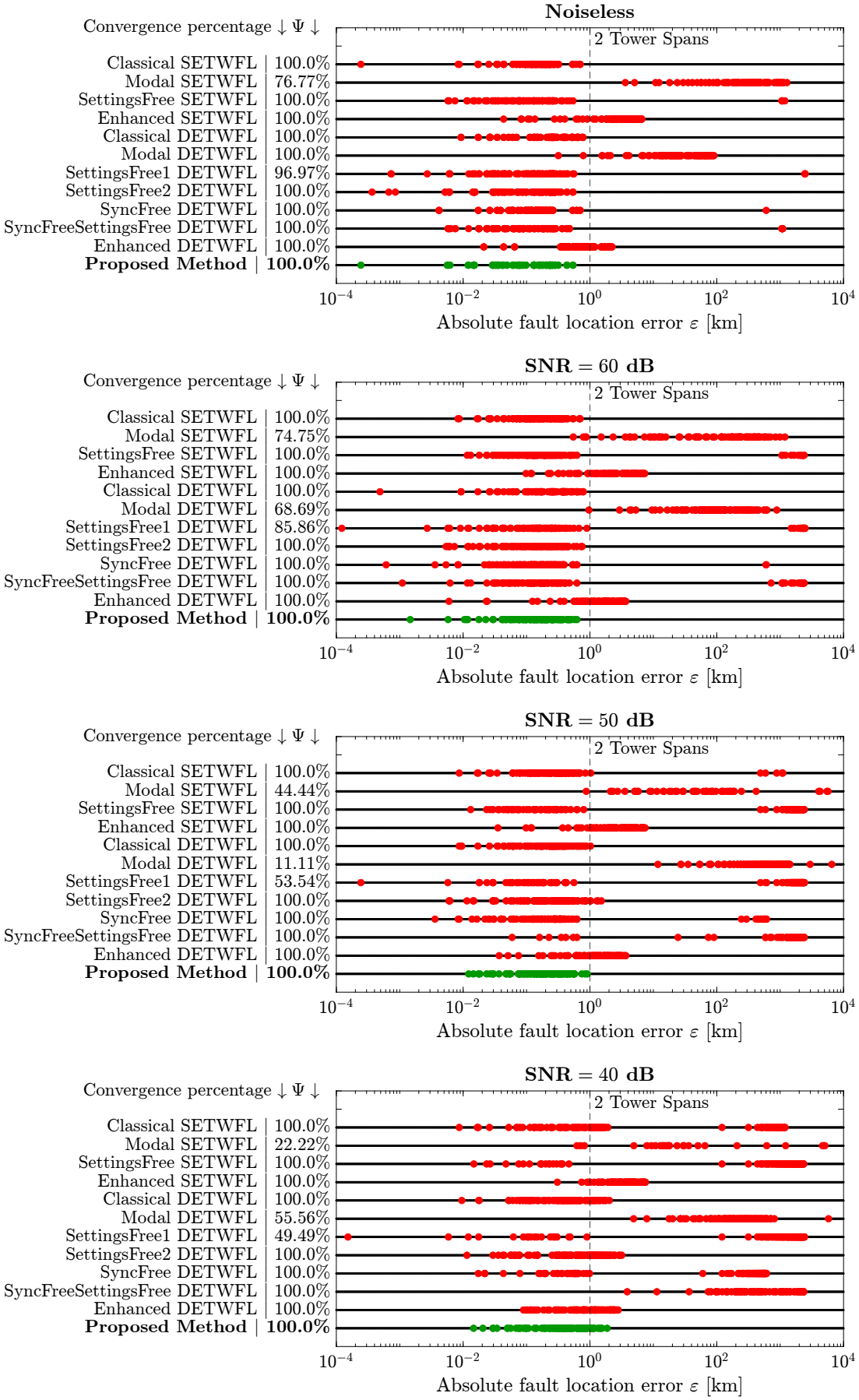

Source: Own Authorship.

5.3.5 Soil Resistivity

All methods listed in Table 3.2 might be affected by the ρ value. Figure 5.16 shows the Ψ and ε values for PG faults, when $R_{\text{Fault}} = 0\ \Omega$ (solid fault), $\kappa = 0$ s, $f_{\text{S}} = 1$ MHz, noiseless signals, and $\rho = 1000\ \Omega{\cdot}$m and $10000\ \Omega{\cdot}$m. From the results, the impact of soil resistivity is not significant for all methods by comparing the considered ρ values. Finally, proposed method shows the best performance, providing a fault location error $\varepsilon < 550$ m in both scenarios.

5.3.6 Sampling Frequency

All methods listed in Table 3.2 are affected by the f_{S}. Figure 5.17 shows the Ψ and ε values for PG faults, when $R_{\text{Fault}} = 0\ \Omega$ (solid fault), $\kappa = 0$ s, noiseless signals, $\rho = 1000\ \Omega{\cdot}$m considering $f_{\text{S}} = 1$ MHz and $f_{\text{S}} = 500$ kHz. From the results, the impact of sampling frequency

Figure 5.16: Convergence percentage Ψ and fault location error ε with different soil resistivity ρ values.

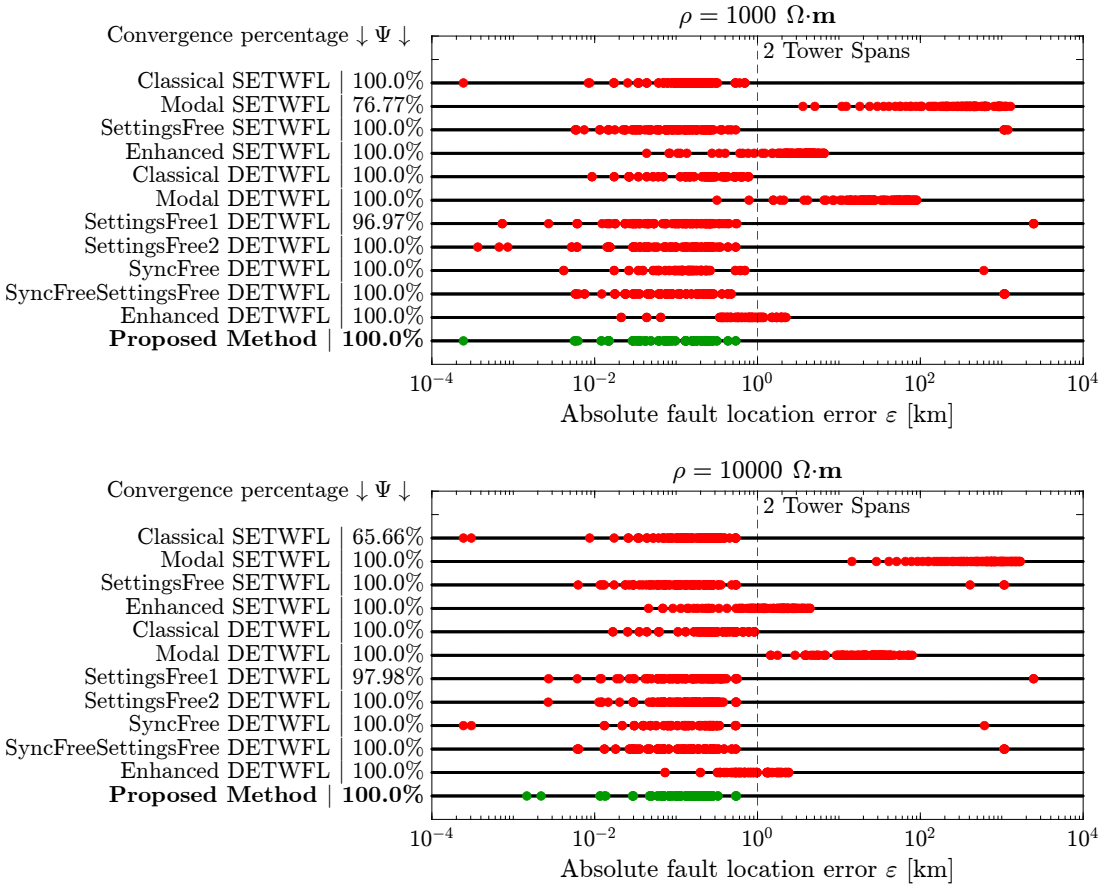

Source: Own Authorship.

is not significant. The proposed method shows the best performance, providing a fault location error $\varepsilon = 540$ m and $\varepsilon < 762$ m using $f_S = 1$ MHz and $f_S = 500$ kHz, respectively. However, as aforementioned, devices using $f_S = 1$ MHz or greater are readily available on the market and have been widely used in real-world applications, therefore, high f_S values are no longer a technological barrier (DONG, 2022; SEL INC., 2022; GE, 2022; SIEMENS, 2023).

5.3.7 The Best Scenario and the Worst Scenario

By knowing that the performance of TWFL methods can vary depending on the variables: fault features (R_{Fault}), signal conditions (κ, SNR, and f_S), external conditions (ρ), and user predefined settings (v_p), studying the contrast between the best scenario and the worst scenario is useful way of identifying how much stable the TWFL methods are when these variables change.

Figure 5.17: Convergence percentage Ψ and fault location error ε with different sampling frequency f_S values.

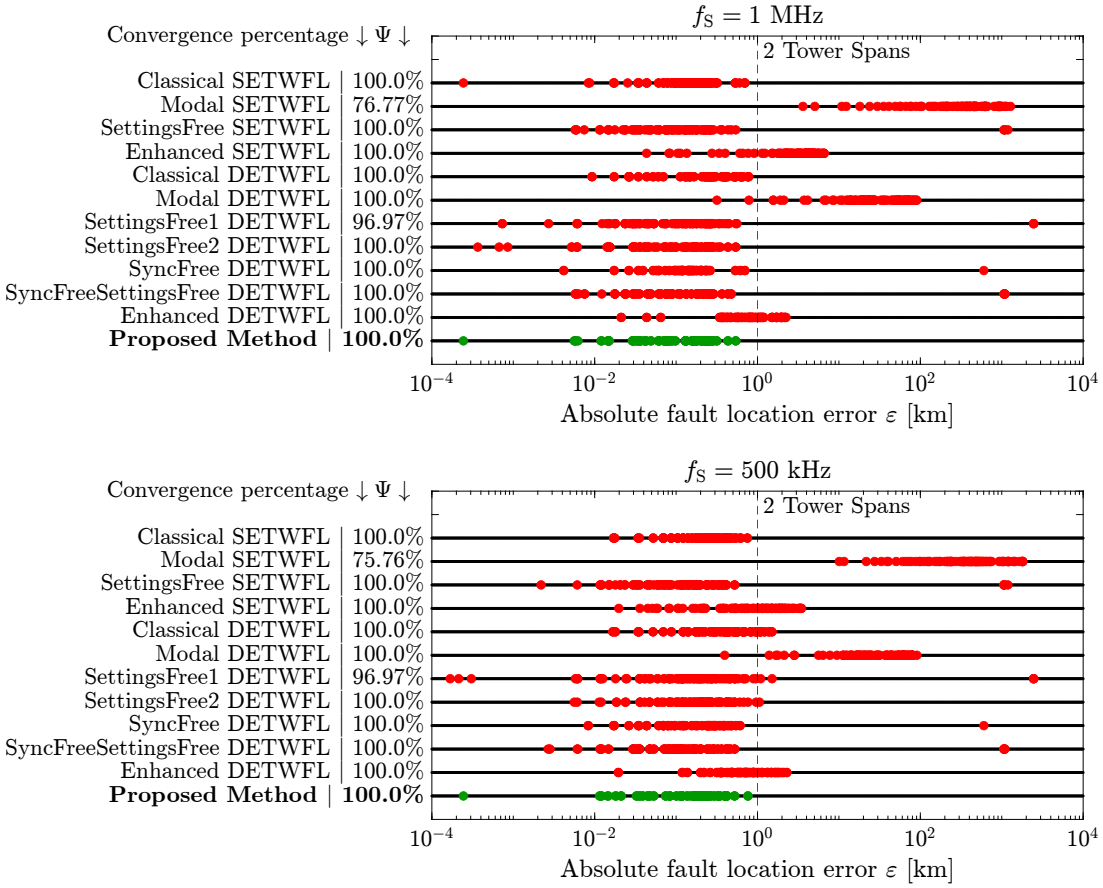

Source: Own Authorship.

The best scenario is created considering solid ($R_{\text{Fault}} = 0\ \Omega$) PG faults using synchronized data ($\kappa = 0$ s), noiseless signals, $f_{\text{S}} = 1$ MHz, and $\rho = 1000\ \Omega$·m. From the previous Subsections, $v_{\text{p,20 kHz}}$ setting resulted in the best results for the TWFL methodologies that require v_{p} settings. Therefore, $v_{\text{p}} = v_{\text{p,20 kHz}}$ is considered in this Subsection. Figure 5.18 presents Ψ and ε for the eleven state-of-the-art TWFL methods, as well as for the proposed method, considering the aforementioned fault features, signal conditions, system topology and settings. From the results, Modal SETWFL and Modal DETWFL presented the worst performances compared to other methods. Their poor performances are due to the fact that these methods depend on ground-mode TWs, which results in uncertainties on the detection of ground-mode TWs and on ground-mode TW propagation velocity. Also, Enhanced SETWFL and Enhanced DETWFl presented significant errors. SettingsFree SETWFL, SettingsFree1 DETWFL, SyncFree DETWFL, and SyncFreeSettingsFree DETWFL methods presented ε greater than hundreds of kilometers are observed in some cases. Finally, Classical SETWFL, Classical DETWFL and SettingsFree2 DETWFL methods presented the best performance among the existing TWFL methods, yielding $\Psi = 100\%$ and $\varepsilon < 0.699$ km, $\varepsilon < 0.776$ km, and $\varepsilon < 0.540$ km, respectively. Even so, the proposed method proved to be more promising, resulting in a $\Psi = 100\%$ and $\varepsilon < 540$ m.

The worst scenario is created considering a PG fault with R_{Fault} equal to 800 Ω, unsynchronized data with misalignments of $\kappa = 1$ ms, SNR equal to 40 dB, $f_{\text{S}} = 500$ kHz, and $\rho = 10000\ \Omega$·m. In addition, when $v_{\text{p,Light}}$ was set in all setting-dependent TWFL methods, uncertainties in the line electrical parameters resulted in higher fault location errors. Therefore,

Figure 5.18: Convergence percentage Ψ and fault location error ε in the best scenario.

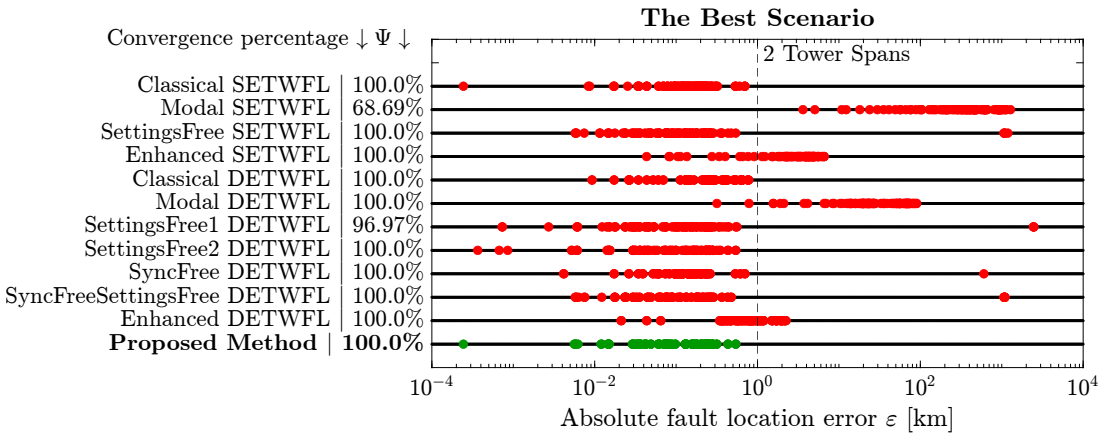

Source: Own Authorship.

Figure 5.19: Convergence percentage Ψ and fault location error ε in the worst scenario.

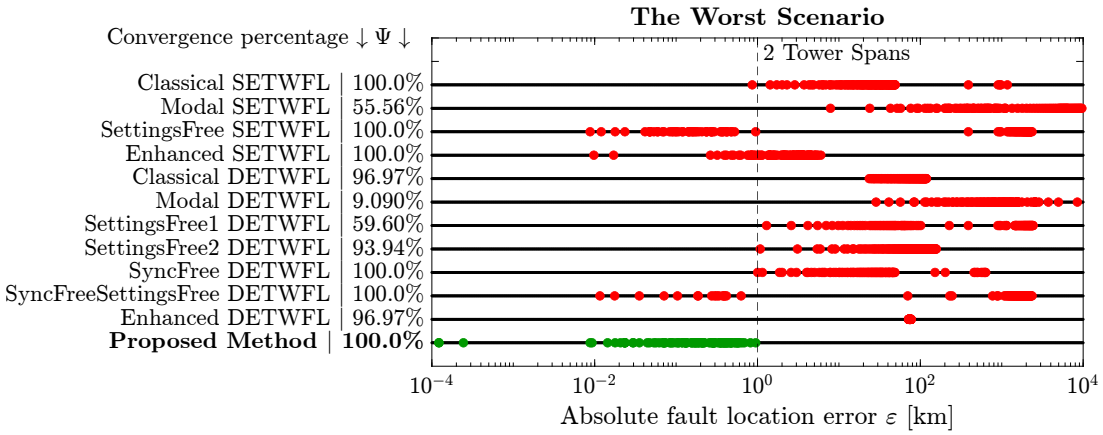

Source: Own Authorship.

$v_{\mathrm{p}} = v_{\mathrm{p,Light}}$ is set here. In this critical scenario, Figure 5.19 shows Ψ and ε for each TWFL method. The Enhanced SETWFL method resulted in a maximum fault location error of 5.989 km. All other existing TWFL methods presented errors in the order of tens of kilometers. On the other hand, the proposed method showed a stable and accurate performance, resulting in $\Psi = 100\%$ and $\varepsilon < 0.949$ km.

CHAPTER 6

CONCLUSIONS

This thesis proposes a double-ended TW-based PG fault location method for HVDC lines. An analysis of the TW phenomenon on HVDC systems finds that refracted TWs are detectable in PG faults. Based on this finding, a PG fault location method is proposed. This method is free from TW propagation velocity settings and data synchronization means. Simulations in the Rio Madeira HVDC system were carried out using the ATP. Results show that the method is accurate, presenting fault location errors smaller than 0.6 km (0.02 % of the line length) in most cases. Moreover, the method shows to be robust under different data synchronization misalignments, fault resistances, noise levels, soil resistivities, and sampling frequencies. Finally, a comparative study proves that the method is more robust and accurate than the state-of-the-art TWFL methods, with a relatively simple procedure.

Future directions:

- The proposed method is based on the HVDC converter topology. Therefore, testing the proposed method with other HVDC converter topologies, such as VSC and MMC, is a future activity to prove the versatility of the proposed method;
- The proposed method was implemented using a high-pass filter. Aiming to prove the robustness of the proposed solution, testing the proposed method with other filtering techniques, such as wavelet transform-based filters, differentiator-smother filter etc;
- To test the proposed method on close-in faults;
- Simplicity is an important advantage of the proposed method. To evaluate the proposed method's performance embedded in a real-time digital simulator;
- To test the proposed method on real-world fault cases from different HVDC systems;
- The proposed method was tested on a point-to-point HVDC line. When a fault takes place in multi-terminal HVDC systems, multiple TW reflections can arise, which can affect the

detection of refracted TWs of the proposed method. Therefore, testing the proposed method in multi-terminal HVDC systems and, if necessary, propose adaptations.

REFERENCES

AIEE Committee Report. Bibliography and summary of fault location methods [includes discussion]. *Transactions of the American Institute of Electrical Engineers. Part III: Power Apparatus and Systems*, v. 74, p. 1423–1428, 1 1955. ISSN 2379-6766. Cited in page 17.

ALASSI, A.; BAÑALES, S.; ELLABBAN, O.; ADAM, G.; MACIVER, C. Hvdc transmission: Technology review, market trends and future outlook. *Renewable and Sustainable Energy Reviews*, Elsevier Ltd, v. 112, p. 530–554, 9 2019. ISSN 18790690. Cited in page 1.

ALLEN, J. E.; GROSS, G. J. A method for locating faults on overhead transmission lines by means of high frequency. *Edison Electric Institute Bulletin*, v. 3, p. 309–315, 8 1935. Cited in page 17.

ANDO, M.; SCHWEITZER, E. O.; BAKER, R. A. Development and field-data evaluation of single-end fault locator for two-terminal hvdc transmission lines - part 1: Data collection system and field data. *IEEE Transactions on Power Apparatus and Systems*, PAS-104, p. 3524–3530, 12 1985. ISSN 0018-9510. Cited in page 19.

ANDO, M.; SCHWEITZER, E. O.; BAKER, R. A. Development and field-data evaluation of single-end fault locator for two-terminal hvdc transmission lines - part 2: Algorithm and evaluation. *IEEE Transactions on Power Apparatus and Systems*, PAS-104, p. 3531–3537, 12 1985. ISSN 0018-9510. Cited 5 times in pages 19, 20, 24, 29, and 31.

AURANGZEB, M.; CROSSLEY, P. A.; GALE, P. Fault location on a transmission line using high frequency travelling waves measured at a single line end. In: . [S.l.: s.n.], 2000. v. 4, p. 2437–2442 vol.4. Cited in page 6.

BEWLEY, L. V. Traveling waves due to lightning. *Transactions of the American Institute of Electrical Engineers*, v. 48, n. 3, p. 1050–1064, July 1929. ISSN 2330-9431. Cited in page 17.

BEWLEY, L. V. Traveling waves on transmission systems. *Transactions of the American Institute of Electrical Engineers*, v. 50, n. 2, p. 532–550, June 1931. ISSN 2330-9431. Cited 2 times in pages 9 and 17.

CARSON, J. R. Theory of the transient oscillations of electrical networks and transmission systems. *Transactions of the American Institute of Electrical Engineers*, XXXVIII, p. 345–427, 1919. Cited in page 6.

CARSON, J. R. Electric circuit theory and the operational calculus. *The Bell System Technical Journal*, v. 4, p. 685–761, 1925. Cited in page 6.

CARSON, J. R. Wave propagation in overhead wires with ground return. *The Bell System Technical Journal*, v. 5, n. 4, p. 539–554, Oct 1926. ISSN 0005-8580. Cited in page 17.

CARSON, J. R. The present status of wire transmission theory and some of its outstanding problems. *The Bell System Technical Journal*, v. 7, p. 268–280, 1928. Cited in page 6.

CHEN, P.; XU, B.; LI, J. A traveling wave based fault locating system for hvdc transmission lines. In: . [S.l.]: 2006 International Conference on Power System Technology, 2006. Cited in page 20.

CHEN, W.; WANG, D.; CHENG, D.; LIU, X. Travelling wave fault location approach for mmc-hvdc transmission line based on frequency modification algorithm. *International Journal of Electrical Power and Energy Systems*, Elsevier Ltd, v. 143, 12 2022. ISSN 01420615. Cited 4 times in pages 3, 25, 26, and 34.

CROSSLEY, P.; DAVIDSON, M.; GALE, P. Fault location using travelling waves. In: . [S.l.: s.n.], 1993. p. 6/1–6/3. Cited 2 times in pages 17 and 18.

DARDENGO, V. P.; CAVALCANTE, P. A. H.; ALMEIDA, M. C. de. An evaluation of wave speed impacts on fault location methods for hvdc lines. In: . [S.l.: s.n.], 2018. p. 1–5. ISSN 2472-9639. Cited 2 times in pages 23 and 29.

DARDENGO, V. P.; FARDIN, J. F.; ALMEIDA, M. C. de. Single-terminal fault location in hvdc lines with accurate wave velocity estimation. *Electric Power Systems Research*, Elsevier Ltd, v. 194, 5 2021. ISSN 03787796. Cited 2 times in pages 3 and 41.

DATTA, B.; CHATTERJEE, S. A literature review on use of bewley's lattice diagram. In: . [S.l.: s.n.], 2012. p. 1–4. Cited in page 10.

DE MAGALHÃES JR., F. M.; LOPES, F. V. Mathematical Study on Traveling Waves Phenomena on Three Phase Transmission Lines Part I: Fault-Launched Waves. *IEEE Transactions on Power Delivery*, Institute of Electrical and Electronics Engineers Inc., 2021. ISSN 19374208. Cited in page 6.

DE MAGALHÃES JR., F. M.; LOPES, F. V. Mathematical Study on Traveling Waves Phenomena on Three Phase Transmission Lines Part II: Reflection and Refraction Matrices. *IEEE Transactions on Power Delivery*, Institute of Electrical and Electronics Engineers Inc., 2021. ISSN 19374208. Cited 2 times in pages 4 and 8.

DOMMEL, H.; MEYER, W. Computation of Electromagnetic Transients. *Proceedings of the IEEE*, v. 62, p. 983–993, 1974. ISSN 0018-9219. Cited 2 times in pages 12 and 34.

DOMMEL, H. W. Digital computer solution of electromagnetic transients in single-and multiphase networks. *IEEE Transactions on Power Apparatus and Systems*, PAS-88, p. 388–399, 4 1969. ISSN 0018-9510. Cited in page 12.

DOMMEL, H. W. *Electromagnetic Transients Program Reference Manual: EMTP Book*. Portland, USA: Bonneville Power Administration, 1996. Cited in page 36.

DONG, X. *The Theory of Fault Travel Waves and Its Application*. [S.l.]: Springer Singapore, 2022. ISBN 9789811904042. Cited 7 times in pages 6, 8, 20, 30, 34, 42, and 50.

DOWELL, J. C. Attenuation and successive reflections of traveling waves. *Transactions of the American Institute of Electrical Engineers*, v. 50, p. 551–557, 6 1931. ISSN 2330-9431. Cited in page 17.

FARIA, J. A. B.; BRICENO, J. H. On the modal analysis of asymmetrical three-phase transmission lines using standard transformation matrices. *IEEE Transactions on Power Delivery*, v. 12, p. 1760–1765, 10 1997. ISSN 1937-4208. Cited in page 7.

FAYAZI, M.; JOORABIAN, M.; SAFFARIAN, A.; MONADI, M. A single-ended traveling wave based fault location method using dwt in hybrid parallel hvac/hvdc overhead transmission lines on the same tower. *Electric Power Systems Research*, Elsevier Ltd, v. 220, 7 2023. ISSN 03787796. Cited 2 times in pages 3 and 26.

FERNANDES, P. C.; HONORATO, T. R.; LOPES, F. V.; SILVA, K. M.; GONçALVES, H. N. Evaluation of Travelling Wave-Based fault Location Methods Applied to HVDC Systems. *Electric Power Systems Research*, Elsevier Ltd, v. 189, 12 2020. ISSN 03787796. Cited 13 times in pages 3, 4, 5, 7, 8, 20, 21, 22, 23, 24, 31, 34, and 44.

FERRER, H. J. A.; SCHWEITZER, I. E. O. *Modern Solutions for Protection, Control and Monitoring of Electric Power Systems*. [S.l.: s.n.], 2010. Cited in page 6.

FOURIER, J.-B.-J. *Théorie analytique de la chaleur*. [S.l.]: Chez Firmin Didot, père et fils, 1822. Cited in page 13.

GALE, P.; CROSSLEY, P.; BINGYIN, X.; YAOZHONG, G.; CORY, B.; BARKER, J. Fault Location Based on Travelling Waves. In: *Fifth International Conference on Developments in Power System Protection*. [S.l.: s.n.], 1993. p. 54–59. Cited 6 times in pages 17, 18, 20, 21, 29, and 31.

GENERAL ELETRIC. *RPV311 Distributed Multifunction Fault Recorder - Technical Manual*. Boston, Massachusetts, USA, 2022. Cited 2 times in pages 42 and 50.

GILANY, M.; IBRAHIM, D. khalil; ELDIN, E. S. T. Traveling-Wave-Based Fault-Location Scheme for Multiend-Aged Underground Cable System. *IEEE Transactions on Power Delivery*, v. 22, p. 82–89, 1 2007. ISSN 1937-4208. Cited 2 times in pages 21 and 29.

GLOVER, J. D.; OVERBYE, T. J.; SARMA, M. S. *Power System Analysys & Design*. Sixth. [S.l.]: Cengage Learning, 2015. 1-942 p. Cited 3 times in pages 6, 13, and 14.

GREENWOOD, A. *Electrical Transients in Power Systems*. Second. [S.l.]: Wiley-Interscience, 1991. 1-768 p. Cited in page 6.

HALEEM, N. M.; RAJAPAKSE, A. D. A single pole to ground fault location method for hvdc transmission lines based on coupling characteristics. In: . [S.l.: s.n.], 2019. p. 1–6. Cited in page 2.

Hitachi Energy. *High-Voltage Direct Current (HVDC)*. 2023. Online; accessed 28 November 2023. Disponível em: <www.hitachienergy.com/hvdc>. Cited in page 1.

HOFF, A.; ABBOUD, R.; BERNARDES, R.; LIMA, P. Finding Faults Fast Saves Money and Improves Service. In: *48th Annual Western Protective Relay Conference*. Spokane, USA: [s.n.], 2021. p. 1–14. Cited 2 times in pages 1 and 2.

HUAI, Q.; LIU, K.; HOOSHYAR, A.; DING, H.; QIN, L.; CHEN, K. Line fault location for multi-terminal mmc-hvdc system based on swt and svd. *IET Renewable Power Generation*, v. 14, p. 4043–4052, 2020. Disponível em: <https://ietresearch.onlinelibrary.wiley.com/doi/abs/10.1049/iet-rpg.2020.0702>. Cited 5 times in pages 3, 4, 9, 20, and 26.

HUAI, Q.; LIU, K.; HOOSHYAR, A.; DING, H.; CHEN, K.; LIANG, Q. Single-ended line fault location method for multi-terminal hvdc system based on optimized variational mode decomposition. *Electric Power Systems Research*, Elsevier Ltd, v. 194, 5 2021. ISSN 03787796. Cited 2 times in pages 3 and 26.

HUAI, Q.; QIN, L.; LIU, K.; DING, H.; LIAO, X.; TAN, T. Combined line fault location method for mmc-hvdc transmission systems. *IEEE Access*, Institute of Electrical and Electronics Engineers Inc., v. 8, p. 170794–170806, 2020. ISSN 21693536. Cited 4 times in pages 3, 24, 25, and 29.

HUGHES, R. W.; WEINTRAUB, N. Fault location by pulse time modulation. *Electrical Engineering*, v. 69, p. 1009–1011, 11 1950. ISSN 2376-7804. Cited in page 17.

IZYKOWSKI, J. *Fault Location on Power Transmission Lines*. [S.l.]: Oficyna Wydawnicza Politechniki Wroclawskiej, 2008. Cited in page 6.

KARAPETOFF, V. A graphical theory of traveling electric waves between parallel conductors. *Transactions of the American Institute of Electrical Engineers*, v. 48, p. 508–522, 4 1929. ISSN 2330-9431. Cited in page 17.

KASZTENNY, B.; GUZMáN, A.; FISCHER, N.; MYNAM, M. V.; TAYLOR, D. Practical setting considerations for protective relays that use incremental quantities and traveling waves. In: . [S.l.: s.n.], 2016. p. 1–25. Cited in page 8.

KIMBARK, E. W. Transient overvoltages caused by monopolar ground fault on bipolar dc line: Theory and simulation. *IEEE Transactions on Power Apparatus and Systems*, PAS-89, n. 4, p. 584–592, April 1970. ISSN 0018-9510. Cited in page 31.

LAN, S.; CHEN, M. J.; CHEN, D. Y. A novel hvdc double-terminal non-synchronous fault location method based on convolutional neural network. *IEEE Transactions on Power Delivery*, Institute of Electrical and Electronics Engineers Inc., v. 34, p. 848–857, 6 2019. ISSN 19374208. Cited in page 3.

LAN, T.; LI, Y.; DUAN, X. High fault-resistance tolerable traveling wave protection for multi-terminal vsc-hvdc. *IEEE Transactions on Power Delivery*, Institute of Electrical and Electronics Engineers Inc., v. 36, p. 943–956, 4 2021. ISSN 19374208. Cited in page 31.

LEWIS, L. J. Traveling wave relations applicable to power-system fault locators. *Transactions of the American Institute of Electrical Engineers*, v. 70, p. 1671–1680, 7 1951. ISSN 2330-9431. Cited in page 17.

LIN, X.; ZHENG, Y.; TONG, N.; LI, Z.; SUI, Q. Fast mutual-speed-up protection adaptive to dead-zone grounding-fault identification for vsc-mtdc. *IEEE Transactions on Power Delivery*, v. 36, p. 3393–3403, 12 2021. ISSN 1937-4208. Cited 3 times in pages 4, 8, and 31.

LIU, Y.; SHENG, G.; HE, Z.; JIANG, X. A Traveling Wave Fault Location Method for Earth Faults Based on Mode Propagation Time Delays of Multi-Measuring Points. *Przeglad Elektrotechniczny*, 2012. ISSN 0033-2097. Cited 3 times in pages 3, 21, and 29.

LIU, Z.; GAO, H.; LUO, S. Non-unit protection for long-distance lcc-hvdc transmission lines based on waveform characteristics of voltage travelling waves. *International Journal of Electrical Power & Energy Systems*, Elsevier BV, v. 150, p. 109079, 8 2023. ISSN 01420615. Cited 5 times in pages 3, 7, 22, 33, and 44.

LOPES, F. V. Settings-Free Traveling-Wave-Based Earth Fault Location Using Unsynchronized Two-Terminal Data. *IEEE Transactions on Power Delivery*, v. 31, p. 2296–2298, 10 2016. ISSN 1937-4208. Cited 3 times in pages 3, 22, and 29.

LOPES, F. V.; DANTAS, K. M.; SILVA, K. M.; COSTA, F. B. Accurate Two-Terminal Transmission Line Fault Location Using Traveling Waves. *IEEE Transactions on Power Delivery*, v. 33, n. 2, p. 873–880, 2018. Cited 3 times in pages 3, 23, and 29.

LOPES, F. V.; REIS, R. L. A.; SILVA, K. M.; MARTINS-BRITTO, A.; RIBEIRO, E. P. A.; MORAES, C. M.; RODRIGUES, M. A. M. Past, Present, and Future Trends of Traveling Wave-Based Fault Location Solutions. In: *2021 Workshop on Communication Networks and Power Systems (WCNPS)*. [S.l.: s.n.], 2021. p. 1–6. ISSN 2768-0045. Cited 4 times in pages 8, 19, 20, and 25.

LOPES, F. V.; SILVA, K. M.; COSTA, F. B.; NEVES, W. L. A.; FERNANDES, D. Real-time traveling-wave-based fault location using two-terminal unsynchronized data. *IEEE Transactions on Power Delivery*, v. 30, p. 1067–1076, 6 2015. ISSN 1937-4208. Cited 2 times in pages 3 and 9.

LUZ, G.; JUNIOR, D.; JUNIOR, S. HVDC Transmission Line Modeling Analysis in PSCAD and ATP Programs. In: *Symposium of Specialists in Electric Operational and Expansion Planning*. [S.l.: s.n.], 2014. p. 1–10. Cited in page 36.

MAGNAGO, F. H.; ABUR, A. Fault Location Using Wavelets. *IEEE Transactions on Power Delivery*, v. 13, p. 1475–1480, 10 1998. ISSN 1937-4208. Cited 2 times in pages 7 and 20.

MARIHART, D. J.; HAAGENSON, N. W. Automatic fault locator for bonneville power administration. In: . [S.l.: s.n.], 1972. p. 1–6. Cited 2 times in pages 18 and 19.

MARTI, J. R. Accurate Modelling of Frequency-Dependent Transmission Lines in Electromagnetic Transient Simulations. *IEEE Transactions on Power Apparatus and Systems*, PAS-101, p. 147–157, 1 1982. ISSN 0018-9510. Cited in page 36.

MARTI, J. R.; MARTI, L.; DOMMEL, H. W. Transmission line models for steady-state and transients analysis. In: . [S.l.: s.n.], 1993. v. 2, p. 744–750. Cited in page 7.

MCEACHRON, K. B.; HEMSTREET, J. G.; RUDGE, W. J. Traveling waves on transmission lines with artificial lightning surges. *Transactions of the American Institute of Electrical Engineers*, v. 49, n. 3, p. 885–894, July 1930. ISSN 2330-9431. Cited in page 17.

MCEACHRON, K. B.; HEMSTREET, J. G.; SEELYE, H. P. Study of the effect of short lengths of cable on traveling waves. *Transactions of the American Institute of Electrical Engineers*, v. 49, p. 1432–1441, 1930. Cited in page 17.

MEYER, W. S.; LIU, T. *Alternative Transients Program (ATP) Rule Book*. [S.l.]: Canadian/American EMTP User Group, 1992. Cited in page 36.

MONTEIRO, R. D.; CRUZ, M. C.; LOPES, F. V.; MEDEIROS, J. O.; MEDEIROS, M. F. Parameters-free non-iterative two-terminal measurements synchronization algorithm. *International Journal of Electrical Power and Energy Systems*, Elsevier Ltd, v. 138, 6 2022. ISSN 01420615. Cited 3 times in pages 3, 9, and 21.

NAIDU, O. D.; PRADHAN, A. K. A Traveling Wave-Based Fault Location Method Using Unsynchronized Current Measurements. *IEEE Transactions on Power Delivery*, v. 34, p. 505–513, 4 2019. ISSN 1937-4208. Cited 2 times in pages 23 and 29.

NANAYAKKARA, K.; RAJAPAKSE, A. D.; WACHAL, R. Fault location in extra long hvdc transmission lines using continuous wavelet transform. In: . [S.l.: s.n.], 2011. p. 1–7. Cited in page 21.

National Institute of Standards and Technology (NIST). *SI REDEFINITION - Meet the Constants*. 2023. Accessed: 2023-08-10. Disponível em: <https://www.nist.gov/si-redefinition/meet-constants>. Cited in page 43.

OLIVEIRA, A. P.; MOREIRA, F. A.; PICANCO, A. F. Application of hilbert-huang and stockwell transforms to fault location in transmission lines using traveling wave theory. In: . IEEE, 2022. p. 1–6. ISBN 978-1-6654-7982-0. Disponível em: <https://ieeexplore.ieee.org/document/9830381/>. Cited in page 26.

PHADKE, A. G.; THORP, J. S. *Computer Relaying for Power Systems*. Second. [S.l.]: John Wiley & Sons, 2009. 1-326 p. Cited in page 6.

RIBEIRO, C. M. S.; LOPES, F. V.; SILVA, K. M. Assessment of traveling wave propagation velocity on hvdc transmission lines. In: *2022 Workshop on Communication Networks and Power Systems (WCNPS)*. [S.l.: s.n.], 2022. p. 1–6. Cited 2 times in pages 7 and 22.

ROHRIG, J. Location of faulty places by measuring with cathode ray oscillographs. *Elektrotech Zeits*, v. 8, n. 2, p. 241–242, 1931. Cited in page 17.

RORDEN, H. L. Solution of circuits subjected to traveling waves. *Transactions of the American Institute of Electrical Engineers*, v. 51, p. 824–836, 9 1932. ISSN 2330-9431. Cited in page 17.

SAHA, M. M.; IZYKOWSKI, J.; ROSOLOWSKI, E. *Fault Location on Power Networks*. [S.l.]: Springer, 2010. Cited 3 times in pages 6, 8, and 9.

SCHWEITZER, E. O.; GUZMáN, A.; MYNAM, M.; SKENDZIC, V.; KASZTENNY, B. Accurate Single-End Fault Location and Line-Length Estimation Using Traveling Waves. In: *13th International Conference on Developments in Power System Protection*. [S.l.: s.n.], 2016. p. 1–6. Cited 4 times in pages 3, 20, 22, and 29.

SCHWEITZER, E. O.; GUZMáN, A.; MYNAM, M. V.; SKENDZIC, V.; KASZTENNY, B.; MARX, S. Locating faults by the traveling waves they launch. In: . [S.l.: s.n.], 2013. Cited in page 3.

SCHWEITZER ENGINEERING LABORATORIES INC. *SEL-T401L Relay Time-Domain Protection Instruction Manual*. Pullman, WA, 2022. Cited 3 times in pages 3, 42, and 50.

SIEMENS AG. *SIPROTEC 7SE20 Traveling Wave Recorder*. Erlangen, Germany, 2023. Cited 2 times in pages 42 and 50.

SILVA, D. M. da; COSTA, F. B.; MIRANDA, V.; LEITE, H. Wavelet-based analysis and detection of traveling waves due to dc faults in lcc hvdc systems. *International Journal of Electrical Power and Energy Systems*, Elsevier Ltd, v. 104, p. 291–300, 1 2019. ISSN 01420615. Cited in page 24.

SNEDDOM, M.; GALE, P. Fault location on transmission lines. In: . [S.l.: s.n.], 1997. p. 2/1–2/3. Cited 3 times in pages 17, 18, and 19.

STEINMETZ, C. P. The general equations of the electric circuit. *Transactions of the American Institute of Electrical Engineers*, XXVII, p. 1231–1305, 6 1908. ISSN 2330-9431. Cited in page 6.

STEINMETZ, C. P. *Theory and Calculation of Transient Electric Phenomena and Oscillations*. [S.l.]: McGraw Hill, 1909. 1-556 p. Cited in page 6.

STEVENS, R. F.; STRINGFIELD, T. W. A transmission line fault locator using fault-generated surges. *Transactions of the American Institute of Electrical Engineers*, v. 67, p. 1168–1179, 1 1948. ISSN 2330-9431. Cited in page 17.

STRINGFIELD, T. W.; MARIHART, D. J.; STEVENS, R. F. Fault location methods for overhead lines. *Transactions of the American Institute of Electrical Engineers. Part III: Power Apparatus and Systems*, v. 76, p. 518–529, 4 1957. ISSN 2379-6766. Cited 3 times in pages 17, 18, and 19.

TüNNERHOFF, P.; RUFFING, P.; SCHNETTLER, A. Comprehensive fault type discrimination concept for bipolar full-bridge-based mmc hvdc systems with dedicated metallic return. *IEEE Transactions on Power Delivery*, v. 33, p. 330–339, 2 2018. ISSN 1937-4208. Cited in page 2.

VIEIRA, J. C. C.; FERNANDES, D.; NEVES, W. L. A.; LOPES, F. V. Fault diagnosis in bipolar hvdc systems based on traveling wave theory by monitoring data from one terminal. *Electric Power Systems Research*, v. 223, p. 109594, 10 2023. ISSN 03787796. Cited 3 times in pages 4, 8, and 23.

VIEIRA, J. C. C.; JUNIOR, D. F.; NEVES, W. A.; LOPES, F. V. Challenges in application of the traveling wave-based fault location methods applied to hvdc systems: Evaluation of classical one- and two-terminal methods. In: . IEEE, 2022. p. 1–6. ISBN 978-1-6654-1639-9. Disponível em: <https://ieeexplore.ieee.org/document/9808569/>. Cited in page 26.

WANG, D.; CHENG, D.; SUN, X.; CHEN, W.; QIAO, F.; LIU, X.; HOU, M. Novel travelling wave directional pilot protection approach for lcc-mmc-mtdc overhead transmission line. *International Journal of Electrical Power and Energy Systems*, Elsevier Ltd, v. 144, 1 2023. ISSN 01420615. Cited in page 34.

WANG, D.; FU, J.; HOU, M.; QIAO, F.; GAO, M. Novel travelling wave fault location principle for vsc-hvdc transmission line. *Electric Power Systems Research*, Elsevier Ltd, v. 196, 7 2021. ISSN 03787796. Cited 6 times in pages 3, 25, 26, 29, 34, and 43.

WANG, D.; HOU, M.; GAO, M.; QIAO, F. Travelling wave directional pilot protection for hybrid hvdc transmission line. *International Journal of Electrical Power and Energy Systems*, Elsevier Ltd, v. 107, p. 615–627, 5 2019. ISSN 01420615. Cited in page 31.

WANG, D.; HOU, M.; GAO, M.; QIAO, F. Travelling wave directional pilot protection for hybrid lcc-mmc-hvdc transmission line. *International Journal of Electrical Power and Energy Systems*, Elsevier Ltd, v. 115, 2 2020. ISSN 01420615. Cited in page 34.

WANG, D.; LIU, H.; ZHANG, D.; QIAO, F.; LIU, X.; HOU, M. Travelling wave fault location for lcc–mmc–mtdc transmission lines based on frequency-dependent characteristic. *International Journal of Electrical Power and Energy Systems*, Elsevier Ltd, v. 138, 6 2022. ISSN 01420615. Cited in page 34.

WANG, J.; ZHANG, Y. Traveling wave propagation characteristic-based lcc-mmc hybrid hvdc transmission line fault location method. *IEEE Transactions on Power Delivery*, Institute of Electrical and Electronics Engineers Inc., v. 37, p. 208–218, 2 2022. ISSN 19374208. Cited in page 31.

WANG, J.; ZHANG, Y. Traveling wave propagation characteristic-based lcc-mmc hybrid hvdc transmission line fault location method. *IEEE Transactions on Power Delivery*, Institute of Electrical and Electronics Engineers Inc., v. 37, p. 208–218, 2 2022. ISSN 19374208. Cited in page 36.

WEI, X.; ZOU, G.; CHEN, C.; ZHANG, S.; ZHOU, C.; SONG, S. Single-ended dc line protection scheme based on first peak time of current-limiting reactor voltage. *International Journal of Electrical Power and Energy Systems*, Elsevier Ltd, v. 150, 8 2023. ISSN 01420615. Cited 5 times in pages 3, 7, 22, 33, and 44.

WU, J.-Y.; LAN, S.; XIAO, S.-J.; YUAN, Y.-B. Single pole-to-ground fault location system for mmc-hvdc transmission lines based on active pulse and ceemdan. *IEEE Access*, v. 9, p. 42226–42235, 5 2021. ISSN 2169-3536. Cited 2 times in pages 1 and 2.

YU, S.; WANG, X.; ZHANG, X.-P. A sensitive single-end dc line fault detection method for mmc-hvdc grids using reactor voltage ratio. *International Journal of Electrical Power & Energy Systems*, Elsevier BV, v. 148, p. 108953, 6 2023. ISSN 01420615. Cited in page 31.

ZENG, R.; WU, Q.; ZHANG, L. Two-terminal traveling wave fault location based on successive variational mode decomposition and frequency-dependent propagation velocity. *Electric Power Systems Research*, Elsevier Ltd, v. 213, 12 2022. ISSN 03787796. Cited in page 26.

ZHANG, C.; SONG, G.; WANG, T.; YANG, L. Single-ended traveling wave fault location method in dc transmission line based on wave front information. *IEEE Transactions on Power Delivery*, v. 34, p. 2028–2038, 10 2019. ISSN 1937-4208. Cited 4 times in pages 3, 4, 23, and 26.

ZHANG, Y.; TAI, N.; XU, B. Fault Analysis and Traveling-Wave Pprotection Scheme for Bipolar HVDC Lines. *IEEE Transactions on Power Delivery*, v. 27, p. 1583–1591, 2012. ISSN 08858977. Cited in page 31.

ZHANG, Y.; WANG, S.; LIU, T.; ZHANG, S.; LU, Q. A traveling-wave-based protection scheme for the bipolar voltage source converter based high voltage direct current (vsc-hvdc) transmission lines in renewable energy integration. *Energy*, Elsevier Ltd, v. 216, 2 2021. ISSN 03605442. Cited in page 31.

ZHU, X.; LI, S.; GUO, Y.; CHEN, X.; HE, C.; DENG, J. Novel wavefront detection and fault location method based on hilbert-huang transform for long hvdc transmission lines. *Electric Power Systems Research*, Elsevier Ltd, v. 211, 10 2022. ISSN 03787796. Cited 10 times in pages 3, 4, 7, 8, 9, 20, 21, 22, 23, and 26.

APPENDIX A

PUBLICATIONS

The results of this PhD research were published in the following papers.

- **RIBEIRO, C. M. S.**; LOPES, F. V.; SILVA, K. M. 'Double-Ended Traveling Wave-Based Method for Pole-to-Ground Fault Location on HVDC Transmission Lines'. Submitted to *IEEE Transactions on Instrumentation and Measurement*.

- **RIBEIRO, C. M. S.**; SILVA, K. M.; GAMA, L. A. 'A Systematic Review of Traveling Wave-Based Fault Location Methods for HVDC Transmission Lines'. To be submitted to *Protection and Control of Modern Power Systems*.

- REIS, R. L. A.; LOPES, F. V.; NEVES, W. L. A.; FERNANDES JR., D.; **RIBEIRO, C. M. S.** ; CUNHA, G. A. 'An Improved Single-Ended Correlation-Based Fault Location Technique Using Traveling Waves'. *International Journal of Electrical Power & Energy Systems*. 2021. DOI: 10.1016/j.ijepes.2021.107167

- **RIBEIRO, C. M. S.**; LOPES, F. V.; SILVA, K. M.; 'Assessment of Traveling Wave Propagation Velocity on HVDC Transmission Lines'. In: 7th Workshop on Communication Networks and Power Systems 2022 (WCNPS 2022). DOI: 10.1109/WCNPS56355.2022.9969692

- **RIBEIRO, C. M. S.**; LOPES, F. V. 'Funções de Proteção de Sistemas Elétricos Baseadas na Transformada de Stockwell: Revisão Bibliográfica e Implementação'. In: VIII Simpósio Brasileiro de Sistemas Elétricos 2020. DOI: 10.48011/sbse.v1i1.2364.